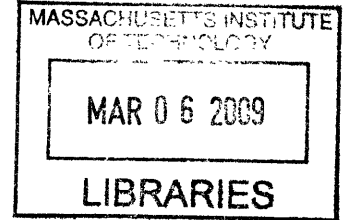


The Role of Fuel in Determining the High Load Limit of Controlled Auto-Ignition Engines

by

Amir Gamal Maria

B.A.Sc., Mechanical Engineering (2005)
University of Toronto



Submitted to the Department of Mechanical Engineering
in partial fulfillment of the requirements for the degree of

Master of Science in Mechanical Engineering

at the

MASSACHUSETTS INSTITUTE OF TECHNOLOGY

January 2009

[Feb]

© 2009 Massachusetts Institute of Technology
All rights reserved

A handwritten signature in black ink, appearing to read "Amir Gamal Maria".

Signature of Author

.....
Department of Mechanical Engineering

Certified by

.....
Wai K. Cheng
Professor of Mechanical Engineering
Thesis Supervisor

Accepted by

.....
David E. Hardt
Chairman, Department Committee on Graduate Students

The Role of Fuel in Determining the High Load Limit of Controlled Auto-Ignition Engines

by

Amir Gamal Maria

Submitted to the Department of Mechanical Engineering in partial fulfillment of the requirements for the degree of Master of Science in Mechanical Engineering

Abstract

Controlled Auto-Ignition (CAI) engines have the potential to increase fuel economy while lowering nitrogen oxide and soot emissions. One hurdle that is currently being faced is the engine's inability to operate at high loads due to a large Maximum Pressure Rise Rate (MPRR). To address this issue, this research has been focused on analytically determining the optimum fuel that can be used in a CAI engine to reduce the MPRR and extend the high load limit. The strategy is to use the fuel ignition characteristics to maximize the impact of stratification on reducing the MPRR with sequential ignitions.

To quantify the impact of the selected fuel on the high load limit, the fuel's ignition delay curve under constant volume conditions, as a function of the initial concentration and temperature was used. A parametric model of the fuel chemistry was created so that different functional dependences of the ignition delay curve could be produced through adjustment of the model parameters. Then, the ignition delay curve was parameterized, and various artificial fuels were created. The artificial fuels were then tested in an engine simulation under different operating conditions and temperature distributions.

The results from the engine simulations provide insight into the characteristics of the optimum fuel ignition delay time versus temperature relationship. As expected, the conclusions depend on the initial boundary conditions applied; particularly the initial cylinder temperature distribution. With a constant temperature applied to the entire charge, the MPRR is reduced when ignition occurs in the Negative Temperature Coefficient (NTC) region. When ignition occurs in the NTC region, the radical concentration in the later stages of the combustion process is reduced, which reduces the MPRR. When an initial quadratic temperature distribution is applied, different regions of the combustion chamber can ignite at different periods, hence reducing the MPRR. However, ignition in the NTC region negates this positive effect, and should therefore be avoided. The functional dependency of the ignition delay time versus initial temperature for the optimum fuel must therefore be created based on the expected initial charge temperature distribution.

Thesis Supervisor: Wai K. Cheng
Title: Professor of Mechanical Engineering

Acknowledgments

I would like to express my gratitude to Prof. Wai Cheng for his guidance. Working with him in the Sloan Automotive Laboratory has been a great opportunity and a very valuable learning experience. I would also like to thank Dr. Kenneth Kar for the important input he has provided that has helped shape this project.

This project has been sponsored by Chevron Corporation. Special thanks to Dr. William Cannella who has been my main contact with Chevron. It has been a pleasure to work with him, and I look forward to further contacts with him as this project develops in the coming years.

Finally, I would like to thank my family and friends for their encouragement. In particular, I would like to thank my parents for their love, prayers, and unwavering support.

Amir Gamal Maria
January 2009

Table of Contents

ABSTRACT	3
ACKNOWLEDGMENTS	5
TABLE OF CONTENTS	7
LIST OF FIGURES	9
LIST OF TABLES	13
NOMENCLATURE	15
CHAPTER 1. INTRODUCTION	17
1.1 MOTIVATION AND BACKGROUND	17
1.2 LITERATURE REVIEW	21
1.2.1 <i>Fuel Chemistry Models</i>	21
1.2.2 <i>CAI Engine Simulation Models</i>	22
1.3 RESEARCH APPROACH AND OBJECTIVES	24
1.4 REPORT OUTLINE	25
CHAPTER 2. MODELS USED TO STUDY IGNITION DELAY CHARACTERISTICS	27
2.1 FUEL CHEMISTRY MODEL: MODIFIED SHELL MODEL	27
2.1.1 <i>Description of Modified Shell Model</i>	27
2.1.2 <i>Choice of parameters and fit to the prescribed $\tau(T,M)$</i>	28
2.2 CAI ENGINE SIMULATION MODEL: MULTI-ZONE ENGINE MODEL	29
CHAPTER 3. MODEL REPRESENTATION FOR ISO-OCTANE AND N-HEPTANE	31
3.1 ISO-OCTANE REPRESENTATION	31
3.2 N-HEPTANE REPRESENTATION	32
CHAPTER 4. REPRESENTATION OF ARTIFICIAL FUELS	35
4.1 DESCRIPTION OF ARTIFICIAL FUELS	35
4.2 SINGLE REACTION FUELS	35
4.3 ISO-OCTANE-BASED FUELS	36
4.4 N-HEPTANE-BASED FUELS	38
CHAPTER 5. FUEL EFFECTS ON HIGH LOAD LIMIT	41
5.1 ANALYSIS PROCEDURE	41
5.2 DETERMINATION OF THE MAXIMUM PRESSURE RISE RATE	42
5.3 IGNITION TEMPERATURES.....	43
5.4 SINGLE REACTION FUELS	44
5.4.1 <i>Sensitivity to Pre-Exponential Factor</i>	44
5.4.2 <i>Sensitivity to Slope of Ignition Delay versus Temperature</i>	47
5.4.3 <i>Single Reaction Fuels Summary</i>	52
5.5 COMPARISON OF ISO-OCTANE AND N-HEPTANE	54
5.6 ISO-OCTANE-BASED FUELS	57
5.6.1 <i>Sensitivity to T_A</i>	57
5.6.2 <i>Sensitivity to D_A</i>	58
5.6.3 <i>Sensitivity to n_1</i>	60
5.6.4 <i>Sensitivity to n_2</i>	60
5.6.5 <i>Sensitivity to γ_{NTC}</i>	62
5.6.6 <i>Sensitivity to Low Temperature Branching Global Parameter</i>	63
5.6.7 <i>Sensitivity to High Temperature Branching Global Parameter</i>	65
5.7 N-HEPTANE-BASED FUELS	66

5.7.1	<i>Sensitivity to T_A</i>	66
5.7.2	<i>Sensitivity to D_A</i>	67
5.7.3	<i>Sensitivity to n_1</i>	68
5.7.4	<i>Sensitivity to n_2</i>	69
5.7.5	<i>Sensitivity to y_{NTC}</i>	70
5.7.6	<i>Sensitivity to Low Temperature Branching Global Parameter</i>	71
5.7.7	<i>Sensitivity to High Temperature Branching Global Parameter</i>	72
CHAPTER 6.	DISCUSSION AND SUMMARY	75
6.1	MINIMIZING MPRR IN A CHARGE WITH A UNIFORM TEMPERATURE DISTRIBUTION	75
6.2	MINIMIZING MPRR IN A CHARGE WITH A QUADRATIC TEMPERATURE DISTRIBUTION.....	76
REFERENCES		77
APPENDIX A		81
APPENDIX B		85
APPENDIX C		89
APPENDIX D		91
APPENDIX E		93
APPENDIX F		99

List of Figures

FIGURE 1-1	COMPARISON OF THE MAIN FEATURES OF SPARK IGNITION, CAI, AND DIESEL ENGINES	17
FIGURE 1-2	EXAMPLE CONSTANT VOLUME BATCH REACTOR SIMULATION: N-HEPTANE, $T_0=800$ K.....	19
FIGURE 1-3	EXAMPLE CAI ENGINE SIMULATION PRESSURE CURVES: (A) ISO-OCTANE (B) N-HEPTANE	19
FIGURE 1-4	FUEL EFFECT ON RATE OF PRESSURE RISE	21
FIGURE 3-1	ISO-OCTANE REPRESENTATION OF (A) TOTAL AND (B) FIRST-STAGE IGNITION DELAY VERSUS TEMPERATURE [$M_0 = 3.2E-4$ MOL/ CM^3 , $\Phi = 0.5$]	31
FIGURE 3-2	ISO-OCTANE REPRESENTATION CONCENTRATION EFFECTS: (A) FUEL CONCENTRATION [$T_0 = 780$ K, $M_0 = 3.2E-4$ MOL/ CM^3] (B) TOTAL CONCENTRATION [$T_0 = 780$ K, $\Phi = 0.5$]	31
FIGURE 3-3	SHELL MODEL ISO-OCTANE REPRESENTATION IN SINGLE ZONE ENGINE COMBUSTION MODEL: (A) $T_0 = 420$ K, $M_0 = 3.4E-5$ MOL/ CM^3 , $\Phi = 0.5$, CR = 16 (B) $T_0 = 420$ K, $M_0 = 3.4E-5$ MOL/ CM^3 , $\Phi = 0.3$, CR = 16	32
FIGURE 3-4	N-HEPTANE REPRESENTATION OF (A) TOTAL AND (B) FIRST-STAGE IGNITION DELAY VERSUS TEMPERATURE [$M_0 = 3.2E-4$ MOL/ CM^3 , $\Phi = 0.5$]	33
FIGURE 3-5	N-HEPTANE REPRESENTATION CONCENTRATION EFFECTS: (A) FUEL CONCENTRATION [$T_0 = 800$ K, $M_0 = 3.2E-4$ MOL/ CM^3] (B) TOTAL CONCENTRATION [$T_0 = 800$ K, $\Phi = 0.5$]	33
FIGURE 3-6	SHELL MODEL N-HEPTANE REPRESENTATION IN SINGLE ZONE ENGINE COMBUSTION MODEL: (A) $T_0 = 320$ K, $M_0 = 3.4E-5$ MOL/ CM^3 , $\Phi = 0.5$, CR = 16 (B) $T_0 = 345$ K, $M_0 = 3.4E-5$ MOL/ CM^3 , $\Phi = 0.3$, CR = 16	33
FIGURE 4-1	IGNITION DELAY CURVE PARAMETERIZATION	35
FIGURE 4-2	IGNITION DELAY CURVES FOR SINGLE REACTION (INITIATION REACTION) FUELS: (A) SCALE PRE-EXPONENTIAL FACTOR (B) CHANGE SLOPE, AND PIVOT AROUND 900 K	36
FIGURE 4-3	ISO-OCTANE BASED ARTIFICIAL FUELS: (A) T_A VARIATION (B) D_A VARIATION (C) N_1 VARIATION (D) N_2 VARIATION (E) Y_{NTC} VARIATION	37
FIGURE 4-4	ISO-OCTANE BASED ARTIFICIAL FUELS WITH VARIATION IN GLOBAL PARAMETERS: (A) A_{F1} (B) A_{F2}	38
FIGURE 4-5	N-HEPTANE BASED ARTIFICIAL FUELS: (A) T_A VARIATION (B) D_A VARIATION (C) N_1 VARIATION (D) N_2 VARIATION (E) Y_{NTC} VARIATION	39
FIGURE 4-6	N-HEPTANE BASED ARTIFICIAL FUELS WITH VARIATION IN GLOBAL PARAMETERS: (A) A_{F1} (B) A_{F2}	39
FIGURE 5-1	SAMPLE PRESSURE VERSUS CRANK ANGLE CURVES DURING COMBUSTION EVENT.....	43
FIGURE 5-2	MAXIMUM MOTORED TEMPERATURE VERSUS INITIAL TEMPERATURE AND COMPRESSION RATIO	44
FIGURE 5-3	MPPRR FOR SINGLE REACTION FUEL, EFFECT OF POSITION: (A) CONSTANT VOLUME, UNIFORM TEMPERATURE DISTRIBUTION (B) CONSTANT VOLUME, QUADRATIC TEMPERATURE DISTRIBUTION (C) VARIABLE VOLUME, UNIFORM TEMPERATURE DISTRIBUTION (D) VARIABLE VOLUME, QUADRATIC TEMPERATURE DISTRIBUTION	45
FIGURE 5-4	MAXIMUM MOTORED TEMPERATURES FOR SINGLE REACTION FUELS, EFFECT OF POSITION: (A) UNIFORM TEMPERATURE DISTRIBUTION (B) QUADRATIC TEMPERATURE DISTRIBUTION	45
FIGURE 5-5	SLOPE OF IGNITION DELAY VERSUS TEMPERATURE FOR IGNITION DELAY CURVES GIVEN IN FIGURE 4-2 (A)	46
FIGURE 5-6	MPPRR FOR SINGLE REACTION FUEL, EFFECT OF SLOPE WITH PIVOT AT 900 K: (A) CONSTANT VOLUME, UNIFORM TEMPERATURE DISTRIBUTION (B) CONSTANT VOLUME, QUADRATIC TEMPERATURE DISTRIBUTION (C) VARIABLE VOLUME, UNIFORM TEMPERATURE DISTRIBUTION (D) VARIABLE VOLUME, QUADRATIC TEMPERATURE DISTRIBUTION.....	47
FIGURE 5-7	MAXIMUM MOTORED TEMPERATURES FOR SINGLE REACTION FUELS, EFFECT OF SLOPE WITH PIVOT AT 900 K: (A) UNIFORM TEMPERATURE DISTRIBUTION (B) QUADRATIC TEMPERATURE DISTRIBUTION	48
FIGURE 5-8	SLOPE OF IGNITION DELAY VERSUS TEMPERATURE FOR IGNITION DELAY CURVES GIVEN IN FIGURE 4-2 (B)	49
FIGURE 5-9	MPPRR FOR SINGLE REACTION FUEL, EFFECT OF SLOPE WITH PIVOT AT 900 K, CONSTANT VOLUME, QUADRATIC TEMPERATURE DISTRIBUTION WITH CONSTANT HEAT RELEASE RATE AFTER COMBUSTION INITIATION AND WORK TRANSFER BETWEEN ZONES NOT INCLUDED	50
FIGURE 5-10	ZONE TEMPERATURES IN THE CONSTANT VOLUME, MULTI-ZONE SIMULATION FOR $T_0=800$ K: (A) $SF=10^{-6}$ (B) $SF=10^{-6}$..	51
FIGURE 5-11	MPPRR FOR SINGLE REACTION FUEL, EFFECT OF SLOPE WITH PIVOT AT 900 K, VARIABLE VOLUME, QUADRATIC TEMPERATURE DISTRIBUTION WITH CONSTANT HEAT RELEASE RATE AFTER COMBUSTION INITIATION: (A) WORK TRANSFER BETWEEN ZONES NOT INCLUDED (B) WORK TRANSFER INCLUDED	52
FIGURE 5-12	MPPRR AND MAXIMUM MOTORED TEMPERATURE FOR ISO-OCTANE AND N-HEPTANE: (A) UNIFORM TEMPERATURE DISTRIBUTION (B) QUADRATIC TEMPERATURE DISTRIBUTION	54
FIGURE 5-13	PRESSURE CURVES FOR ISO-OCTANE AND N-HEPTANE: (A),(B),(C) UNIFORM TEMPERATURE DISTRIBUTION, CR=12,16,20, RESPECTIVELY	55

FIGURE 5-41	MAXIMUM MOTORED TEMPERATURE FOR N-HEPTANE BASED FUEL, IMPACT OF A_{F1} : (A) VARIABLE VOLUME, UNIFORM TEMPERATURE DISTRIBUTION (B) VARIABLE VOLUME, QUADRATIC TEMPERATURE DISTRIBUTION.....	72
FIGURE 5-42	MPPRR FOR N-HEPTANE BASED FUEL, IMPACT OF A_{F2} : (A) VARIABLE VOLUME, UNIFORM TEMPERATURE DISTRIBUTION (B) VARIABLE VOLUME, QUADRATIC TEMPERATURE DISTRIBUTION	73
FIGURE 5-43	MAXIMUM MOTORED TEMPERATURE FOR N-HEPTANE BASED FUEL, IMPACT OF A_{F2} : (A) VARIABLE VOLUME, UNIFORM TEMPERATURE DISTRIBUTION (B) VARIABLE VOLUME, QUADRATIC TEMPERATURE DISTRIBUTION.....	73
FIGURE C-1	IGNITION CHARACTERISTICS	89
FIGURE C-2	FIRST STAGE IGNITION DELAY TIME USING BRANCHING AGENT CONCENTRATION	90
FIGURE E-1	INITIAL TEMPERATURE FOR SINGLE REACTION FUELS, EFFECT OF POSITION: (A) UNIFORM TEMPERATURE DISTRIBUTION (B) QUADRATIC TEMPERATURE DISTRIBUTION	93
FIGURE E-2	INITIAL TEMPERATURE FOR SINGLE REACTION FUELS, EFFECT OF SLOPE WITH PIVOT AT 900 K: (A) UNIFORM TEMPERATURE DISTRIBUTION (B) QUADRATIC TEMPERATURE DISTRIBUTION	93
FIGURE E-3	INITIAL TEMPERATURE FOR ISO-OCTANE AND N-HEPTANE SIMULATIONS: (A) UNIFORM TEMPERATURE DISTRIBUTION (B) QUADRATIC TEMPERATURE DISTRIBUTION	94
FIGURE E-4	INITIAL TEMPERATURE FOR ISO-OCTANE BASED FUEL, IMPACT OF T_A : (A) VARIABLE VOLUME, UNIFORM TEMPERATURE DISTRIBUTION (B) VARIABLE VOLUME, QUADRATIC TEMPERATURE DISTRIBUTION.....	94
FIGURE E-5	INITIAL TEMPERATURE FOR ISO-OCTANE BASED FUEL, IMPACT OF D_A : (A) VARIABLE VOLUME, UNIFORM TEMPERATURE DISTRIBUTION (B) VARIABLE VOLUME, QUADRATIC TEMPERATURE DISTRIBUTION.....	94
FIGURE E-6	INITIAL TEMPERATURE FOR ISO-OCTANE BASED FUEL, IMPACT OF N_1 : (A) VARIABLE VOLUME, UNIFORM TEMPERATURE DISTRIBUTION (B) VARIABLE VOLUME, QUADRATIC TEMPERATURE DISTRIBUTION.....	95
FIGURE E-7	INITIAL TEMPERATURE FOR ISO-OCTANE BASED FUEL, IMPACT OF N_2 : (A) VARIABLE VOLUME, UNIFORM TEMPERATURE DISTRIBUTION (B) VARIABLE VOLUME, QUADRATIC TEMPERATURE DISTRIBUTION.....	95
FIGURE E-8	INITIAL TEMPERATURE FOR ISO-OCTANE BASED FUEL, IMPACT OF Y_{NTC} : (A) VARIABLE VOLUME, UNIFORM TEMPERATURE DISTRIBUTION (B) VARIABLE VOLUME, QUADRATIC TEMPERATURE DISTRIBUTION.....	95
FIGURE E-9	INITIAL TEMPERATURE FOR ISO-OCTANE BASED FUEL, IMPACT OF A_{F1} : (A) VARIABLE VOLUME, UNIFORM TEMPERATURE DISTRIBUTION (B) VARIABLE VOLUME, QUADRATIC TEMPERATURE DISTRIBUTION.....	96
FIGURE E-10	INITIAL TEMPERATURE FOR ISO-OCTANE BASED FUEL, IMPACT OF A_{F2} : (A) VARIABLE VOLUME, UNIFORM TEMPERATURE DISTRIBUTION (B) VARIABLE VOLUME, QUADRATIC TEMPERATURE DISTRIBUTION.....	96
FIGURE E-11	INITIAL TEMPERATURE FOR N-HEPTANE BASED FUEL, IMPACT OF T_A : (A) VARIABLE VOLUME, UNIFORM TEMPERATURE DISTRIBUTION (B) VARIABLE VOLUME, QUADRATIC TEMPERATURE DISTRIBUTION.....	96
FIGURE E-12	INITIAL TEMPERATURE FOR N-HEPTANE BASED FUEL, IMPACT OF D_A : (A) VARIABLE VOLUME, UNIFORM TEMPERATURE DISTRIBUTION (B) VARIABLE VOLUME, QUADRATIC TEMPERATURE DISTRIBUTION.....	97
FIGURE E-13	INITIAL TEMPERATURE FOR N-HEPTANE BASED FUEL, IMPACT OF N_1 : (A) VARIABLE VOLUME, UNIFORM TEMPERATURE DISTRIBUTION (B) VARIABLE VOLUME, QUADRATIC TEMPERATURE DISTRIBUTION.....	97
FIGURE E-14	INITIAL TEMPERATURE FOR N-HEPTANE BASED FUEL, IMPACT OF N_2 : (A) VARIABLE VOLUME, UNIFORM TEMPERATURE DISTRIBUTION (B) VARIABLE VOLUME, QUADRATIC TEMPERATURE DISTRIBUTION.....	97
FIGURE E-15	INITIAL TEMPERATURE FOR N-HEPTANE BASED FUEL, IMPACT OF Y_{NTC} : (A) VARIABLE VOLUME, UNIFORM TEMPERATURE DISTRIBUTION (B) VARIABLE VOLUME, QUADRATIC TEMPERATURE DISTRIBUTION.....	98
FIGURE E-16	INITIAL TEMPERATURE FOR N-HEPTANE BASED FUEL, IMPACT OF A_{F1} : (A) VARIABLE VOLUME, UNIFORM TEMPERATURE DISTRIBUTION (B) VARIABLE VOLUME, QUADRATIC TEMPERATURE DISTRIBUTION.....	98
FIGURE E-17	INITIAL TEMPERATURE FOR N-HEPTANE BASED FUEL, IMPACT OF A_{F2} : (A) VARIABLE VOLUME, UNIFORM TEMPERATURE DISTRIBUTION (B) VARIABLE VOLUME, QUADRATIC TEMPERATURE DISTRIBUTION.....	98
FIGURE F-1	SUMMARY OF IMPACT OF IGNITION DELAY CURVE FEATURES ON MPPRR.....	99

List of Tables

TABLE 5-1	ENGINE OPERATING PARAMETERS	41
TABLE A-1	MODIFIED SHELL MODEL.....	81

Nomenclature

ACRONYMS

CAI	Controlled Auto-Ignition
CFD	Computational Fluid Dynamics
CR	Compression Ratio
EGR	Exhaust Gas Recirculation
LLNL	Lawrence Livermore National Laboratory
MPRR	Maximum Pressure Rise Rate
NTC	Negative Temperature Coefficient
NVH	Noise Vibration and Harshness
SCCI	Stratified Charge Compression Ignition
SF	Scale Factor
TDC	Top Dead Center

SYMBOLS

ϕ	Fuel-air equivalence ratio
\emptyset	Branching factor
τ	Ignition delay time
γ	Specific heat ratio
$[X]$	Molar concentration of species χ
A	Pre-exponential factors
B	Branching agent species in Shell Model
c_v	Constant volume specific heat
c_p	Constant pressure specific heat
D_A	Ignition delay time at the start of the NTC region
E	Activation Energy
f	Shell Model reaction rate coefficient
k	Shell Model reaction rate coefficient
m	Number of hydrogen pairs in fuel
M	Total charge molar concentration
MO	Initial total charger molar concentration
M_i	Total charge molar concentration in zone i
n	Number of carbon atoms in fuel
n_1	Low temperature region logarithmic slope
n_2	High temperature region logarithmic slope
N	Total number of moles
N_i	Total number of moles in zone i
N_x	Number of moles of species χ
p	Number of oxygen molecules consumed in each propagation cycle
P	Pressure
Q	Intermediate species in Shell Model
Q_1	Total exothermicity of one propagation cycle
Q_2	Heating value of CO to CO ₂ reaction

R	Radical species in Shell Model
\bar{R}	Equilibrium radical species concentration
RH	Fuel species in Shell Model
R_u	Universal gas constant
t	Time
T	Temperature
T_0	Initial temperature
T_A	Temperature at the start of the NTC region
T_i	Temperature in zone i
V	Total charge volume
V_i	Charge volume in zone i
v_q	Rate of radical generation due to primary initiation
x_j	Oxygen concentration constant in shell model
x_{NTC}	Difference in the initial temperature at the beginning and end of the NTC region
y_j	Fuel concentration constant in shell model
y_{NTC}	Difference in the ignition delay times at the beginning and end of the NTC region

Chapter 1. Introduction

1.1 Motivation and Background

The development of Controlled Auto-Ignition (CAI) engines can contribute to reducing the automotive industry's reliance on oil, while also reducing harmful emissions. It has been demonstrated that CAI engines can have low emissions of oxides of nitrogen (NO_x) and particulate matter (PM) while establishing a high part load thermal efficiency [1].

The main features of CAI engine operation, when compared to spark ignition and diesel (diffusion-controlled) engines is presented in Figure 1-1. The main distinguishing feature is that CAI engines do not rely on a spark plug or fuel injection to initiate combustion. The premixed charge is simply compressed until auto-ignition. This allows for a higher compression ratio, the elimination of a throttle, and shorter combustion durations [2]. All three of these features contribute to the higher thermal efficiency obtained with CAI engines. Since the fuel and air are typically premixed and diluted, NO_x and PM emissions are also reduced.

Spark Ignition Engines	CAI Engines	Diesel Engines
Premixed fuel/air charge		Fuel injected late in compression stroke
Combustion initiated with spark plug	Auto-ignition due to compression	Combustion initiated with fuel injection
Turbulent premixed flame propagation	No flame - kinetically controlled	Turbulent diffusion flame
Low compression ratio		High compression ratio
Load limited by throttling	Load limited by amount of fuel injected	

Figure 1-1 Comparison of the main features of spark ignition, CAI, and diesel engines

Since CAI engines depend on auto-ignition to initiate the combustion process, fuel chemical kinetics plays an important role in the engine's operation and control. The fuel chemical kinetics can be described with detailed reaction mechanisms, which outline the reaction pathways a fuel molecule can take during oxidation. Typical reaction mechanisms are described by low and high temperature reaction pathways. There is a transition temperature range in which the low temperature path is switched off, but the high temperature regime has yet to commence. Therefore, combustion initiating at low temperatures can exhibit a two-stage heat release process as the fuel molecules pass through both the low and high temperature pathways. Both ignition pathways are controlled by a degenerative chain branching process. In the low temperature pathway, alkyl-peroxy radicals, RO_2 , undergo an isomerization process above 800 K [3], leading to the formation of a branching agent and subsequently two additional radicals. In the high temperature reaction pathway (900 K to 1100 K), chain branching is introduced through hydrogen peroxide decomposition [3].

An example constant volume batch reactor simulation with n-heptane is shown in Figure 1-2. It can be seen that there is a first stage ignition at approximately 1 ms, followed by the main ignition at 2 ms. When the main ignition time versus initial temperature is plotted, the fuel ignition delay curve is created. The ignition delay time typically decreases as temperature increases, except in the Negative Temperature Coefficient (NTC) region. In this region, the low temperature pathway is less reactive since additional non-branching propagation channels begin to dominate leading to the formation of cyclic ethers, conjugate olefins, and β -decomposition products [4]. The temperature is also not high enough for the high temperature branching pathways to initiate.

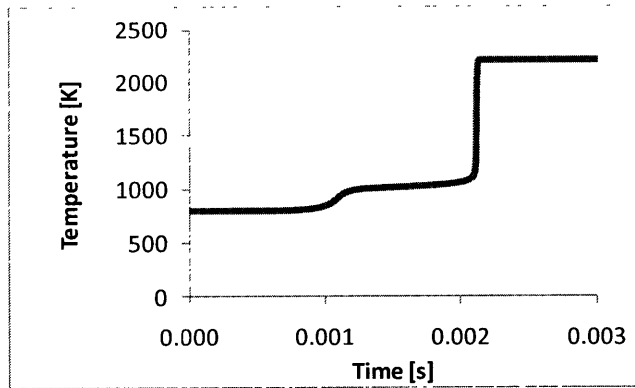


Figure 1-2 Example constant volume batch reactor simulation: n-heptane, $T_0=800$ K.

The dependence of CAI combustion on fuel kinetics is illustrated in Figure 1-3. The low temperature reaction pathway in branched-chain paraffins such as iso-octane is much less reactive than in straight-chain paraffins such as n-heptane [3]. Therefore, for iso-octane, significant heat release occurs at a higher temperature and the process manifests as a single-stage ignition only; see Figure 1-3 (a). This single stage heat release results in a significantly rapid rate of pressure rise. Note that the combustion durations in both the single and two-stage processes are still much shorter than what is seen in spark ignition and diffusion controlled engines.

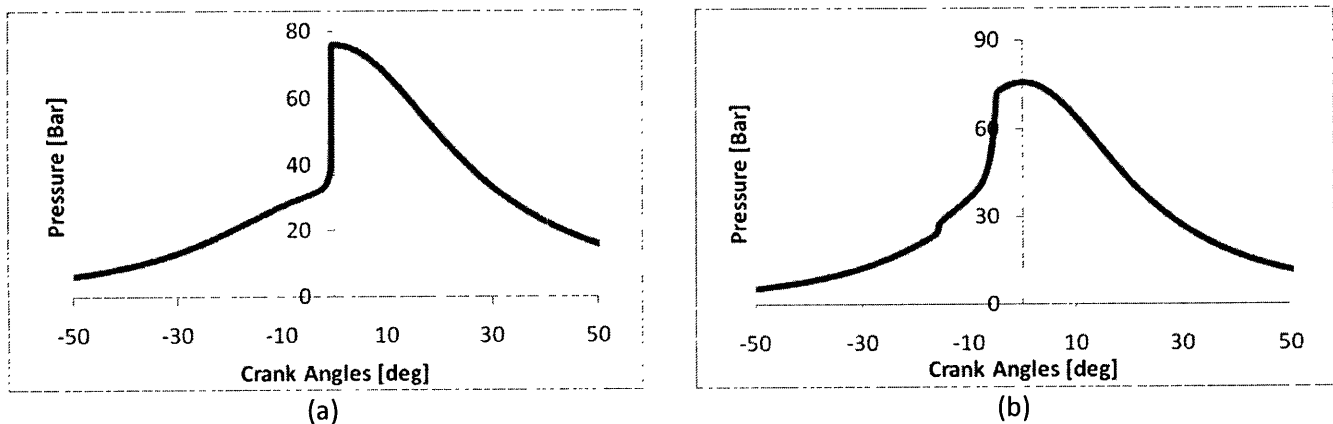


Figure 1-3 Example CAI engine simulation pressure curves: (a) iso-octane (b) n-heptane

Though there is a lot of promise in CAI engines, one hurdle that is currently being faced is the engine's inability to operate at high loads due to the presence of knock [5]. The presence of knock is dictated by the formation of pressure waves during combustion. A pressure wave forms when the

acoustic expansion cannot accommodate the thermal expansion [5]. A measure of the threshold for knock is given by the ringing index [5]:

$$\text{Ringing Index} = \frac{\sqrt{\gamma R_u T_{max}}}{2\gamma P_{max}} \left[\beta \left(\frac{dP}{dt} \right)_{max} \right]^2 \quad [1.1]$$

Equation [1.1] shows that the knock threshold is dependent on the Maximum Pressure Rise Rate (MPRR). Knock is an issue for CAI engines due to the rapid heat release and relatively short combustion duration, which lead to a large rate of pressure rise. One method that can be used to increase the combustion duration is to create a non-homogeneous charge, by a species concentration and/or a temperature distribution [2]. This is referred to as Stratified Charge Compression Ignition (SCCI), and will be studied in this report. Another method used to increase the high load limit is to increase the inlet pressure. Christensen [6] studied this effect using boost pressures of 0 bars to 2 bars, and iso-octane, ethanol, and natural gas as fuels.

This report will present an analytical assessment on the potential of selecting and optimizing a fuel to extend the high load limit of CAI engines. It has been shown that the high load limit, which is constrained by the engine Noise Vibration and Harshness (NVH), can be extended by reducing the MPRR during combustion. The MPRR in a CAI engine is governed by the engine operating conditions, temperature/charge stratification in the combustion chamber, and the fuel combustion chemistry (see Figure 1-4). The selected fuel can have a direct impact on the MPRR through its combustion chemistry, or an indirect impact through its sensitivity to the engine operating conditions and stratification.

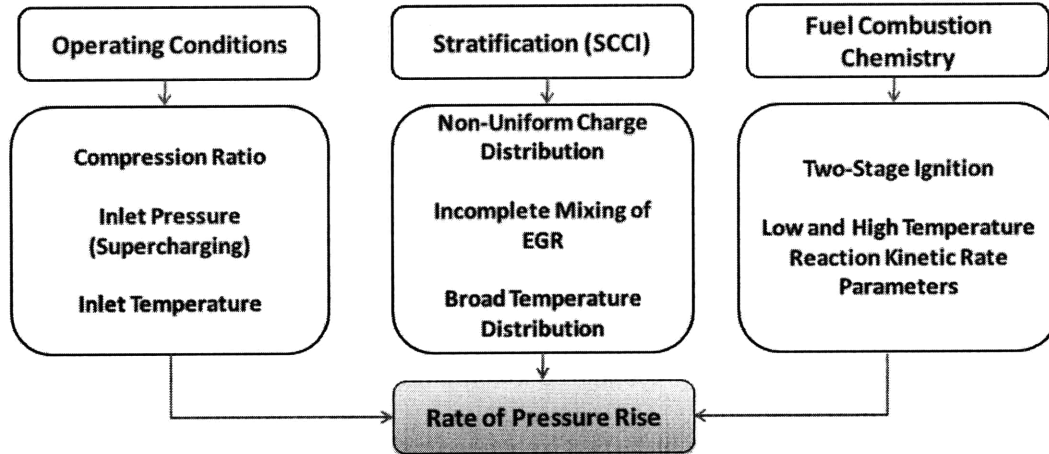


Figure 1-4 Fuel effect on rate of pressure rise

1.2 Literature Review

A fuel chemistry model and engine simulation model are required to analytically assess the impact of fuel of the MPRR in CAI engines. It is therefore worthwhile to examine the past literature to help select the appropriate models for the purpose of this research.

1.2.1 Fuel Chemistry Models

Fuels are typically described by a detailed reaction mechanism outlining all of the possible reaction pathways the fuel molecule can pass through during oxidation. Reaction mechanisms for fuels such as iso-octane [7], n-heptane [8], ethanol [9], and toluene [10] have been published. These mechanisms typically consist of thousands of species and would therefore be too computationally demanding to be used in a fuel optimization study. Also, the fuel would have to be described only by fractions of the known fuels, rather than actual fuel characteristics (such as the ignition delay curve).

There have been attempts to reduce the size of the detailed reaction mechanisms to include only the predominant reactions. For example, Tanaka [11] produced a combined iso-octane and n-heptane

reaction mechanism with only 32 species. However, this would still be computationally expensive for optimization studies.

A detailed summary of the different reduced kinetic models that have been developed to decrease the computational cost of simulating combustion systems has been prepared by Griffiths [12]. One model that is described in [12] is referred to as the Shell Model [13, 14], which is considered to be a generalized mechanism. This model represents the minimum number of reactions that are required to describe the two-stage degenerately branched reaction mechanism seen in most fuels. This is accomplished by grouping the species into three groups - radicals, branching agents, and intermediate species – along with the fuel and oxygen molecules. The parameters (26 in total) for each of the reactions can be set based on a desired ignition delay curve.

1.2.2 CAI Engine Simulation Models

A number of models ranging in complexity have been developed to simulate the thermodynamics of CAI engine operation. Wang [15] provides a good summary of the different modeling techniques that can be used, along with their advantages, disadvantages, and approximate computational cost.

The most computationally intensive models involve Computational Fluid Dynamics (CFD) coupled with a detailed chemistry model [16, 17]. Wang [16] incorporated a spray and turbulence dispersion model into a 3D CFD simulation coupled with a detailed chemical mechanism. He found that a stratified charge, which improves the high load limit, can be obtained using a second fuel injection. Kong [17] coupled CHEMKIN detailed chemistry into KIVA-3V to simulate CAI combustion. Fuel spray dynamics and flow turbulence were also included.

To reduce the computational cost, CFD can be coupled with a simplified combustion model, as opposed to using detailed chemistry. This approach was adopted by Li [18]. The Ricardo Two-Zone Flamelet (RTZF) combustion model was developed in [18] as a substitute to using detailed chemistry. The approach involves combining a one equation ignition delay probability integral with a flamelet

combustion model using a two-zone gas representation. The gas is divided into burned and unburned zones, while the unburned zone is further subdivided into mixed and segregated regions. Through fluid motion and diffusion, the fuel and air are transformed from the segregated zone to the mixed zone, then finally to the burned zone. One interesting feature of this model is its ability to model turbulence controlled combustion as opposed to only chemical kinetics controlled combustion. It was found that turbulence controlled combustion becomes more important during the later stages of combustion [18].

The next level of simplification involves using CFD and detailed chemistry sequentially. This approach was used by Aceves [19, 20]. The first stage of the simulation involves using the CFD code KIVA, without any chemical reactions, to obtain the temperature distributions in the cylinder up to 20 degrees after TDC. Then, the cylinder is divided into ten zones by grouping different temperature ranges. The zones are created such that the hottest zones contain the most mass. The temperature history of each zone is then inserted as a boundary condition into CHEMKIN to solve the detailed chemical kinetics. The CHEMKIN simulation follows the KIVA temperature history for each zone until 5% of the total heat release occurs. Work transfer is incorporated between the zones, but no heat transfer or mass transfer is added.

The above models have demonstrated good accuracy when compared to experimental results; however they would be difficult to use when conducting a detailed fuel optimization study. A number of models have been developed that do not incorporate CFD, and would therefore be less computationally intensive. One model that is frequently used is a multi-zone detailed chemistry model [21]. To allow for stratification, the cylinder is divided into multiple zones. The zones can interact through work, heat, and mass transfer, depending on how each individual zone is defined. Detailed chemistry is then solved in each zone, and is coupled with the thermodynamic model describing the zone interactions.

The simplest CAI engine simulation models involve single zone combustion with detailed chemistry [15]. These models have been used to predict the start of ignition. However, since charge stratification cannot be incorporated, these models have limited use when predicting the MPRR.

1.3 Research Approach and Objectives

Previously published literature has established a number of different techniques of modeling the fuel chemistry and CAI engine simulations. This report will combine both the fuel and engine modeling to develop general guidelines for the optimum fuel characteristics that are desired to extend the high load limit of CAI engines.

A method of defining and distinguishing the fuel characteristics is needed so that the optimum fuel can be described. An attribute that would quantify the impact of the selected fuel on the effects shown in Figure 1-4 is the fuel's ignition delay curve, $\tau(T,M)$ under constant volume conditions, as a function of the initial temperature (T) and molar concentration (M). In the analytical assessment presented in this report, the different fuels are distinguished only through the shape of their ignition delay curve, $\tau(T,M)$. Therefore, a parametric model of the fuel chemistry is needed so that different functional dependences of $\tau(T,M)$ may be produced by adjustment of the model parameters. Then, various artificial fuel ignition characteristics can be created and tested in an engine simulation under different operating conditions and stratification strategies.

The specific objectives of this analytical assessment are:

1. To develop a parametric model of the fuel chemistry that is capable of describing different functional dependencies of $\tau(T,M)$.
2. To adjust the fuel chemistry model parameters to create a number of artificial test fuels with pre-defined ignition delay curves.

3. Insert the artificial fuels into an engine simulation to determine the ideal shape of the ignition delay curve to reduce the MPRR.

1.4 Report Outline

The following chapter of this report will provide an outline of the fuel and engine models that have been developed for the purpose of this analytical assessment. The artificial fuels created with the parameterized fuel chemistry model will then be presented in Chapter 3 and Chapter 4. The MPRR obtained from the engine simulations corresponding to the different artificial fuels will then be examined in Chapter 5 to determine the optimum fuel ignition delay curve. Chapter 6 will then provide a summary of the main conclusions.

Chapter 2. Models used to study ignition delay characteristics

2.1 Fuel Chemistry Model: Modified Shell Model

2.1.1 Description of Modified Shell Model

A parameterized pseudo-chemical model is used to produce different shapes of the fuel ignition delay versus temperature curve. The model must encompass the low and high temperature reactions in real fuels, along with the NTC region that connects these reaction regimes. It is also important that the total number of parameters in the model is minimized so that these parameters can be more readily selected to match the pre-defined ignition delay curve. Finally, the reaction pathway that leads to ignition should be similar to the real fuel reaction scheme, which is a degenerately branched chain mechanism.

To meet the above requirements, the Shell Model [13] described in Appendix A was chosen. In order to simulate the amount of heat release for the individual reaction steps, the following modification was used. The existing Shell Model assumes a ratio of CO/CO₂ in the final combustion products, and determines the heat of reaction based on this assumption. The heat release in the intermediate generic reactions is not modeled. If the fuel burns to completion, there cannot be any CO in the combustion products. However, if the ratio above is simply set to zero, there would be too much heat release during the low temperature reactions, where little CO₂ is expected in the products. Therefore, to resolve this problem, the following scheme is used. The shell model assumes that the rate of fuel consumption is $1/m$ the chain propagation rate (where $2m$ is the number of hydrogen atoms in the fuel). The carbon of this consumed fuel is assumed to be converted first to CO. Then an additional CO to CO₂ reaction is added to the mechanism, with fixed kinetic rate parameters based on existing validated chemical models.

2.1.2 Choice of parameters and fit to the prescribed $\tau(T,M)$

As described in [13], the Shell Model has 26 parameters that can be adjusted to match a pre-determined ignition delay curve. However, not all of the parameters need to be adjusted, as the effects can be replicated with other parameters. Using the terminology in [13] and in Appendix A, A_{P1} , A_{P2} , and A_{P3} were left constant, while E_{P1} , E_{P2} and E_{P3} were adjusted based on the temperature at which the desired NTC region ends, and E_t was left as zero. This leaves seven pre-exponential factors and six activation energies that need to be determined. The remaining six parameters (x_1 , x_3 , x_4 , y_1 , y_3 , y_4) are used to match the desired dependence of fuel, oxygen, and total concentration on ignition delay. Any change in the x_j and y_j parameters is matched with a corresponding change in the appropriate pre-exponential factor, such that the temperature dependence of ignition delay is not affected.

The parameter fitting model created is capable of matching a prescribed data set of ignition delay time (both first and second stage) versus temperature and concentration in four steps. The first three steps match the ignition delay time versus temperature at a given fuel and oxygen concentration. The last step then adjusts the x_j and y_j parameters to match the desired fuel and oxygen concentration dependence. The key model equations are presented in Appendix B. The method the program uses to define the first and second stage ignition delay times is presented in Appendix C.

The first step of the program involves modifying only the seven pre-exponential factors from their default values to move closer to the desired ignition delay time versus temperature curve (at a given concentration). The six activation energies at this stage are scaled from the default values based on the temperature at which the desired NTC region ends. The pre-exponential factors are selected based on a set of seven algebraic equations that were developed to approximate the first stage and second stage ignition delay times (4 equations), the NTC temperature (1 equation), and equilibrium radical concentration scale factors (2 equations). After solving the set of seven equations to determine the pre-

exponential factors, the ignition delay curve resembles the prescribed data set at the low and high temperatures, but not in the NTC region.

The second step of the fitting program involves modifying the six activation energies to better match the prescribed dataset. The pre-exponential factors are calculated by the set of algebraic equations described above every time the activation energies are changed. The optimal activation energies are determined using the Steepest Descent Method.

The third step of the program proceeds through individual incremental changes in the seven pre-exponential factors and six activation energies. This provides a better match of the target ignition delay time versus temperature curve.

The final stage of the fitting program adjusts the x_j and y_j parameters to provide the appropriate ignition delay time versus concentration dependence. This step uses the data points of the prescribed $\tau(T,M)$ at a constant temperature, and different fuel, oxygen, and total concentrations.

2.2 CAI Engine Simulation Model: Multi-Zone Engine Model

After the fuel ignition properties are determined, the last piece required is the engine simulation thermodynamic model. Since one of the goals of this analytical study is to determine the impact of fuel on the effect that temperature/charge stratification has on the MPRR, a multi-zone model is required. For this preliminary analytical assessment, only the work transfer between the combustion zones is considered; there is no heat or mass transfer. This model is described in [21]. The zones are divided such that each zone initially occupies the same volume. The engine model equations associated with the Shell Model are presented in Appendix D.

Chapter 3. Model Representation for Iso-Octane and n-Heptane

3.1 Iso-Octane Representation

To develop a baseline fuel model, the parameter fitting procedure was used to find the appropriate Shell Model parameters that would match the $\tau(T,M)$ produced by the LLNL mechanism for iso-octane. These fuel parameters can then be altered to develop a range of “iso-octane based artificial fuels”.

Following the four-step process outlined in section 2.1.2, the resulting Shell Model representation of the LLNL iso-octane mechanism is shown in Figure 3-1 and Figure 3-2.

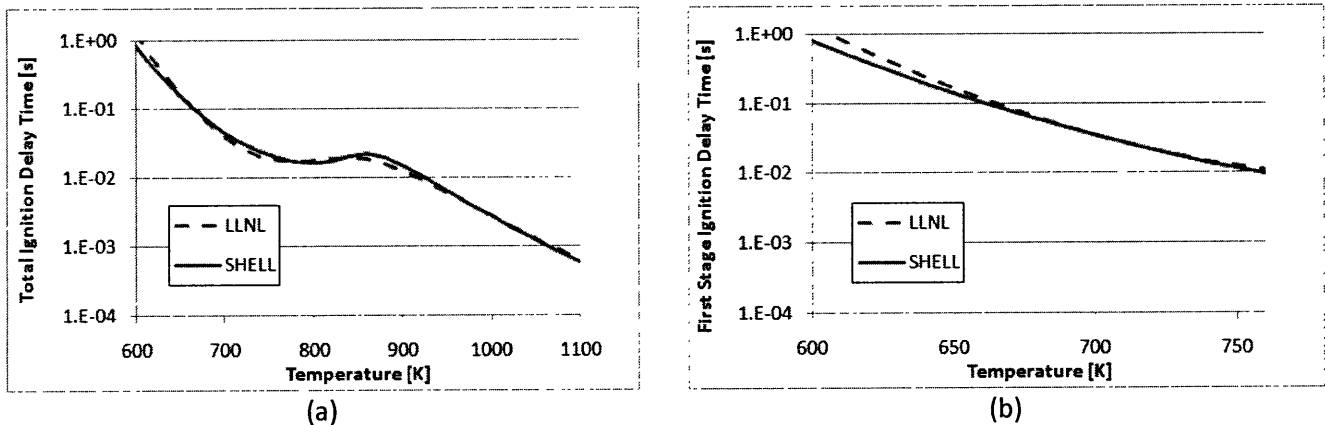


Figure 3-1 Iso-octane representation of (a) total and (b) first-stage ignition delay versus temperature [$M_0 = 3.2E-4$ mol/cm³, $\phi = 0.5$]

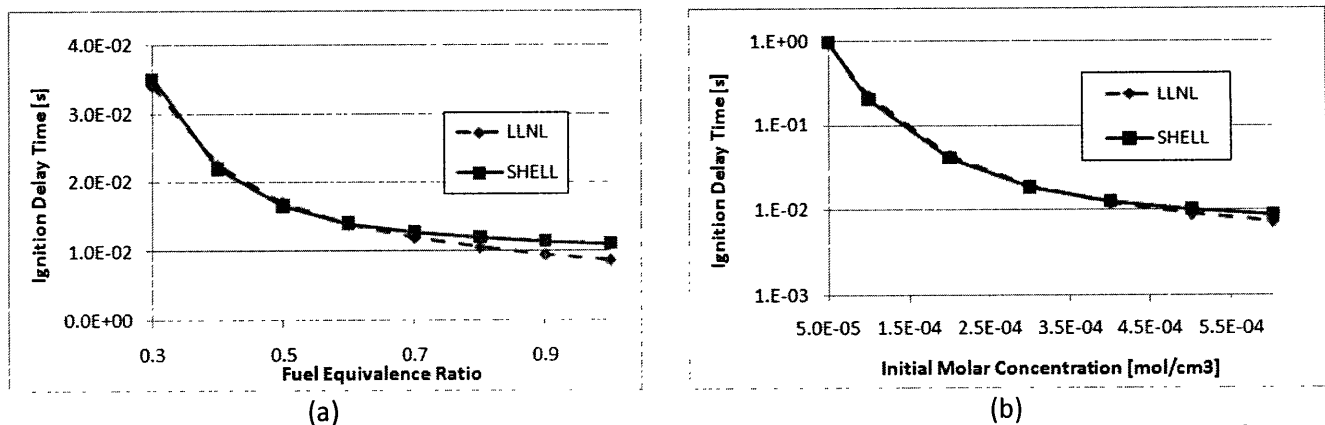


Figure 3-2 Iso-octane representation concentration effects: (a) fuel concentration [$T_0 = 780$ K, $M_0 = 3.2E-4$ mol/cm³] (b) total concentration [$T_0 = 780$ K, $\phi = 0.5$]

The Shell Model representation of the LLNL iso-octane model was then placed in a single zone engine combustion model, and compared to the output from the LLNL mechanism. This comparison was completed to ensure that the appropriate data set range was used in determining the Shell Model parameters. This comparison is given for two different engine operating conditions, and is shown in Figure 3-3.

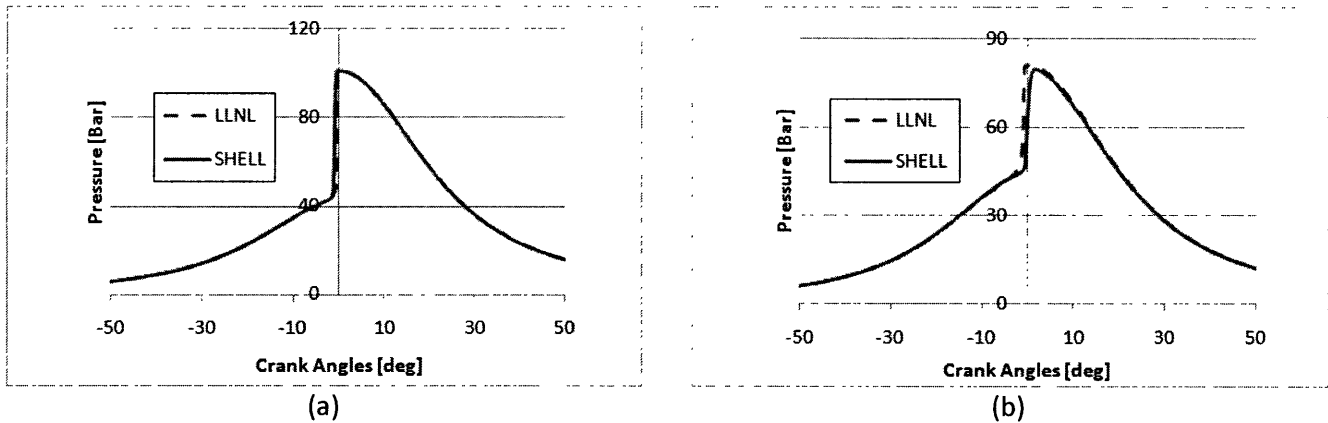
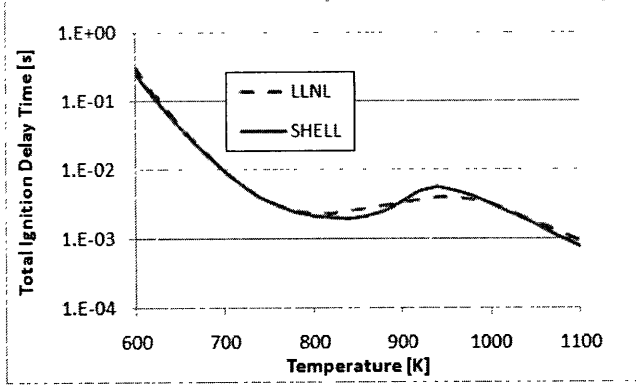


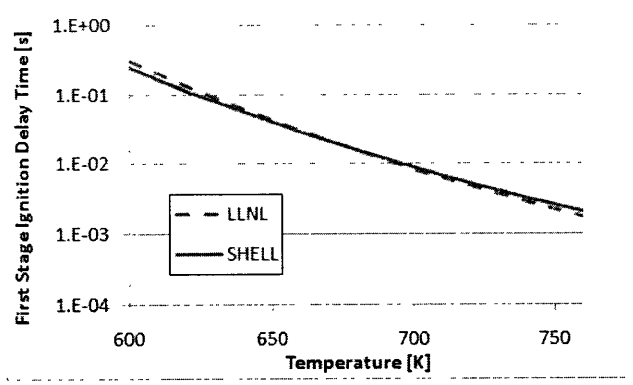
Figure 3-3 Shell Model iso-octane representation in single zone engine combustion model: (a) $T_0 = 420 \text{ K}$, $M_0 = 3.4E-5 \text{ mol/cm}^3$, $\phi = 0.5$, $CR = 16$ (b) $T_0 = 420 \text{ K}$, $M_0 = 3.4E-5 \text{ mol/cm}^3$, $\phi = 0.3$, $CR = 16$

3.2 n-Heptane Representation

The Shell Model parameters that would match the $\tau(T,M)$ relationship produced by the LLNL mechanism for n-heptane were also obtained. Unlike iso-octane, n-heptane produces low first stage ignition delay times, which results in a noticeable two stage ignition profile during engine combustion. This may lead to additional conclusions regarding the impact of fuel on the high load limit, because a fraction of the energy can potentially be released outside of the main ignition. Therefore, it was decided to include n-heptane as a second baseline fuel. The comparison between the Shell Model representation of n-heptane and the LLNL mechanism is given in Figure 3-4 to Figure 3-6.

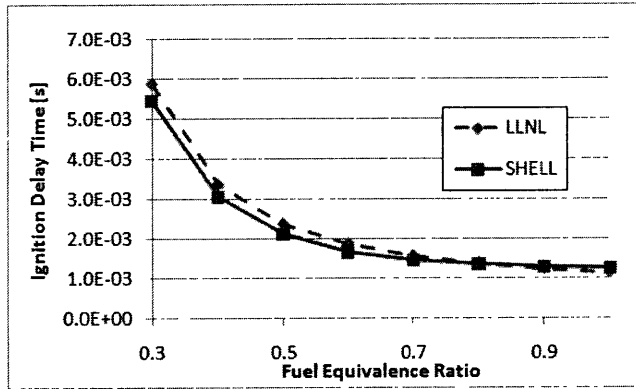


(a)

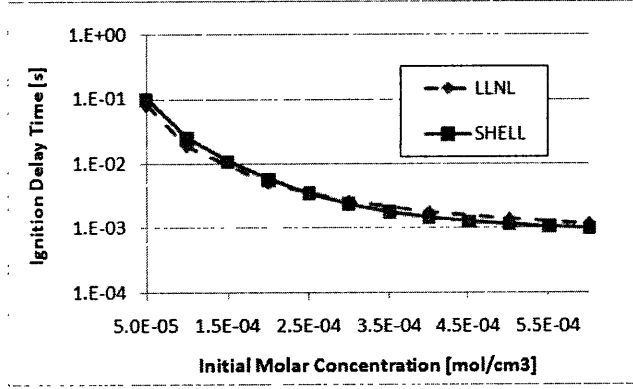


(b)

Figure 3-4 n-Heptane representation of (a) total and (b) first-stage ignition delay versus temperature [$M_0 = 3.2E-4$ mol/cm³, $\phi = 0.5$]

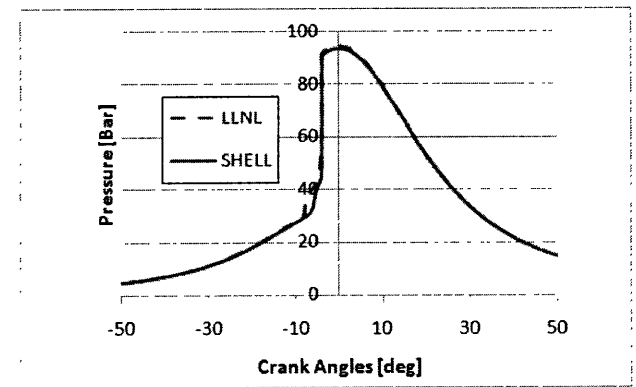


(a)

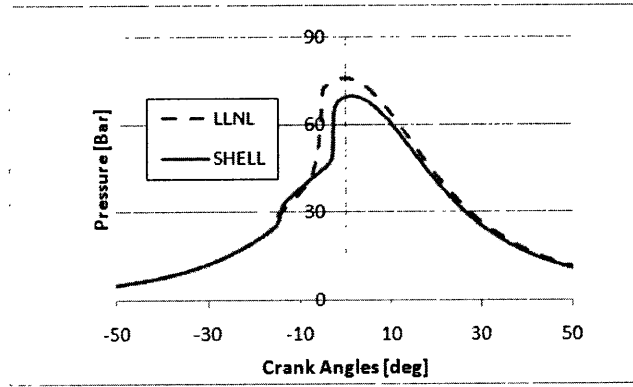


(b)

Figure 3-5 n-Heptane representation concentration effects: (a) fuel concentration [$T_0 = 800$ K, $M_0 = 3.2E-4$ mol/cm³] (b) total concentration [$T_0 = 800$ K, $\phi = 0.5$]



(a)



(b)

Figure 3-6 Shell Model n-heptane representation in single zone engine combustion model: (a) $T_0 = 320$ K, $M_0 = 3.4E-5$ mol/cm³, $\phi = 0.5$, CR = 16 (b) $T_0 = 345$ K, $M_0 = 3.4E-5$ mol/cm³, $\phi = 0.3$, CR = 16

Chapter 4. Representation of Artificial Fuels

4.1 Description of Artificial Fuels

As stated previously, the fuels in this analytical assessment are represented by the constant volume ignition delay curve $\tau(T,M)$. As shown in Figure 4-1, the ignition delay curve can be created by defining the following six main parameters: the temperature (T_A) and ignition delay time (D_A) of point 'A', the logarithmic slopes n_1 and n_2 in the low and high temperature regimes, and the size of the NTC region defined by x_{NTC} and y_{NTC} . Note that the impact of concentration on the ignition delay time is not included in this study, and will remain constant by leaving the Shell Model parameters x_j and y_j unchanged from the baseline fuel. Also note that the ratio of first stage to total ignition delay can impact the rate of pressure rise, but the effect will not be studied.

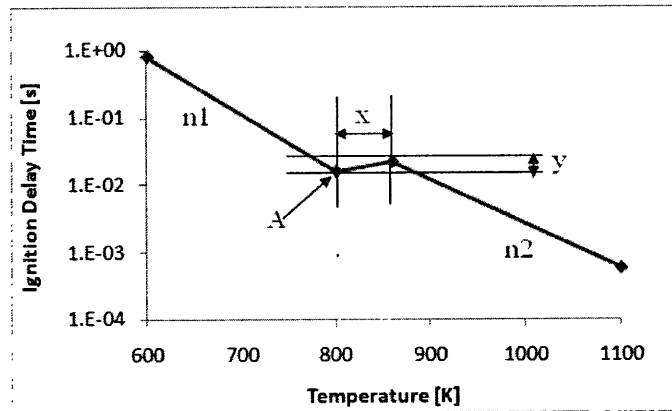


Figure 4-1 Ignition delay curve parameterization

4.2 Single Reaction Fuels

It is instructive to analyze a fuel whose ignition behavior is described by a simple Arrhenius reaction to obtain some general ideas on the impact of fuel on the MPRR. This was accomplished by setting all of the pre-exponential factors in the Shell Model to zero, except for the initiation reaction. The pre-exponential factor and activation energy for the initiation reaction in the baseline case were selected to

match the high temperature region in the iso-octane model. Then the pre-exponential factor was modified to change the magnitude of the ignition delay time while leaving the temperature dependence unchanged (Figure 4-2 (a)): the baseline pre-exponential factor (A) was multiplied by a scale factor (SF), as shown in equation [4.1]. Scale factors of 0.1 and 10 are shown in the Figure.

$$A_{NEW} = (SF) \times (A_{BASE}) \quad [4.1]$$

To change the slope of the ignition delay curve (Figure 4-2 (b)), the curve was pivoted around a selected temperature (T_{PIVOT}) by changing both the pre-exponential scale factor (A) and activation energy (E). The Arrhenius parameters were determined with equations [4.1] and [4.2] for a given scale factor (SF).

$$E_{NEW} = E_{BASE} + (R_u) \times (T_{PIVOT}) \times [\log(SF)] \quad [4.2]$$

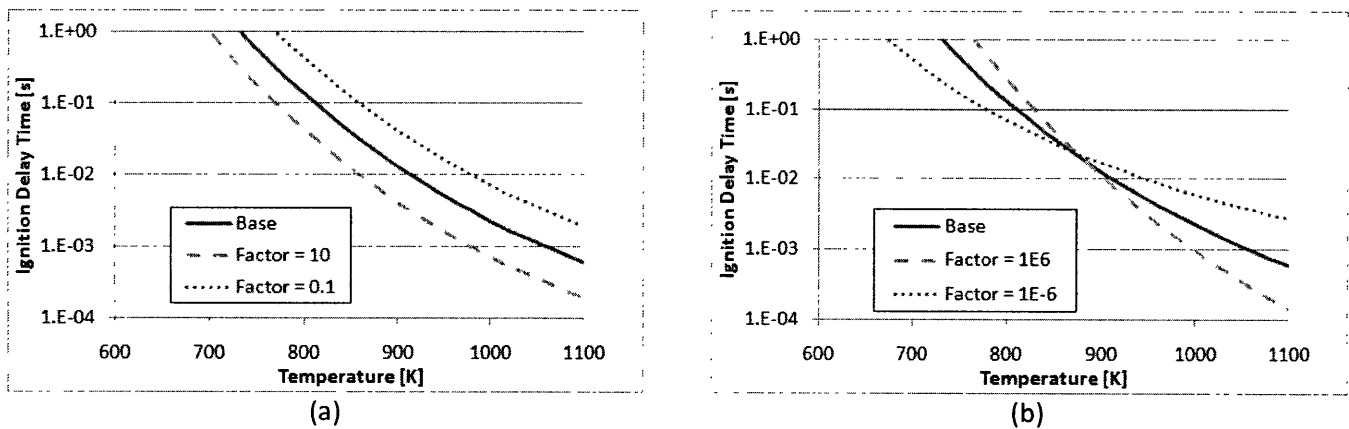


Figure 4-2 Ignition delay curves for single reaction (initiation reaction) fuels: (a) scale pre-exponential factor (b) change slope, and pivot around 900 K

4.3 Iso-Octane-Based Fuels

A number of artificial fuels based on modifications to the iso-octane ignition behavior were created to study the effects of the ignition delay parameters outlined in Figure 4-1. In most of the cases, the parameters for the artificial fuels were obtained from the parameter fitting program (outlined in section 2.1.2). The notable exception to this is the change in n_1 , which can be accomplished by scaling the degenerate branching pre-exponential factor (A_B). The artificial fuels are presented in Figure 4-3.

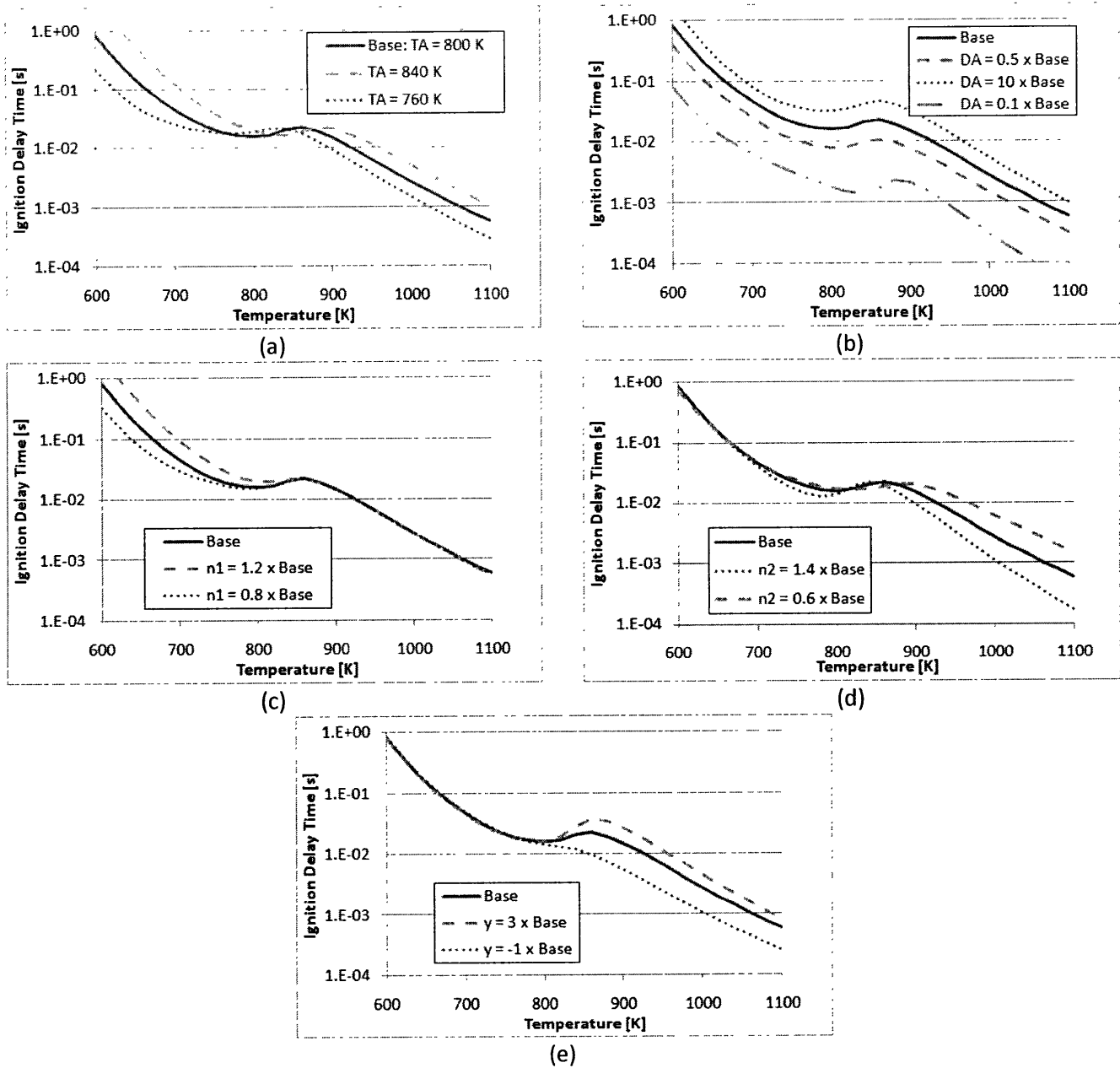


Figure 4-3 Iso-octane based artificial fuels: (a) T_A variation (b) D_A variation (c) n_1 variation (d) n_2 variation (e) γ_{NTC} variation

It should be noted that the x_{NTC} parameter variation (see Figure 4-1) is not included in this study because of difficulties in achieving the desired modifications with the existing chemistry model. It is expected that the effects will be similar to the case when the γ_{NTC} parameter is varied.

In addition to changing the local ignition delay parameters outlined in Figure 4-1 to create the artificial fuels described above, it is instructive to look at the effect of changing two important global

parameters: the low and high temperature pre-exponential factors for branching agent formation, A_{f1} and A_{f2} . The ignition delay curves representing these changes are presented in Figure 4-4.

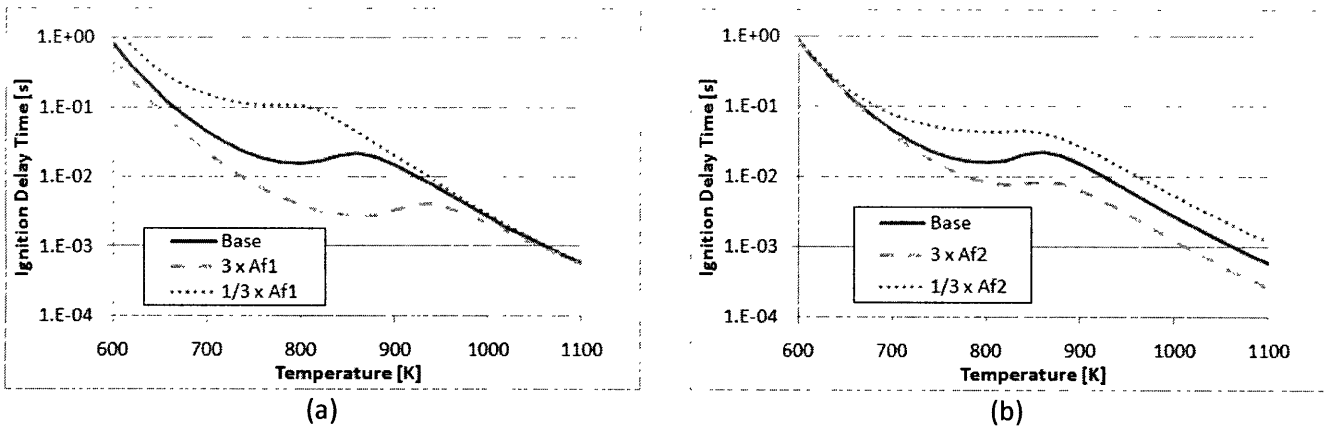
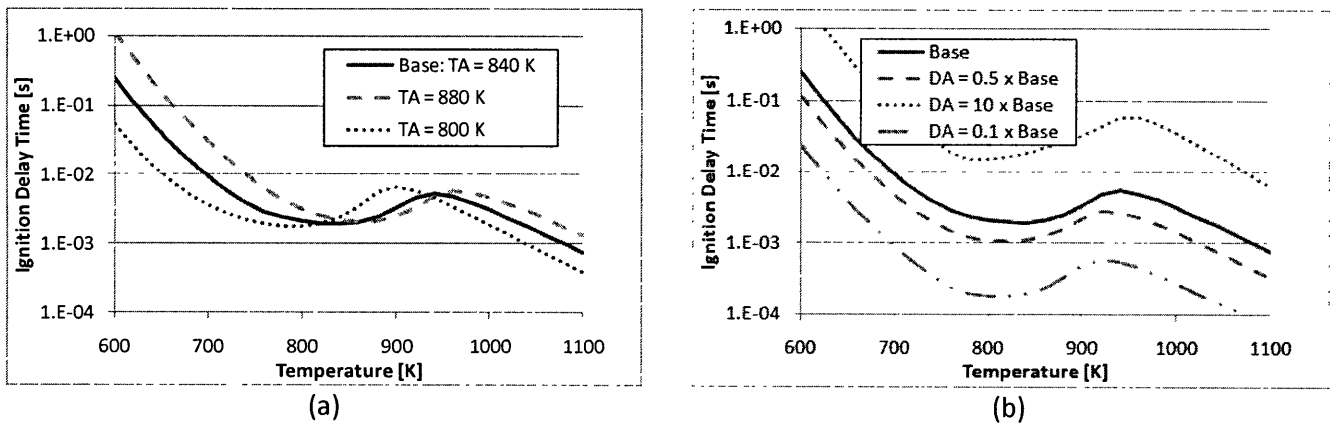
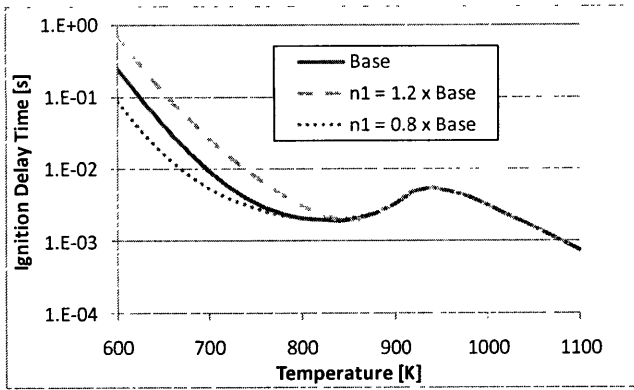


Figure 4-4 Iso-octane based artificial fuels with variation in global parameters: (a) A_{f1} (b) A_{f2}

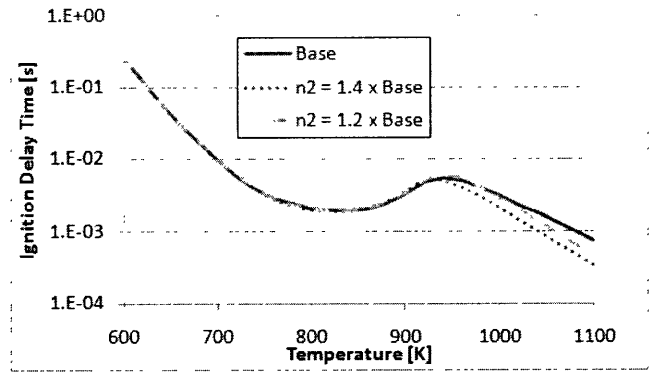
4.4 n-Heptane-Based Fuels

The same parametric variations outlined above were completed for the n-heptane model. The results are shown in Figure 4-5 and Figure 4-6.

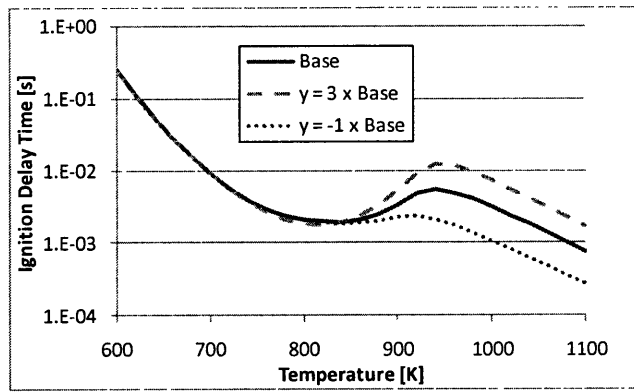




(c)

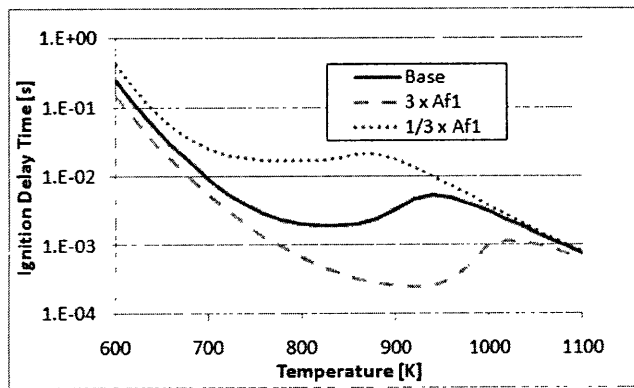


(d)

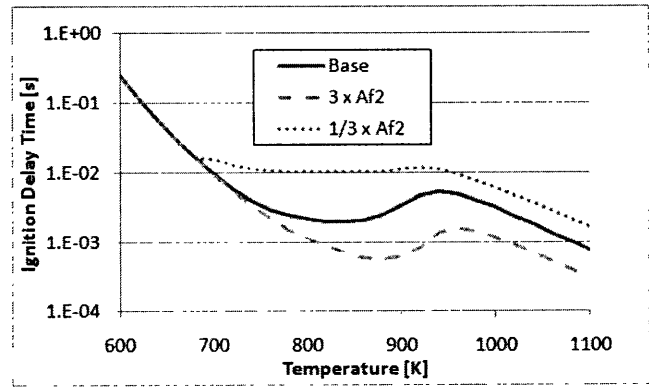


(e)

Figure 4-5 n-Heptane based artificial fuels: (a) T_A variation (b) D_A variation (c) n_1 variation (d) n_2 variation (e) γ_{NTC} variation



(a)



(b)

Figure 4-6 n-Heptane based artificial fuels with variation in global parameters: (a) A_{f1} (b) A_{f2}

Chapter 5. Fuel effects on High Load Limit

5.1 Analysis Procedure

The artificial fuels described in the previous section can now be inserted into an engine simulation to evaluate their impact on the MPRR. As illustrated in Figure 1-4, the fuel can have a direct impact through the chemistry of the heat release process or an indirect impact through its sensitivity to the temperature/charge stratification. Both the direct and indirect impacts of the fuel must be considered in the analysis.

To determine how the fuel affects the impact of the engine operating conditions on the MPRR, an engine with a compression ratio of 12, 16, and 20 was used. The initial charge temperature was modified for each test to ensure that the 50% heat release point occurred at Top Dead Center (TDC). The fuel equivalence ratio and initial total concentration were fixed to 0.5 and 3.4×10^{-5} mol/cm³, respectively. It should be noted that since the concentration parameters (x_j and y_j) in the Shell Model were not modified from the baseline case, it is expected that the different artificial fuels will not significantly impact the dependence of the MPRR on the engine operating condition. The engine size and operating parameters used for the simulations are given in Table 5-1.

Table 5-1 Engine operating parameters

Bore [cm]	8
Stroke [cm]	9
Connecting Rod [cm]	17
Engine Speed [rpm]	1000
Intake Valve Close [degrees]	138 before TDC
Exhaust Valve Open [degrees]	126 after TDC
Compression Ratio	12,16,20
Inlet Temperature	Adjusted for combustion at TDC

To analyze how the fuel affects the impact of temperature stratification on the MPRR, the study has been completed using a uniform temperature distribution and an artificial parabolic temperature distribution. The difference in the maximum and minimum temperature in the artificial distribution is 50 degrees. It should be noted that the effects of equivalence ratio stratification has not been studied in this assessment.

For some select cases, the MPRR was also obtained for a constant volume batch reactor. The fuel equivalence ratio and initial total concentration in the constant volume analyses were fixed to 0.5 and 3.2×10^{-4} mol/cm³, respectively. Additional analyses have also been added in some cases to explain the results. These analyses will be described when they are used. Finally the simulations using a temperature distribution were run predominantly with ten zones. Due to the difficulties in determining the MPRR (as outlined in the next section), the use of more zones will lead to more accurate solutions. An initial validation study has concluded that, for most cases, the use of ten zones leads to an error of about 20% in the MPRR, when compared to simulations with many more zones (up to 50 were tested).

5.2 Determination of the Maximum Pressure Rise Rate

When a uniform temperature, one zone combustion model is used, determining the MPRR is a straightforward task. However, when multiple zones are used, it becomes somewhat difficult to estimate the MPRR. An average pressure rise rate over a pre-defined portion of the combustion event can be easily determined, but this output would depend too heavily on the portion of the combustion event that is selected. Also, the maximum, not average, pressure rise rate is what dictates the high load limit of CAI engines.

The difficulty in determining the MPRR can be seen by examining Figure 5-1, which provides pressure versus crank angle curves for two different fuels. The squares represent the 50% heat release point for each of the ten zones, where each step represents one zone undergoing combustion. At this

point, it is easy to see that using more zones will increase the number of steps, and reduce the interpolation required. From curve (a), it can be argued that a simple curve fit between the 50% heat release points would yield an accurate maximum pressure rise. However, as illustrated in curve (b), a curve fit using all of the 50% heat release points can become challenging for some cases. Therefore, it was decided that a linear interpolation between the 50% heat release points would provide the most straightforward representation of the maximum pressure rise rate.

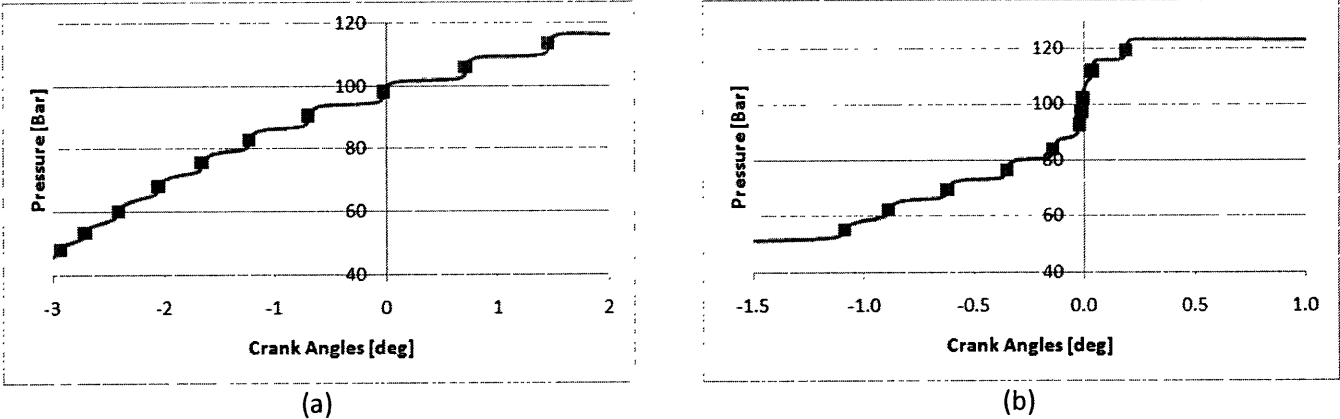


Figure 5-1 Sample pressure versus crank angle curves during combustion event

5.3 Ignition Temperatures

When attempting to explain the dependence of the fuel on the MPRR, it is important to know the temperature of the charge before ignition. This would provide the region of the ignition delay curve that should be focused on. The most direct method of obtaining this temperature is by determining the temperature at top dead center for a motored engine. Recall that the initial temperature of the charge is selected to ensure that the 50% heat release point is at TDC. The relationship between initial temperature, compression ratio, and maximum motored temperature is given in Figure 5-2.

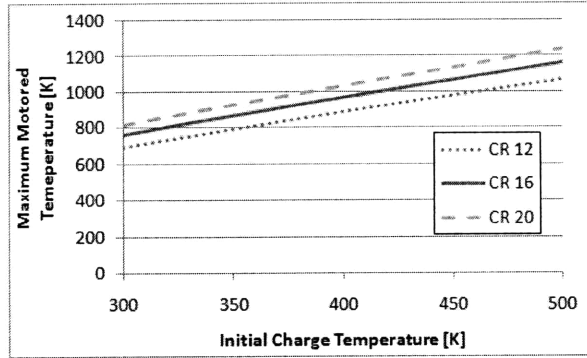


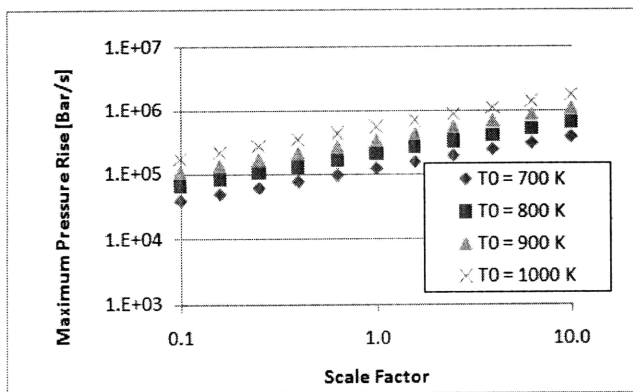
Figure 5-2 Maximum motored temperature versus initial temperature and compression ratio

The maximum motored temperature for the engine simulations will be provided along with the MPRR throughout this report. The initial temperatures used for the engine simulations are provided in Appendix E.

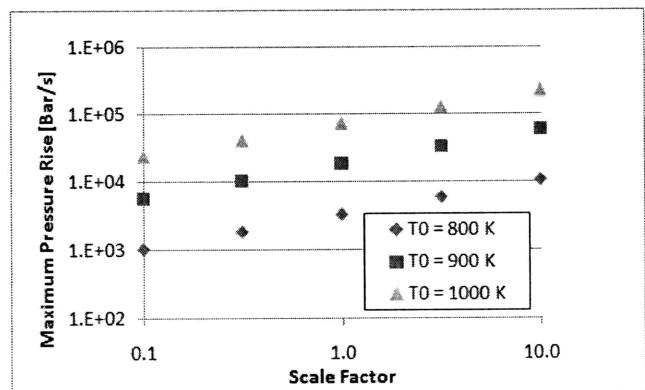
5.4 Single Reaction Fuels

5.4.1 Sensitivity to Pre-Exponential Factor

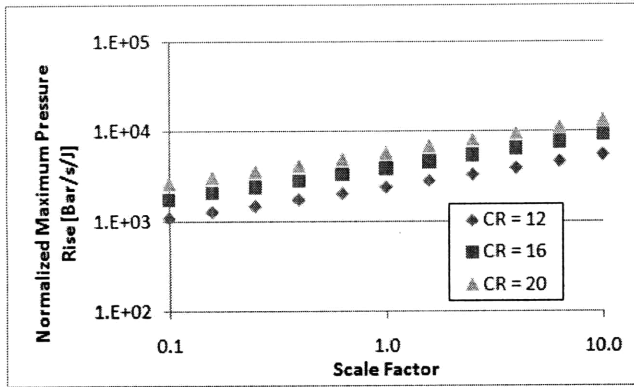
As a baseline example, the single reaction artificial fuels outlined in Figure 4-2 (a) will be analyzed. The ignition delay values as a function of temperature are shifted vertically by scaling the baseline pre-exponential factor. The results from the simulations are given in Figure 5-3. The scale factor used in the figure has been defined in equation [4.1]. The maximum motored temperatures for the engine simulations are presented in Figure 5-4. These were obtained using Figure 5-2.



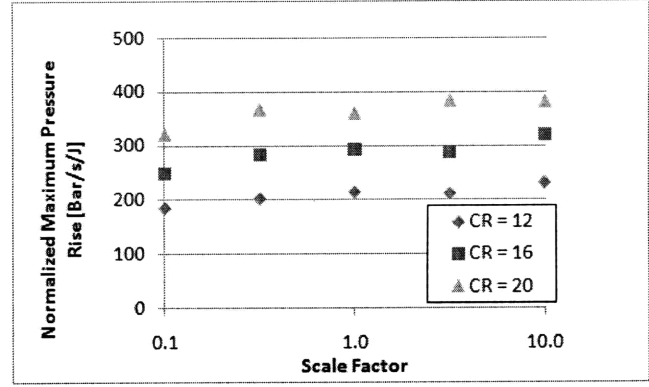
(a)



(b)

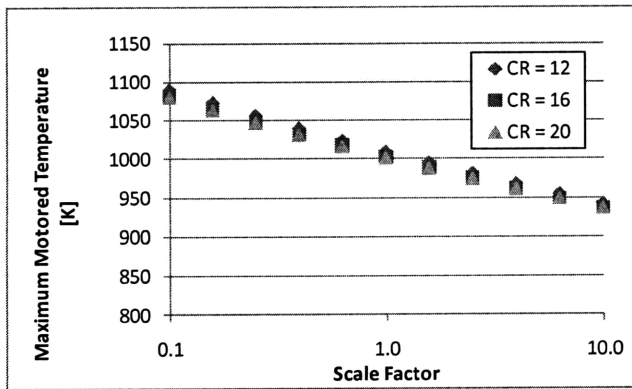


(c)

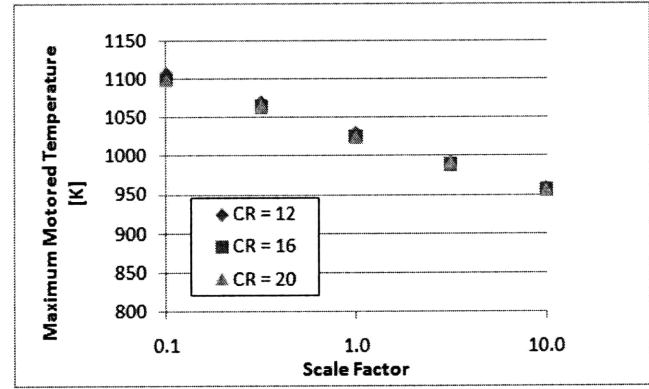


(d)

Figure 5-3 MPRR for single reaction fuel, effect of position: (a) constant volume, uniform temperature distribution (b) constant volume, quadratic temperature distribution (c) variable volume, uniform temperature distribution (d) variable volume, quadratic temperature distribution



(a)



(b)

Figure 5-4 Maximum motored temperatures for single reaction fuels, effect of position: (a) uniform temperature distribution (b) quadratic temperature distribution

It can be seen that as the scale factor increases, and the ignition delay curve is shifted down, the MPRR increases for both single zone models (Figure 5-3 (a) and (c)). This is simply due to the fact that the rate of heat release governed by chemical kinetics increases at the location of MPRR when the pre-exponential factor increases. This effect falls into the combustion chemistry column in Figure 1-4. Note that for the single reaction fuels, the rate of heat release is proportional to A_{NEW} (no other parameters are changed), so it is expected that as the scale factor increases, the rate of heat release at all temperatures will increase.

The increase in rate of pressure rise in the constant volume multi-zone model (Figure 5-3 (b)) is due to a reduction in the slope of the ignition delay curve as the scale factor increases. Note that though the slope appears to be the same in Figure 4-2 (a), this can be deceptive due to the fact that the logarithm of the ignition delay is plotted. The magnitude of the slope of the curves given in Figure 4-2 (a) is presented in Figure 5-5. It can be seen that the slope decreases as the scale factor increases. Therefore, it can be concluded that a reduction in the slope of the ignition delay curve increases the rate of pressure rise for constant volume combustion when temperature stratification is present. This result is somewhat obvious, considering that, when a temperature distribution is present, a smaller slope in the ignition delay curve would lead to a smaller difference in the combustion times of the different zones, and therefore a higher MPRR.

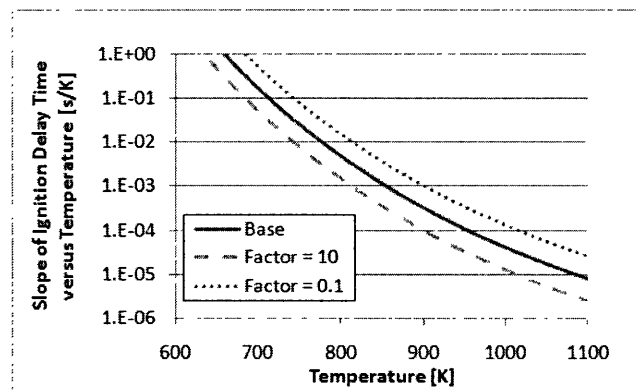


Figure 5-5 Slope of ignition delay versus temperature for ignition delay curves given in Figure 4-2 (a)

Finally, the variable volume, multi-zone results (Figure 5-3 (d)) show that there is little difference in the MPRR when the different fuels are used in an engine simulation. This result may seem surprising, considering that Figure 5-5 shows that the slope in the ignition delay curves do change for the different fuels. However, the comparison between the fuels cannot be done at the same temperature, because the initial temperatures, and consequently the ignition temperatures (given in Figure 5-4), for each simulation are not the same. By comparing the slope of the ignition delay curve for each fuel at the ignition temperature presented in Figure 5-4 (b), it can be seen that the slope is close to constant. This

then explains why the different fuels tested in the engine simulation had similar maximum pressure rise rates.

5.4.2 Sensitivity to Slope of Ignition Delay versus Temperature

The next variable that can be changed in the single reaction fuel model is the slope, as shown in Figure 4-2 (b). The results from the simulations that used these artificial fuels are shown in Figure 5-6. Note that the scale factor used in Figure 5-6 has been defined in equations [4.1] and [4.2]. Figure 5-7 gives the maximum motored temperatures for the engine simulations to help locate region of the ignition delay curve that should be focused on.

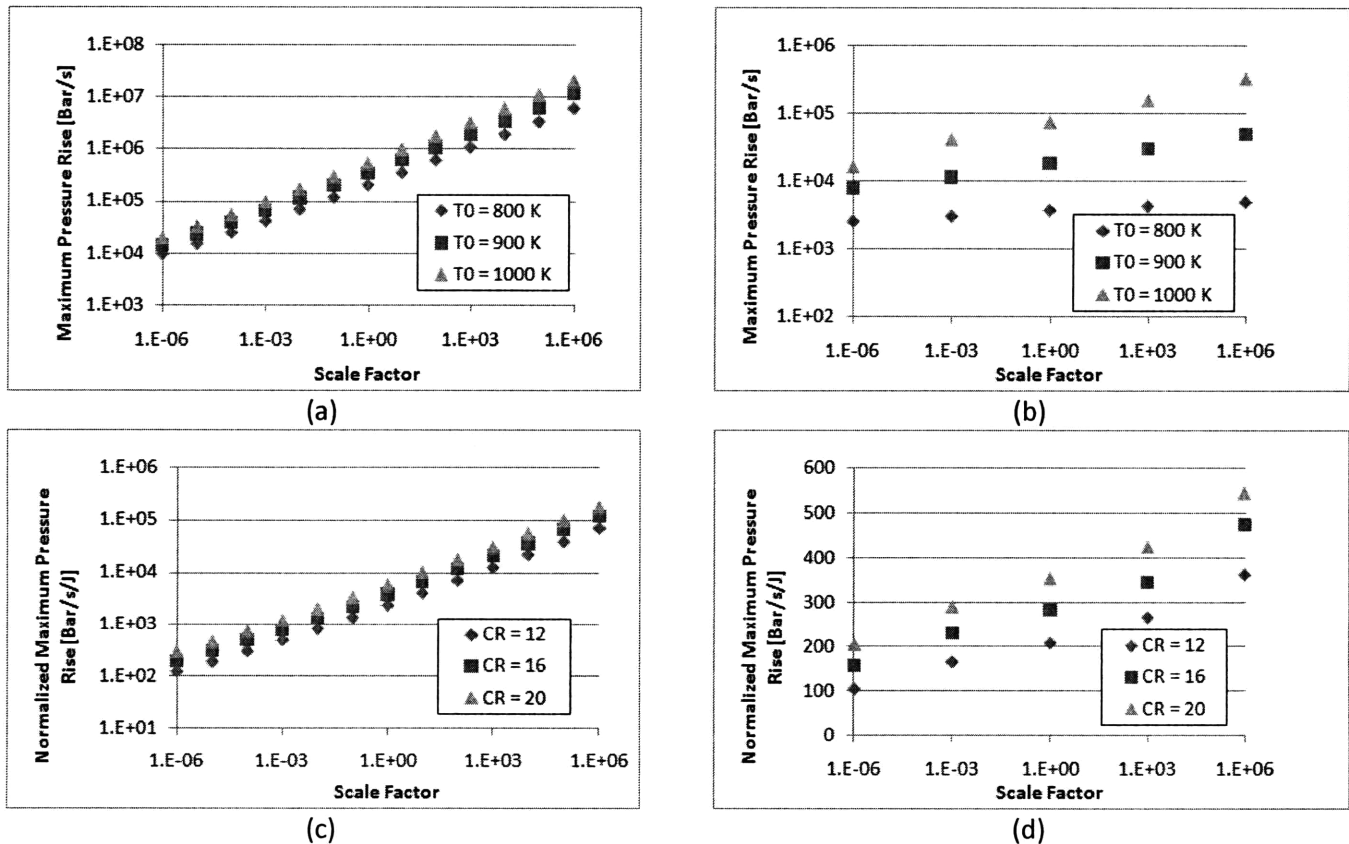


Figure 5-6 MPRR for single reaction fuel, effect of slope with pivot at 900 K: (a) constant volume, uniform temperature distribution (b) constant volume, quadratic temperature distribution (c) variable volume, uniform temperature distribution (d) variable volume, quadratic temperature distribution

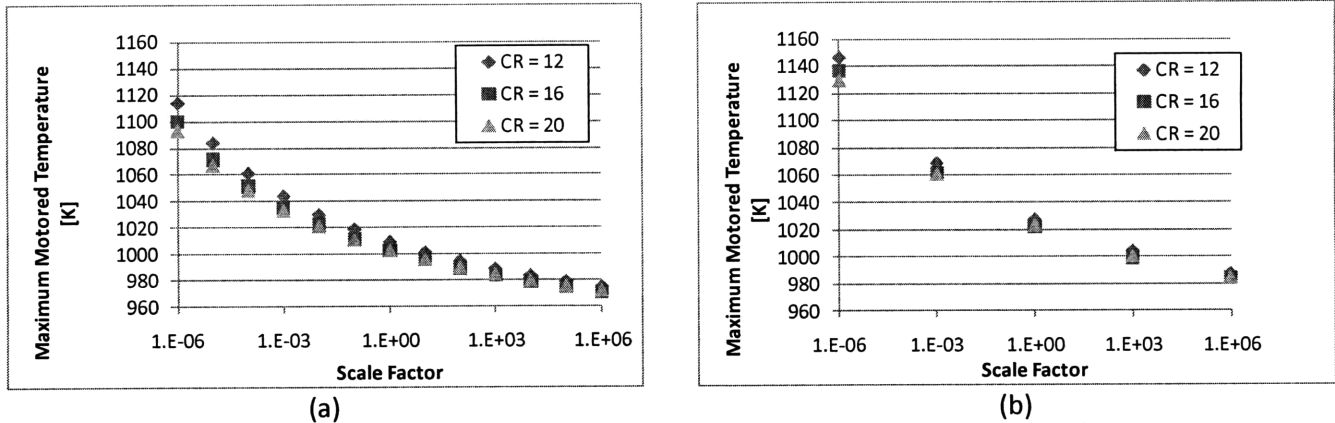


Figure 5-7 Maximum motored temperatures for single reaction fuels, effect of slope with pivot at 900 K: (a) uniform temperature distribution (b) quadratic temperature distribution

It can be seen that the impact of fuel on the single zone constant volume and variable volume simulations (Figure 5-6 (a) and (c)) is similar to the previous case. The kinetic rate equation parameters at the temperature where the MPRR occurs dictate these results. For the single reaction fuels, the rate of heat release is proportional to the product of A_{NEW} and $\exp(-E_{NEW}/RT)$. When equations [4.1] and [4.2] are used, it can be determined that the rate of heat release is proportional to $SF^{(1-TPIVOT/T)}$. Therefore, as long as the temperature at the location of maximum pressure rise rate is larger than the pivot temperature, the maximum heat release rate will increase as the scale factor increases. This has been demonstrated in Figure 5-6 (a) and (c).

With regards to the constant volume simulation, it is instructive to look at the magnitude of the slope of the ignition delay versus temperature curve, given in Figure 5-8. It can be seen that for the case where the maximum temperature is 1000 K, the slope of the ignition delay curve decreases as the scale factor increases, at the temperature of concern. The increase in the rate of pressure rise is then expected, as was described in the previous section. However, for the case where the maximum initial temperature is 800 K, the slope of the ignition delay curve increases as the scale factor increases; yet, the MPRR still increases as the scale factor increases. Therefore, there is clearly another effect present that must be considered in the discussion.

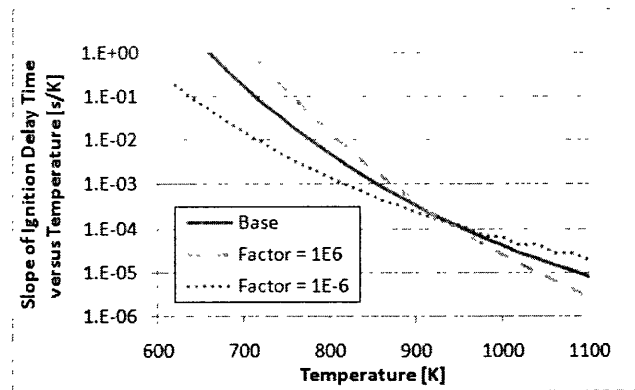


Figure 5-8 Slope of ignition delay versus temperature for ignition delay curves given in Figure 4-2 (b)

It was stated previously that the effect of the temperature distribution is to introduce a delay between zone combustion events, which would reduce the MPRR. Then naturally, it would be expected that if the slope of the ignition delay curve increases, the delay between combustion events would increase, so the MPRR should decrease. However, countering this effect is the energy transfer between the zones due to work interaction. This energy transfer would act to reduce the delay between the zone combustion events.

The impact of the work interaction on the MPRR depends on the fuel in two respects. First, the impact is larger for fuels with larger ignition delay slopes, since the additional energy and subsequent increase in temperature would have a larger impact in accelerating the combustion process. Second, the impact of the work interactions would be less for fuels that have lower heat release rates in each zone due to the kinetic rate parameters. If the rate of heat release in each zone is less, the combustion events between the zones become intertwined, where ignition in one zone occurs before combustion in the previous zone is completed. This would then act to reduce the ability of the work interactions to accelerate ignition in the subsequent zones. Both of these effects can then explain why it is possible to get an increase in the MPRR with an increase in the slope of the ignition delay curve.

The impact of the work interactions has been demonstrated in Figure 5-9 by removing the work interactions that were present in the previous simulation (Figure 5-6 (b)). It can be seen that the rate of

pressure rise now decreases as the scale factor increases for the case with a maximum initial temperature of 800 K. Therefore, the work interactions are clearly responsible for the increase in the rate of pressure rise shown in the original simulation.

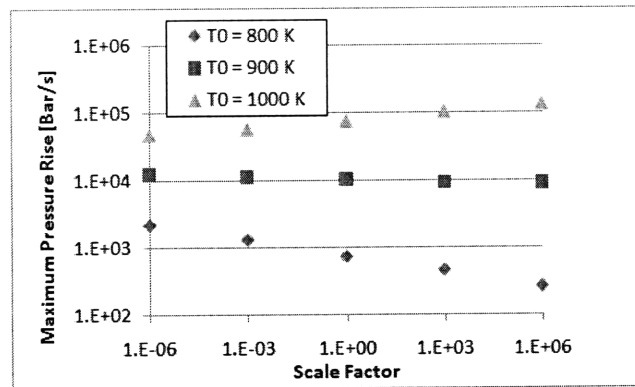


Figure 5-9 MPRR for single reaction fuel, effect of slope with pivot at 900 K, constant volume, quadratic temperature distribution with constant heat release rate after combustion initiation and work transfer between zones not included

To further illustrate the affect of work transfer interactions between the zones in the constant volume, multi-zone model results, the zone temperature evolution for the two fuels at the extremes of the analysis is given in Figure 5-10. It is demonstrated that the time between combustion events decreases much more drastically for the case with the scale factor equal to 10^6 . If no work interactions are present, the time between zone combustion events should increase for the later zones, since a parabolic temperature distribution is used. Figure 5-10 (a) shows that for the lower scale factors, the heat release rate in each zone is much lower. This effect, combined with the smaller ignition delay slope when the initial temperature is 800 K, contribute to the increase in the impact of the work interactions as the scale factor increases.

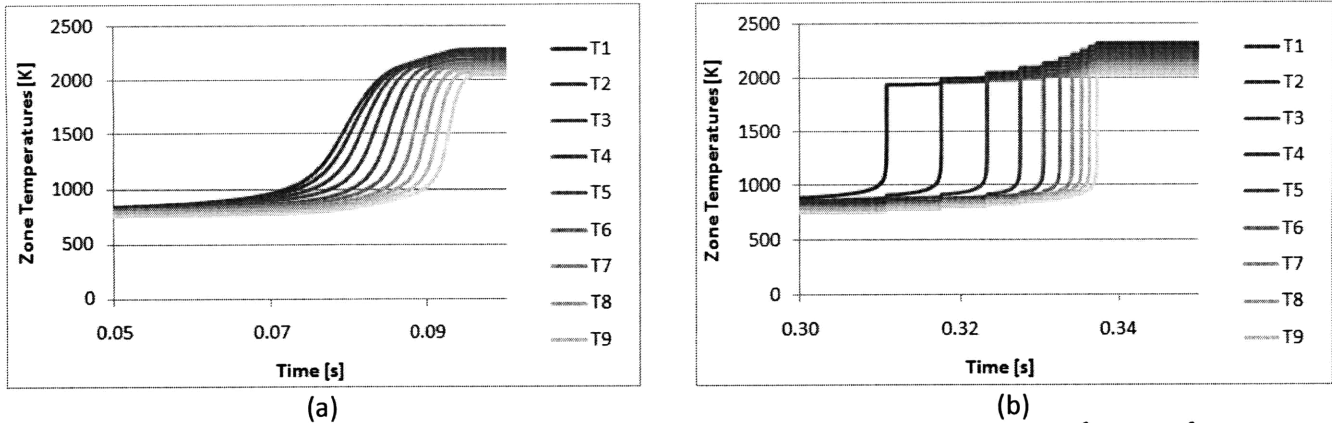


Figure 5-10 Zone temperatures in the constant volume, multi-zone simulation for $T_0=800\text{K}$: (a) $SF=10^{-6}$ (b) $SF=10^6$

Moving to the variable volume, multi-zone case (Figure 5-6 (d)), it can be seen that there is a large increase in the rate of pressure rise as the scale factor increases. This result is somewhat difficult to describe without further analysis. Figure 5-11 provides a sequential build-up to the results shown in Figure 5-6 (d). To eliminate the fuel chemistry related effects, a constant heat release rate was implemented for both Figure 5-11 (a) and (b) after combustion is initiated (identified as the point of 40% total heat release for the individual zone). Also, the energy transfer through work transfer was eliminated in Figure 5-11 (a).

By following the sequence of curves, it can be concluded that for the lower scale factors, the rate of pressure rise is reduced due to fuel combustion chemistry, particularly the low heat release rate within each zone. As the scale factor increases, the fuel chemistry effects no longer dictate the rate of total heat release, since the limiting factor becomes the time between zone combustion events. It is apparent from Figure 5-11 (b) that for the large scale factors, the work transfer has a more predominant effect on increasing the rate of pressure rise. The reason for this is similar to the constant volume simulation discussed above.

Before moving on, it is instructive to look more closely at Figure 5-11 (a), which has a constant heat release rate, thereby eliminating the fuel chemistry effects. Also, the energy transfer due to work interactions between the zones has been eliminated. Therefore, the rate of pressure rise is dictated

only by the delay in ignition between the zones due to the temperature distribution. Based on the initial temperatures, the maximum motored temperatures increase from 980 K to 1120 K as the scale factor decreases (Figure 5-7). The slope of the ignition delay curve at the corresponding motored temperatures slightly increases as the scale factor increases. Therefore it would be expected that as the scale factor increases, the rate of pressure rise should decrease, since no fuel chemistry or work interaction effects are present. This trend is indeed illustrated in Figure 5-11 (a).

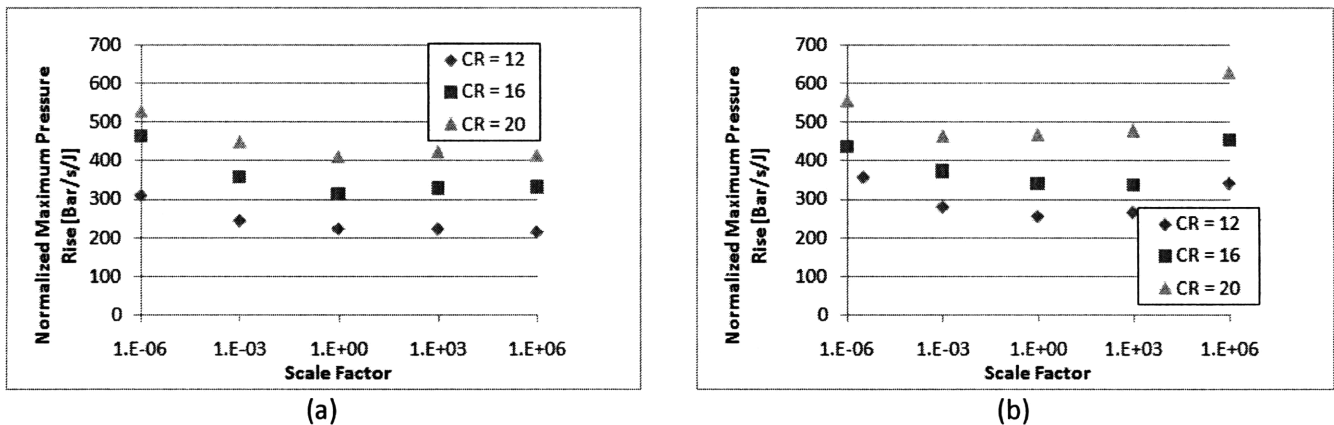


Figure 5-11 MPRR for single reaction fuel, effect of slope with pivot at 900 K, variable volume, quadratic temperature distribution with constant heat release rate after combustion initiation: (a) work transfer between zones not included (b) work transfer included

5.4.3 Single Reaction Fuels Summary

The discussion on single reaction fuels presented a number of general conclusions on potential impacts the shape of the ignition delay curve can have on the rate of pressure rise. Most importantly, it has been demonstrated that fuel ignition properties can have an impact on the MPRR, and there is therefore an opportunity to extend the high load limit by proper fuel selection.

The single reaction fuels lacked the complexity of real fuels, which made the analysis relatively simple. In particular, the ignition delay versus temperature slope in the single reaction fuels followed a simple downward trend. The trend will be much more complicated for real fuels, largely due to the NTC region. The combustion event for the single reaction fuels was also localized near the ignition temperature. Depending on the location of the ignition temperature on the ignition delay curve, real

fuels can potentially exhibit a two stage combustion process, where a considerable amount of the fuel energy is released outside of the main combustion event. These complications will be presented in the remainder of this chapter by examining the iso-octane and n-heptane based fuels.

Before introducing the above complications to the analysis, it is useful to summarize the conclusions that have been presented thus far:

- When no temperature distribution is present, the kinetic rate parameters can have a large affect on the MPRR by increasing the rate of heat release at the temperature of interest. This effect would fall in the “combustion chemistry” column in Figure 1-4. For the simple reaction fuels, the rate of heat release can be easily correlated to the kinetic rate parameters and temperature. Therefore, the effect of changing the kinetic rate parameters can be easily determined.
- When a temperature distribution is present, the absolute slope of the ignition delay versus temperature curve is important. Unfortunately, the relationship between the absolute slope of the ignition delay curve and the rate of pressure rise is not straightforward. Having a larger slope can lead to a larger delay between zone combustion events, and consequently reduce the pressure rise rate. However, having a large slope can also increase the impact of the work interactions between the zones, which acts to increase the pressure rise rate.
- The impact of work interactions between the zones can be reduced when the heat release rate in each zone is reduced. This occurs because the zone combustion events become intertwined, so the work energy transfer has less impact on determining the time of ignition for subsequent zones.
- When comparing the slope of the ignition delay curves for different fuels, it is important to make the comparison at the temperature where the ignition occurs, which has been approximated by using the maximum motored temperature.

5.5 Comparison of Iso-Octane and n-Heptane

With a number of general conclusions in hand, the MPRR can now be evaluated for more complicated fuels. Before proceeding with an evaluation of each of the ignition delay curve parameters described in Figure 4-1, it is useful to compare the two baseline fuels that have been selected: iso-octane and n-heptane.

A general summary of the results obtained with both baseline fuels is given in Figure 5-12. It can be seen that the MPRR is generally lower for n-heptane when a uniform temperature distribution is used. However, the addition of a temperature distribution is more beneficial when iso-octane is used. The maximum motored temperatures are also plotted. The first stage ignition delay times for n-heptane are much lower, which leads to a lower initial temperature and consequently a lower maximum motored temperature.

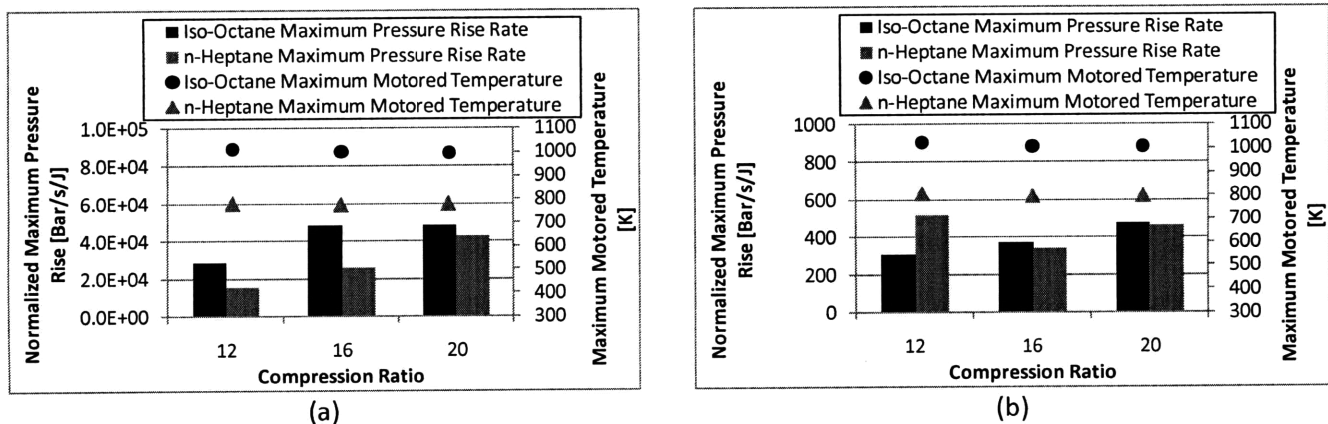


Figure 5-12 MPRR and maximum motored temperature for iso-octane and n-heptane: (a) uniform temperature distribution (b) quadratic temperature distribution

At this point, some general comments can be made regarding both the single zone and multi-zone results. Starting with the single zone results, it has previously been illustrated that the MPRR is governed by the rate of heat release at the temperature where the MPRR occurs. To find the relative rate of heat release, the kinetic parameters in the single reaction fuels were compared. However, with more complicated mechanisms, this approach becomes difficult.

The MPRR occurs at 1700 K for iso-octane, and 1600 K for n-heptane, for all of the simulations. This can be used to explain the lower heat release rate for n-heptane. However, this temperature difference is present for all three compression ratios, yet the difference is much greater for the lower compression ratios. Therefore, another affect is present.

Figure 5-13 presents the pressure traces for the uniform temperature simulations. It can be seen that n-heptane exhibits a two stage ignition, which is more predominant at the lower compression ratios. Two-stage ignition is present for n-heptane because the ignition temperature falls in the NTC region. The two-stage ignition would act to lower the radical concentration at the location of maximum pressure rise, and therefore the heat release rate would also be lowered. This then explains the lower maximum rates of pressure rise obtained with n-heptane compared to iso-octane, for the single zone models.

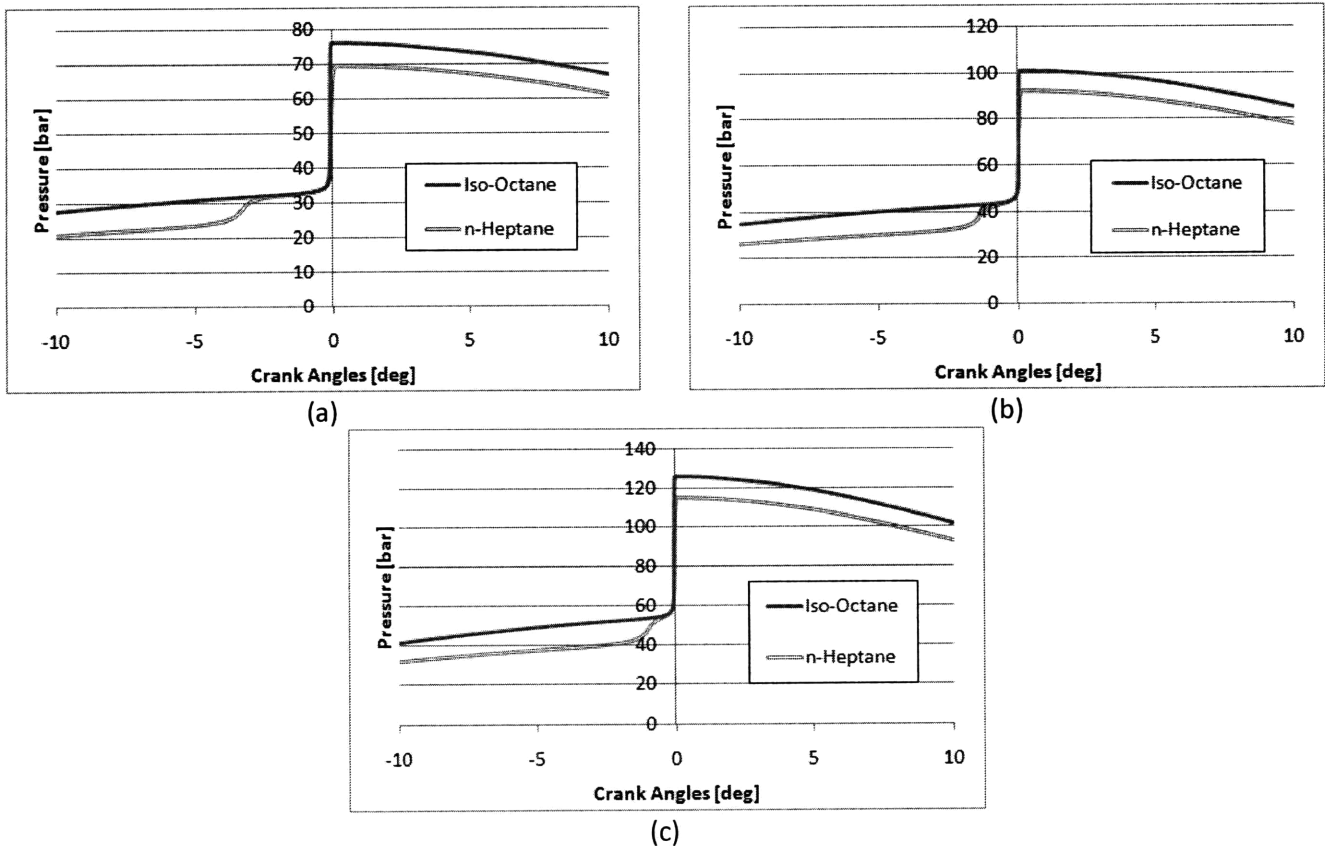


Figure 5-13 Pressure curves for iso-octane and n-heptane: (a),(b),(c) uniform temperature distribution, CR=12,16,20, respectively

With regards to the multi-zone models, Figure 5-12 shows that the temperature distribution was more beneficial when iso-octane was used. The reason for this can be obtained from the pressure traces output by the simulations (Figure 5-14). Each step in the pressure trace corresponds to one zone igniting. It can be seen that the time between zone ignitions for iso-octane is much more uniform than when n-heptane is used. This is because n-heptane ignites in the NTC region, where the ignition delay/temperature dependence becomes flat, or negative (the ignition delay increases as the temperature increases). Then the different zones would not ignite sequentially, and some zones would ignite together, thereby negating the benefits of the temperature distribution.

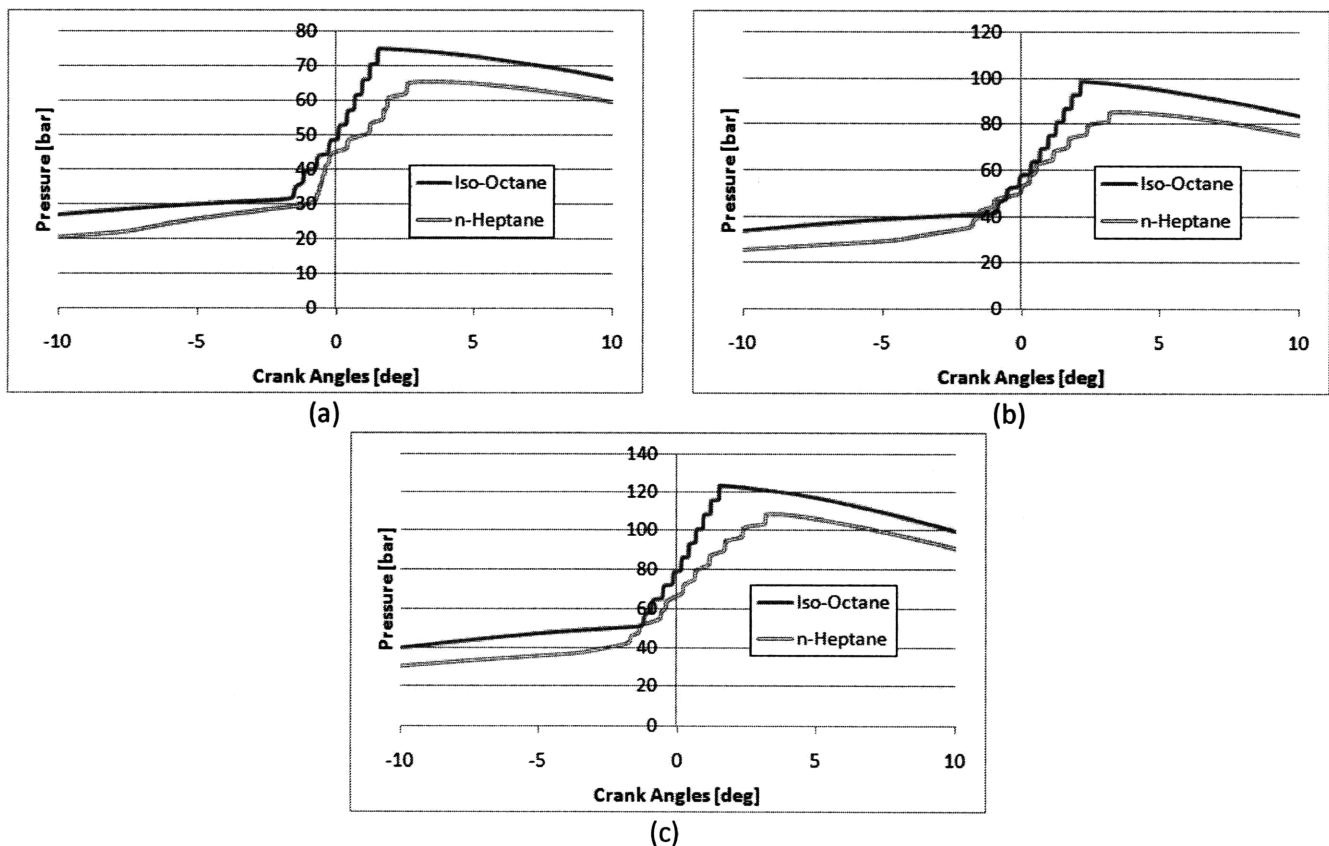


Figure 5-14 Pressure curves for iso-octane and n-heptane: (a),(b),(c) quadratic temperature distribution, CR=12,16,20, respectively

To further illustrate the above point, the zone temperatures for one of the simulations are presented in Figure 5-15. When iso-octane is used, the zones ignite in sequence, with a somewhat

uniform spacing (the spacing is determined by the temperature profile and work interactions). However, when n-heptane is used, the zones ignite in a random pattern, and out of sequence. The zones can ignite out of sequence because the molar concentration in each zone is not the same, and the NTC region can present situations where a higher temperature takes more time to ignite. The random pattern of ignitions consequently leads to the possibility of multiple zones igniting simultaneously, which would reduce or eliminate the benefits of having a temperature distribution.

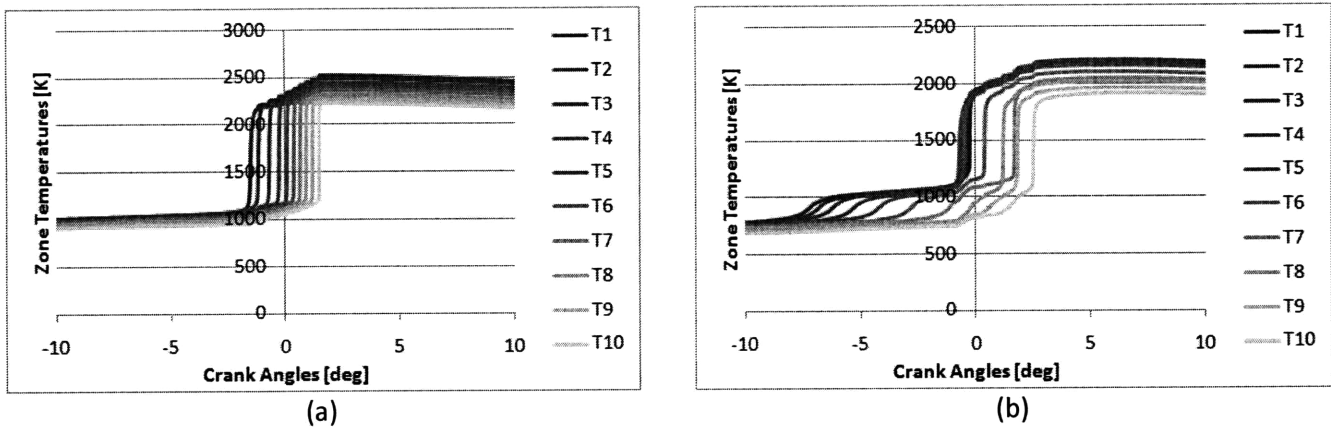


Figure 5-15 Zone temperatures for quadratic temperature distribution, CR=12: (a) iso-octane (b) n-heptane

5.6 Iso-Octane-Based Fuels

At this point, a number of general conclusions have been presented using simple fuels, and the ignition characteristics of the baseline fuels have been compared. The impact of the different ignition delay curve parameters presented in Figure 4-1 can now be studied. This section will present the iso-octane based fuels, while the following section will present the n-heptane based fuels.

5.6.1 Sensitivity to T_A

The parameter T_A represents the horizontal shift in the ignition delay curves; see Figure 4-3 (a). The impact of changing T_A on the MPRR is shown in Figure 5-16. Since there is no shape/slope change in the ignition delay curve, it is not expected that MPRR would change significantly. To obtain combustion at top dead center, the initial temperature would have to be shifted appropriately, such that the ignition

temperature is on the same portion of the curve (Figure 5-17). The small changes in the MPRR in Figure 5-16 are likely due to different specific heat values (due to a different temperature range) and errors in approximating the maximum pressure rise. The change is more pronounced in the single zone model because the curve is governed by the temperature where the maximum pressure rise occurs, which is towards the end of the combustion process. Therefore, the impact of the specific heats would be larger.

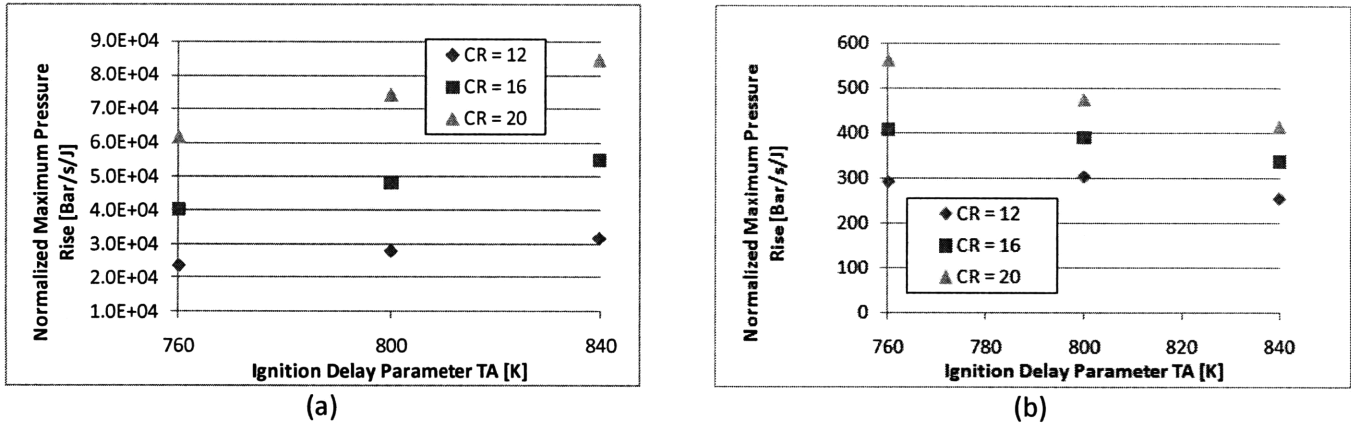


Figure 5-16 MPRR for iso-octane based fuel, impact of T_A : (a) variable volume, uniform temperature distribution (b) variable volume, quadratic temperature distribution

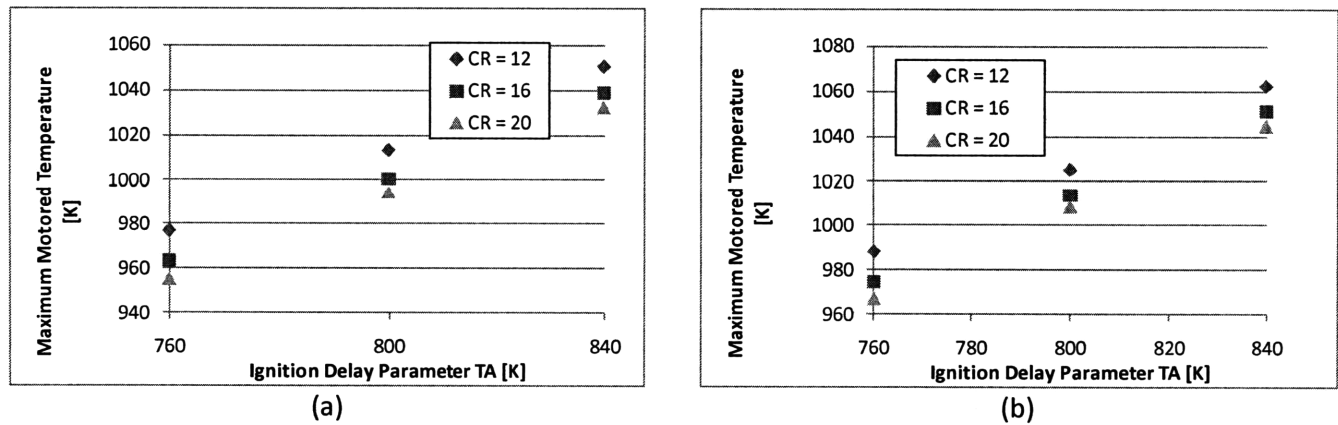
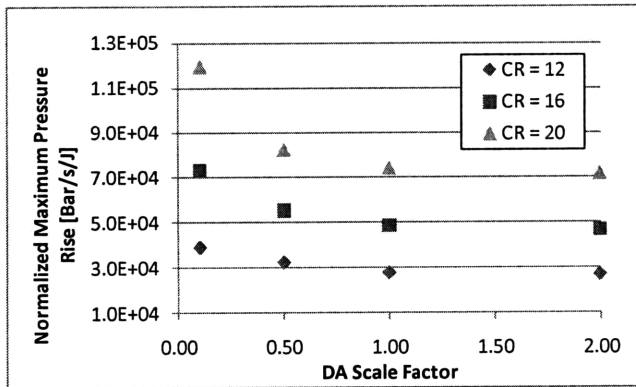


Figure 5-17 Maximum motored temperatures for iso-octane based fuel, impact of T_A : (a) variable volume, uniform temperature distribution (b) variable volume, quadratic temperature distribution

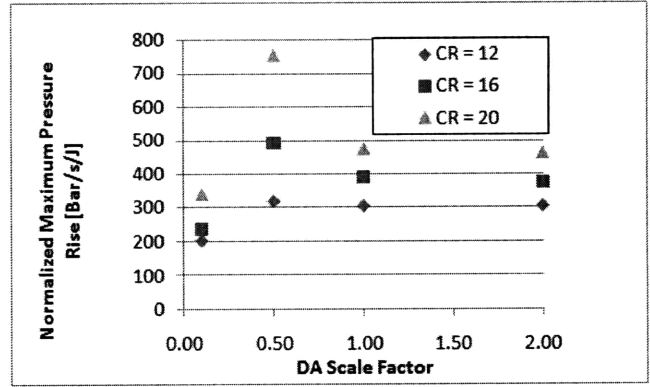
5.6.2 Sensitivity to D_A

The parameter D_A represents the vertical shift in the ignition delay curves; see Figure 4-3 (b). The impact of changing D_A on the MPRR is shown in Figure 5-18. When a uniform temperature distribution

is used, the MPRR stays somewhat constant. When a temperature distribution is added, it can be seen that there is a jump in the rate of pressure rise for the multi-zone case for the artificial fuel with a D_A scale factor of 0.5. In this case, the ignition temperature is around 950 K (Figure 5-19), which would place ignition at the end of the NTC region. This is especially true for the simulation with a compression ratio of 20. It was demonstrated previously that a larger pressure rate in the NTC region is obtained because the slope is flat, which negates the effect of the temperature distribution.

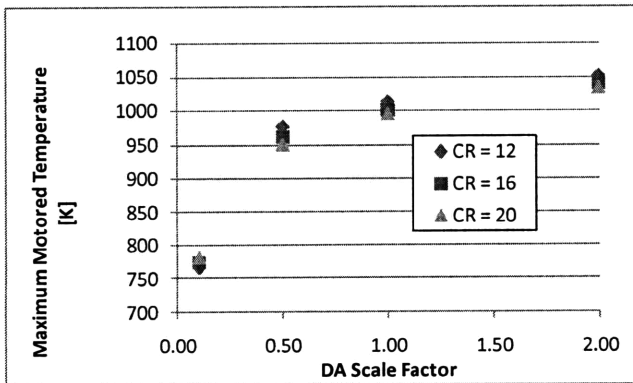


(a)

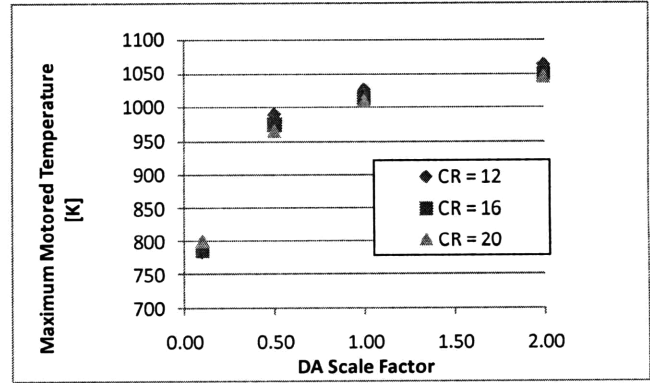


(b)

Figure 5-18 MPRR for iso-octane based fuel, impact of D_A : (a) variable volume, uniform temperature distribution (b) variable volume, quadratic temperature distribution



(a)



(b)

Figure 5-19 Maximum motored temperatures for iso-octane based fuel, impact of D_A : (a) variable volume, uniform temperature distribution (b) variable volume, quadratic temperature distribution

5.6.3 Sensitivity to n_1

The parameter n_1 represents the low temperature logarithmic slope of the ignition delay curves; see Figure 4-3 (c). It can be seen in Figure 5-20 that there is no change in the rate of pressure rise when n_1 is modified. This is expected since the ignition temperature for the baseline fuel is approximately 1000 K (Figure 5-21), which is far from the low temperature region.

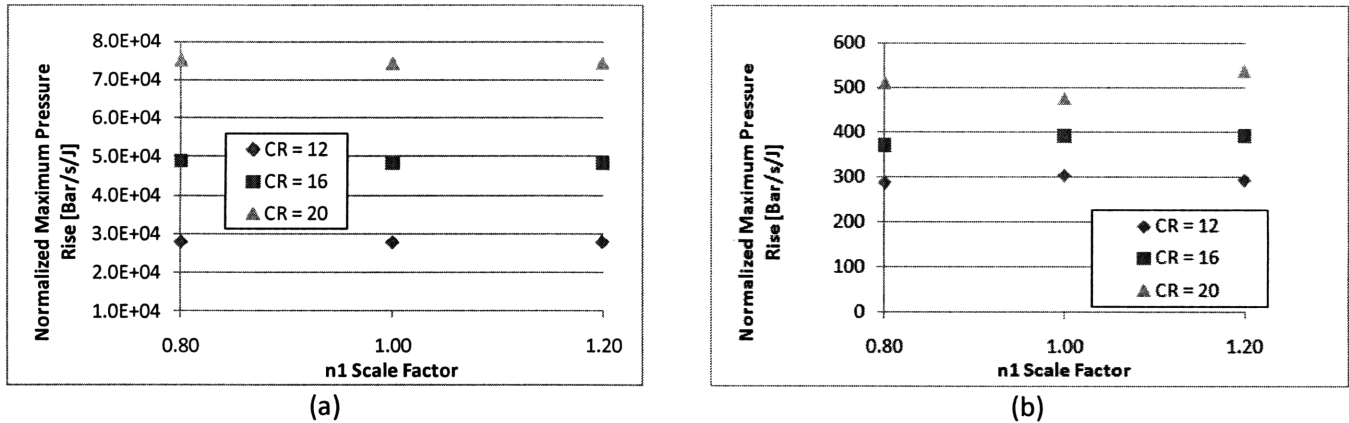


Figure 5-20 MPRR for iso-octane based fuel, impact of n_1 : (a) variable volume, uniform temperature distribution (b) variable volume, quadratic temperature distribution

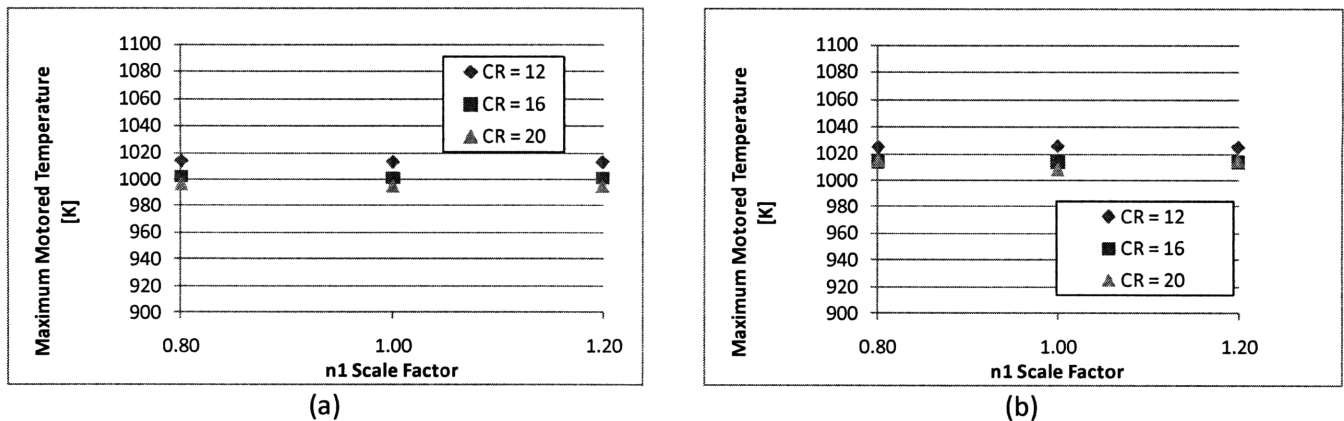


Figure 5-21 Maximum motored temperatures for iso-octane based fuel, impact of n_1 : (a) variable volume, uniform temperature distribution (b) variable volume, quadratic temperature distribution

5.6.4 Sensitivity to n_2

The parameter n_2 represents the high temperature logarithmic slope of the ignition delay curves; see Figure 4-3 (d). The impact of changing n_2 on the rate of pressure rise is shown in Figure 5-22. It can

be seen that with both a uniform and a non-uniform temperature distribution, the rate of pressure rise increases as n_2 increases. Starting with the uniform temperature distribution, the increase in the MPRR as n_2 increases is due to a larger heat release rate at the temperature corresponding to the location of the MPRR. This occurs because to obtain a larger slope, the high temperature kinetic rate parameters must be selected to reduce the reaction time at the higher temperatures. When a temperature distribution is added, the trend is more difficult to describe. At the ignition temperatures (Figure 5-23), the absolute slope is larger when n_2 increases. Note that this is not obvious from the plots in Figure 4-3, which show the logarithm of the ignition delay. It would be expected that the larger slope would lead to a larger delay between zone ignition events, which would then reduce the MPRR. This is indeed the case, when the work interactions are removed. However, as was shown previously, the impact of the work interactions between the zones increases as the slope increases. Therefore, the reason for the increase in the rate of pressure rise as n_2 increases can be attributed to the work interactions. Note that the same trend was established in Figure 5-6 (d) with the single reaction fuels.

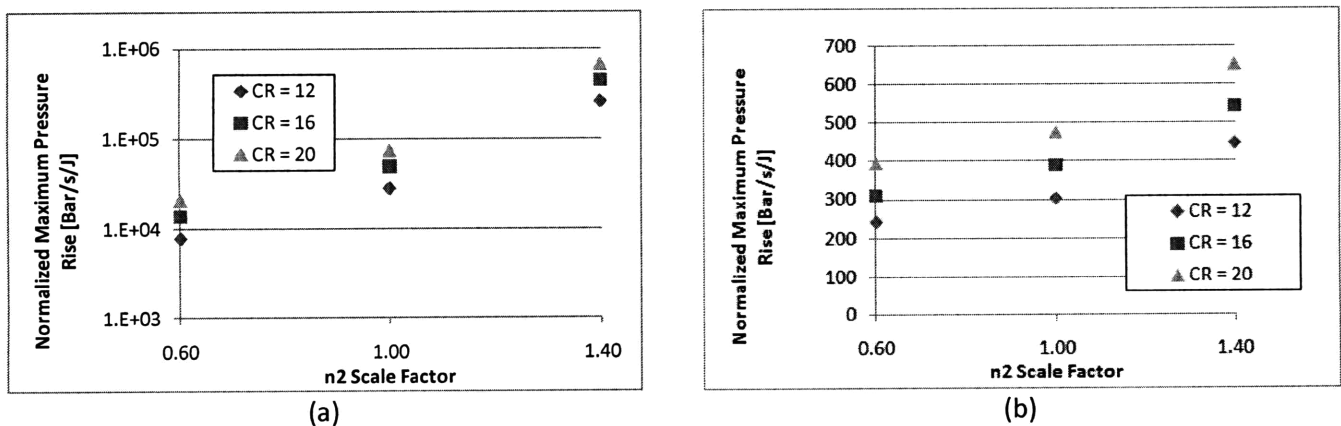


Figure 5-22 MPRR for iso-octane based fuel, impact of n_2 : (a) variable volume, uniform temperature distribution (b) variable volume, quadratic temperature distribution

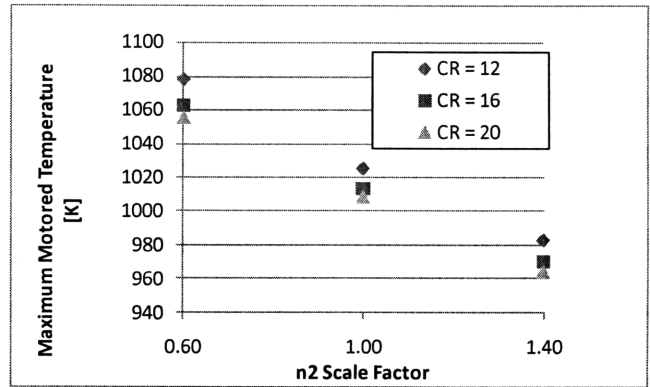
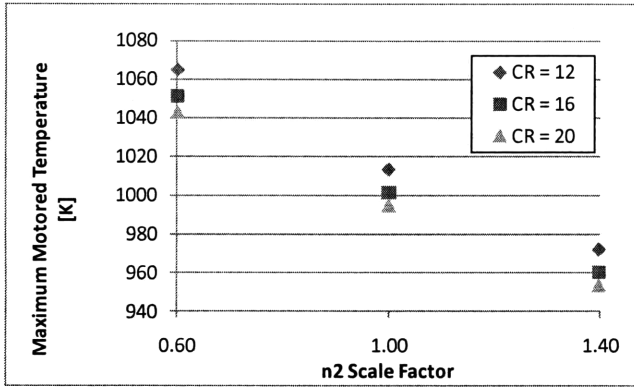


Figure 5-23 Maximum motored temperatures for iso-octane based fuel, impact of n_2 : (a) variable volume, uniform temperature distribution (b) variable volume, quadratic temperature distribution

5.6.5 Sensitivity to y_{NTC}

The parameter y_{NTC} represents the vertical length of the NTC region; see Figure 4-3 (e). The impact of changing y_{NTC} on the MPRR is given in Figure 5-24. For the uniform temperature distribution simulation, the rate of pressure rise increases as the vertical length increases. When a quadratic temperature distribution is added, the difference between the fuels is not significant. The ignition temperatures (Figure 5-25) for each fuel correspond to approximately the same location on each respective curve, so the slope of the ignition delay versus temperature is approximately the same.

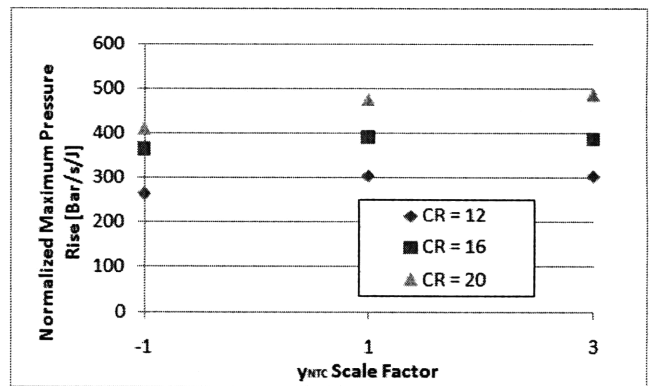
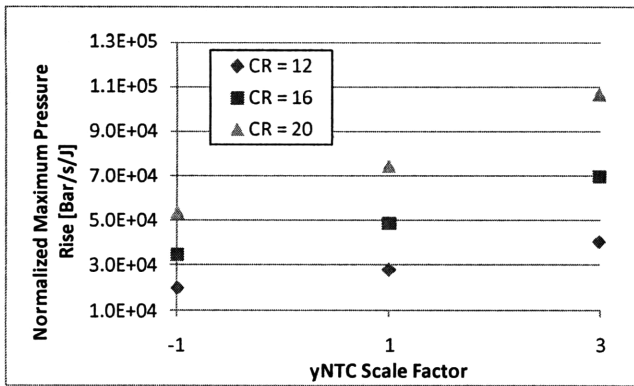


Figure 5-24 MPRR for iso-octane based fuel, impact of y_{NTC} : (a) variable volume, uniform temperature distribution (b) variable volume, quadratic temperature distribution

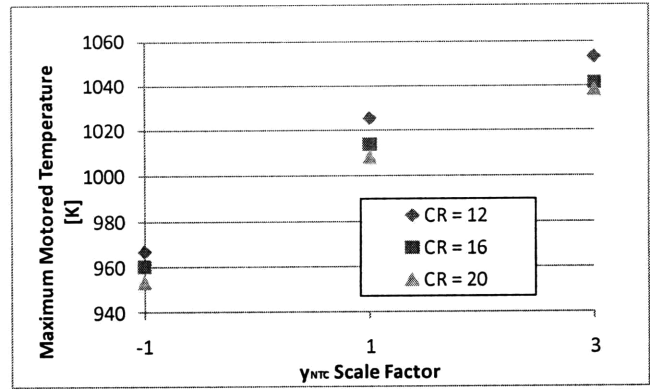
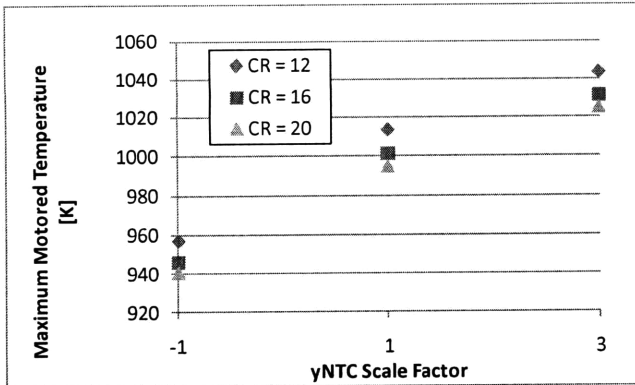


Figure 5-25 Maximum motored temperature for iso-octane based fuel, impact of y_{NTC} : (a) variable volume, uniform temperature distribution (b) variable volume, quadratic temperature distribution

5.6.6 Sensitivity to Low Temperature Branching Global Parameter

The Shell Model parameter A_{f1} was used to change the low temperature branching agent formation rate; see Figure 4-4 (a). The dependence of the rate of pressure rise on A_{f1} is given in Figure 5-26. Examining the single-zone results, it can be seen that the rate of pressure rise decreases abruptly around a scale factor of 2 to 2.5. This result illustrates the impact of the NTC region, and needs to be examined carefully.

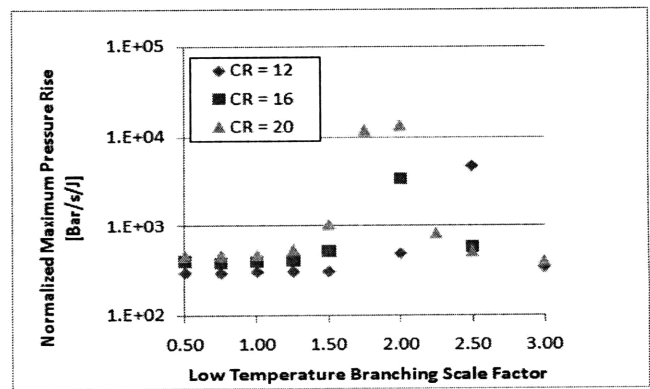
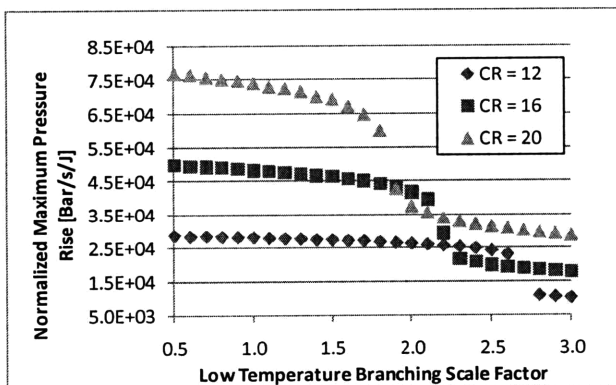


Figure 5-26 MPRR for iso-octane based fuel, impact of A_{f1} : (a) variable volume, uniform temperature distribution (b) variable volume, quadratic temperature distribution

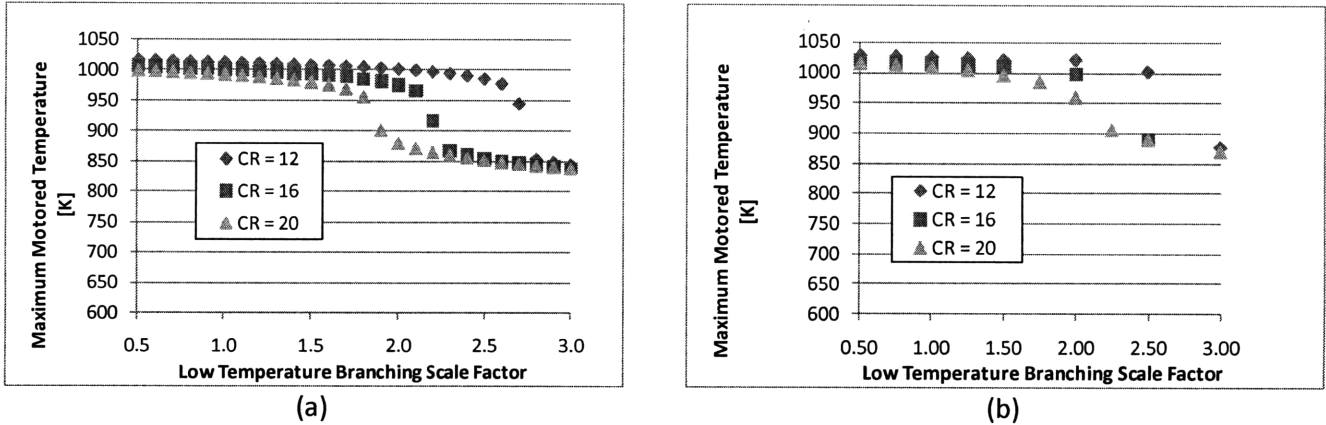


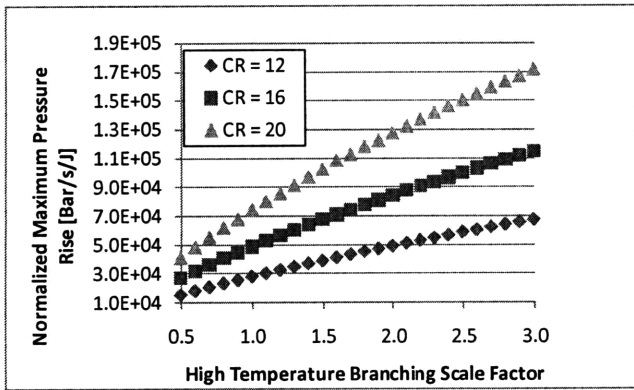
Figure 5-27 Maximum motored temperature for iso-octane based fuel, impact of A_{f1} : (a) variable volume, uniform temperature distribution (b) variable volume, quadratic temperature distribution

The ignition temperatures for the engine simulations are given in Figure 5-27. It can be seen that the ignition temperature suddenly drops also at a scale factor of 2 to 2.5. As A_{f1} increases, the first stage ignition delay times decrease, and the NTC region moves down and to higher temperatures. As a result, ignition moves from the linear high temperature region to the NTC region. This then reduces the radical concentration at the point of maximum pressure rise, which results in a lower heat release rate. It is important to note that this trend was first presented when comparing n-heptane to iso-octane in section 5.5. It was shown that n-heptane had a lower maximum rate of pressure rise with a uniform temperature distribution due to ignition in the NTC region.

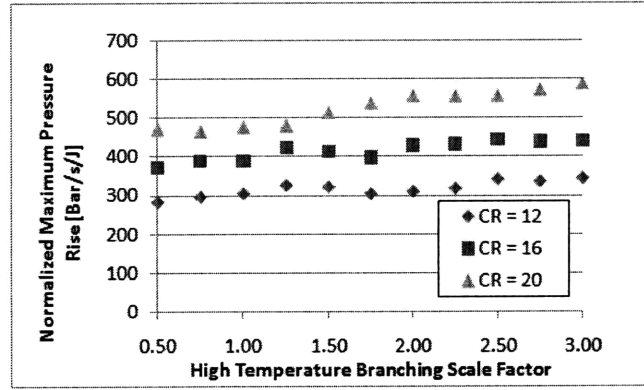
It can be recalled that due to ignition in the NTC region, the benefit of adding a temperature distribution was not as large for n-heptane, compared to iso-octane. This impact is again illustrated in the current simulations (Figure 5-26 (b)), where there is a range of scale factors between 2.0 and 2.5 where the rate of pressure rise increases by an order of magnitude. As previously discussed, the combustion temperature lies in the NTC region for these cases, where the slope is flat. Note that as the scale factor increases past 2.5, ignition occurs before the NTC region, and the MPRR then decreases.

5.6.7 Sensitivity to High Temperature Branching Global Parameter

The Shell Model parameter A_{f2} was used to change the high temperature branching agent formation rate; see Figure 4-4 (b). The impact of changing A_{f2} on the MPRR is given in Figure 5-28. As the rate of formation increases, the rate of pressure rise increases for the single zone simulation. This is due to the higher rate of heat release at the high temperatures where the MPRR occurs. This is a direct result of scaling the A_{f2} kinetic rate parameter, which governs the rate of reaction at high temperatures. When a temperature distribution is added, there is little change in the rate of pressure rise as the high temperature branching agent formation reaction is accelerated. The ignition temperature (Figure 5-29) for each case falls on the same portion of the ignition delay curve.

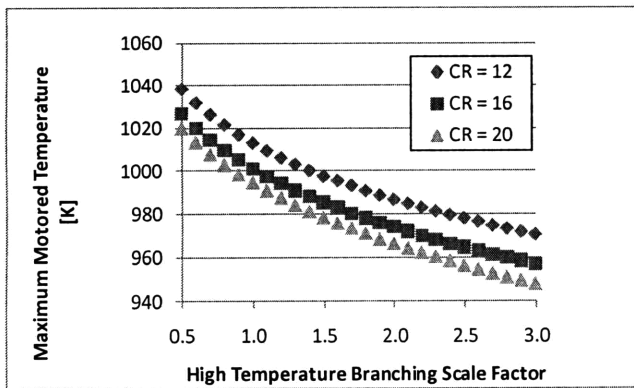


(a)

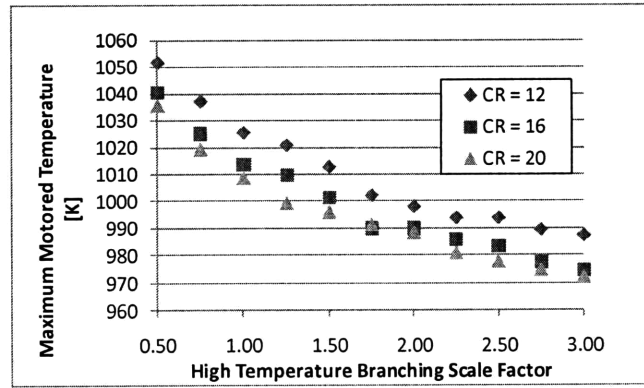


(b)

Figure 5-28 MPRR for iso-octane based fuel, impact of A_{f2} : (a) variable volume, uniform temperature distribution (b) variable volume, quadratic temperature distribution



(a)



(b)

Figure 5-29 Maximum motored temperature for iso-octane based fuel, impact of A_{f2} : (a) variable volume, uniform temperature distribution (b) variable volume, quadratic temperature distribution

5.7 n-Heptane-Based Fuels

It has been demonstrated that ignition in the NTC region can have significant effects on the MPRR. To further study this aspect, the impact of the different ignition delay parameters can now be examined with the n-Heptane-based fuels. Recall that due to the lower first stage ignition delay time, n-heptane based fuels will generally ignite near the NTC region.

5.7.1 Sensitivity to T_A

The parameter T_A represents the horizontal shift in the ignition delay curves; see Figure 4-5 (a). Figure 5-30 shows the impact of changing T_A on the MPRR. To insure that ignition occurs at TDC, the initial charge temperature is increased as T_A is increased. Therefore, ignition will occur approximately in the same portion of the ignition delay curve. This can be seen by examining the ignition temperatures in Figure 5-31. For the iso-octane based fuels, this resulted in little change in MPRR as T_A changed. This is also apparent in the single zone simulation for the n-heptane based fuels, as shown in Figure 5-30 (a). However, for the multi-zone simulations, since ignition occurs in the NTC region, a very small change in the ignition point can lead to a large change in MPRR. This is most evident in the simulation with a compression ratio of 12, because ignition occurs directly in the middle of the NTC region, which is the flattest portion of the ignition delay curve.

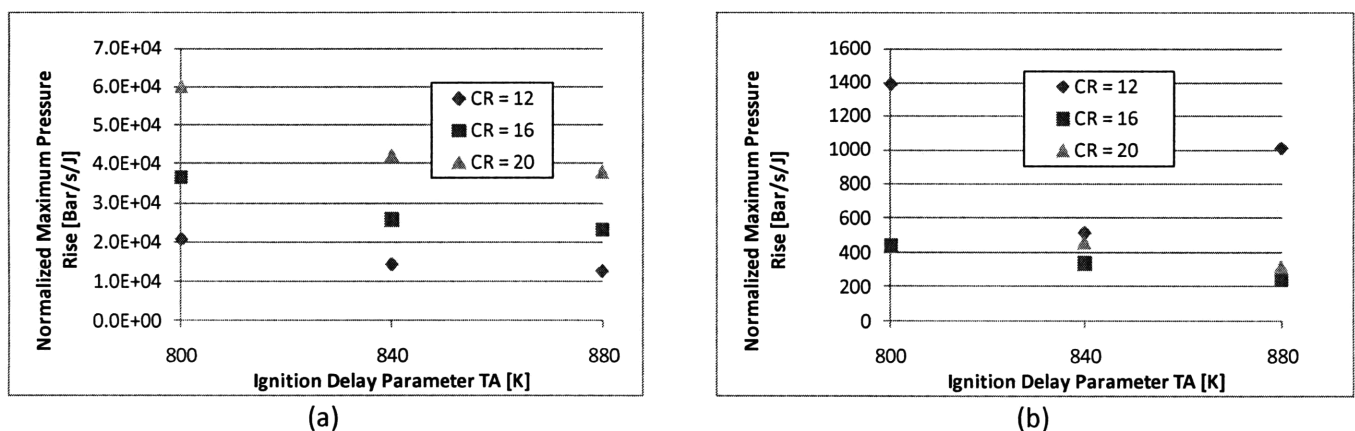


Figure 5-30 MPRR for n-heptane based fuel, impact of T_A : (a) variable volume, uniform temperature distribution (b) variable volume, quadratic temperature distribution

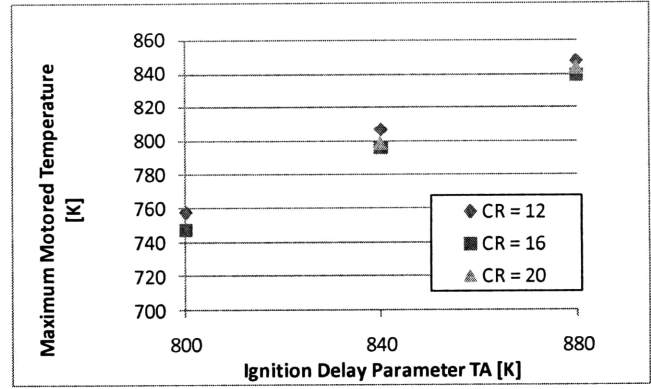
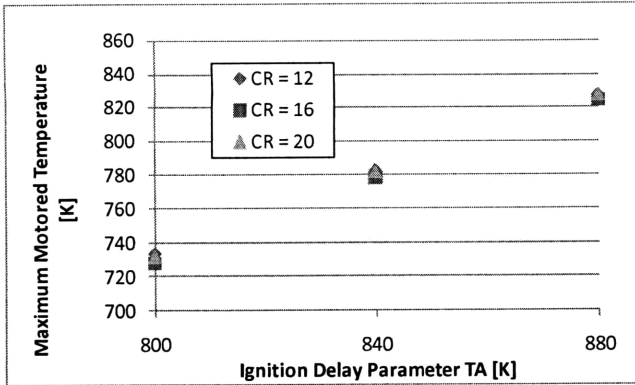


Figure 5-31 Maximum motored temperature for n-heptane based fuel, impact of T_A : (a) variable volume, uniform temperature distribution (b) variable volume, quadratic temperature distribution

5.7.2 Sensitivity to D_A

The parameter D_A represents the vertical shift in the ignition delay curves; see Figure 4-5 (b). The impact of changing D_A is shown in Figure 5-32. Starting with the uniform temperature distribution, it can be seen that at the lowest and highest scale factors, the pressure rise is the highest. This occurs because for the scale factors of 0.1 and 10, combustion occurs outside of the NTC region. The combustion temperature can be obtained from Figure 5-33. Therefore, as demonstrated in the comparison between iso-octane and n-heptane, the two-stage ignition would lead to a lower radical concentration during the main combustion, which would decrease the rate of heat release. With regards to the simulations with a temperature distribution, it is much more difficult to notice a trend.

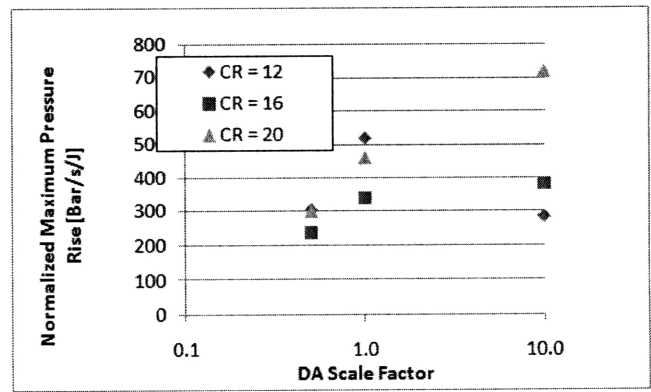
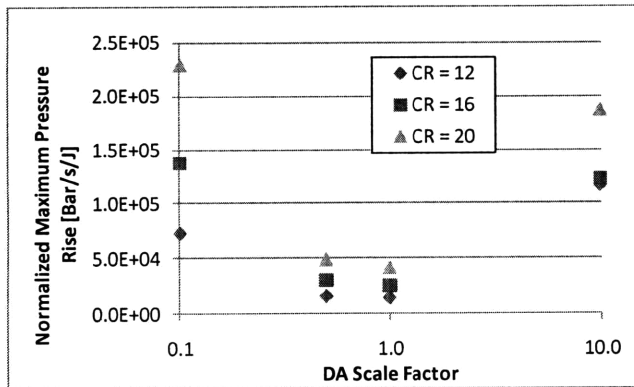


Figure 5-32 MPRR for n-heptane based fuel, impact of D_A : (a) variable volume, uniform temperature distribution (b) variable volume, quadratic temperature distribution

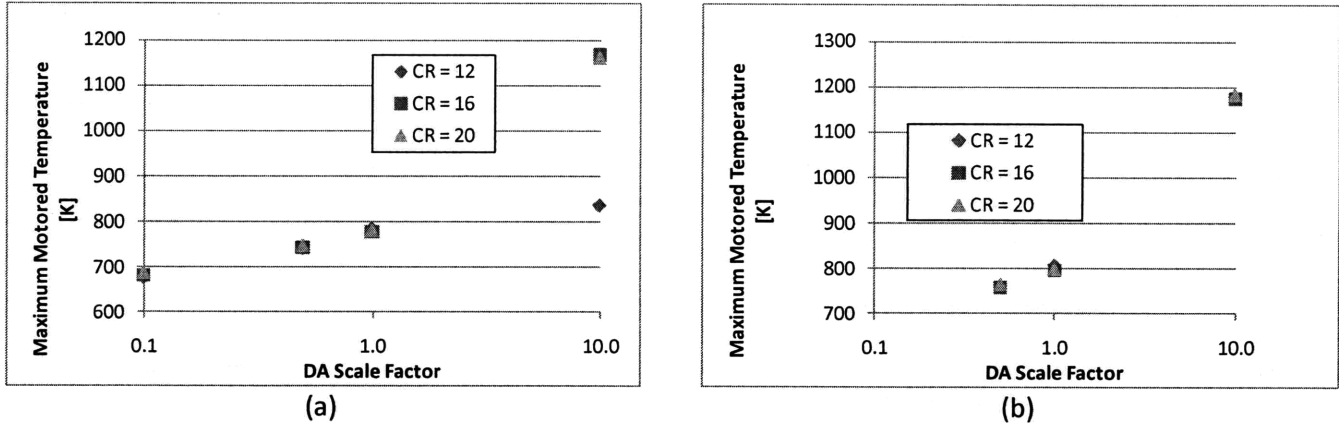


Figure 5-33 Maximum motored temperature for n-heptane based fuel, impact of D_A : (a) variable volume, uniform temperature distribution (b) variable volume, quadratic temperature distribution

5.7.3 Sensitivity to n_1

The parameter n_1 represents the low temperature logarithmic slope of the ignition delay curves; see Figure 4-5 (c). The impact of changing n_1 on the MPRR is given in Figure 5-34. Unlike the iso-octane based fuels, the n-heptane based fuels ignite in the low temperature and NTC regions, as seen in Figure 5-35; therefore the slope is expected to impact the rate of pressure rise. Starting with the uniform temperature distribution simulations, it can be seen that increasing the slope slightly increases the rate of pressure rise. The larger slope typically leads to combustion outside of the NTC region, which can lead to a larger radical concentration and faster heat release rates. With regards to the simulations with a parabolic temperature distribution, a significant drop in the rate of pressure rise is obtained as the slope increases. This occurs because with the larger slope, ignition occurs slightly before the NTC region, away from the flat region of the curve.

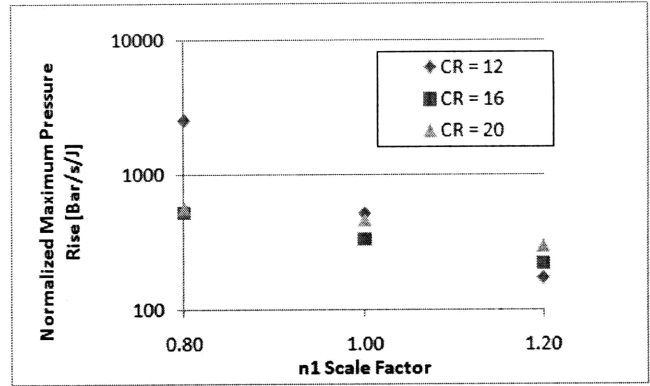
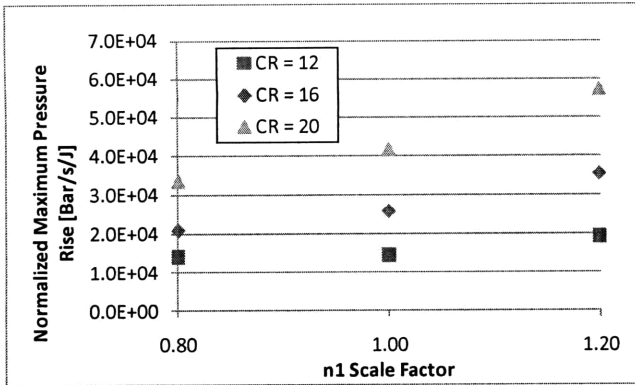


Figure 5-34 MPRR for n-heptane based fuel, impact of n_1 : (a) variable volume, uniform temperature distribution (b) variable volume, quadratic temperature distribution

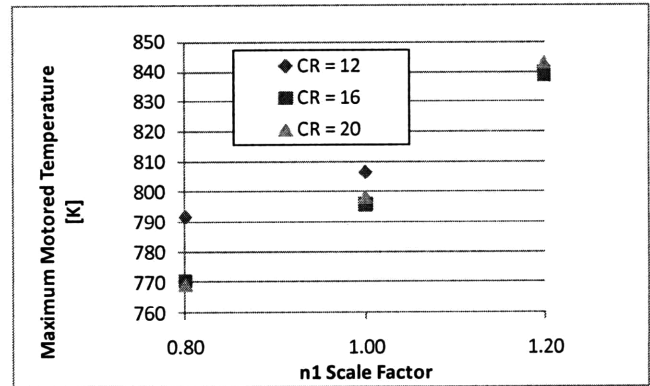
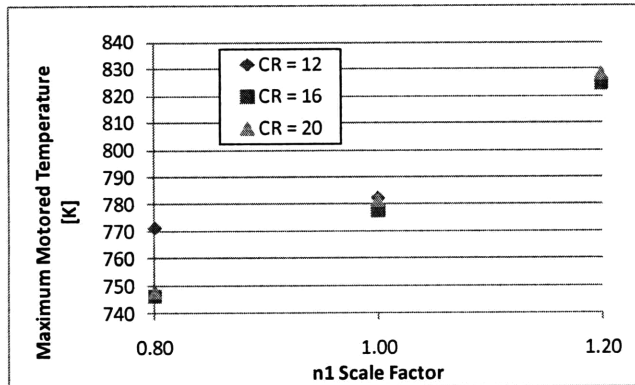
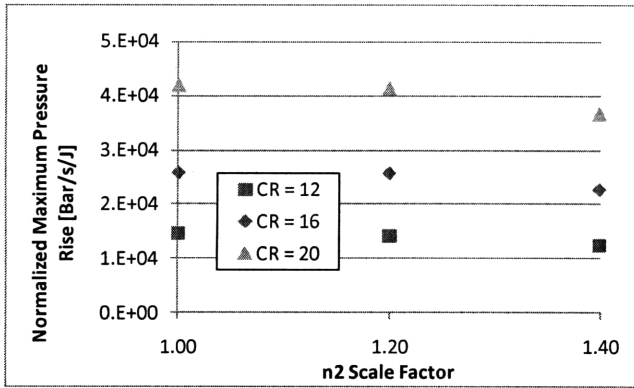


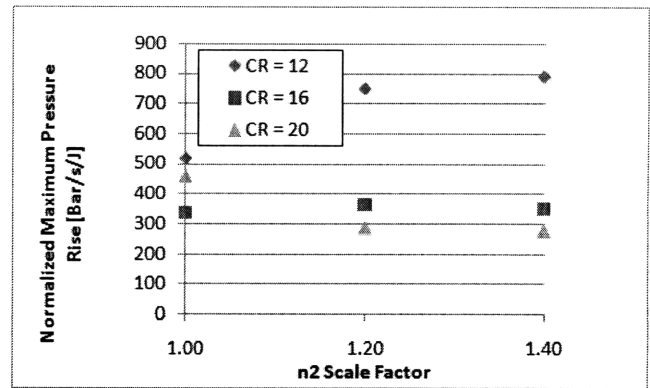
Figure 5-35 Maximum motored temperature for n-heptane based fuel, impact of n_1 : (a) variable volume, uniform temperature distribution (b) variable volume, quadratic temperature distribution

5.7.4 Sensitivity to n_2

The parameter n_2 represents the high temperature logarithmic slope of the ignition delay curves; see Figure 4-5 (d). The impact of changing n_2 on the MPRR is given in Figure 5-36. Since ignition occurs in the low temperature and NTC region (based on Figure 5-37), there does not seem to be a large impact when n_2 is changed.

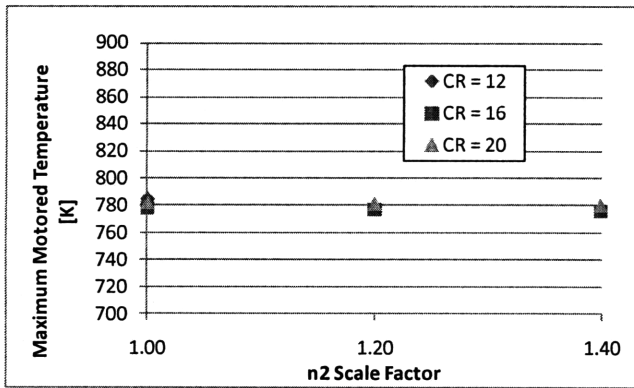


(a)

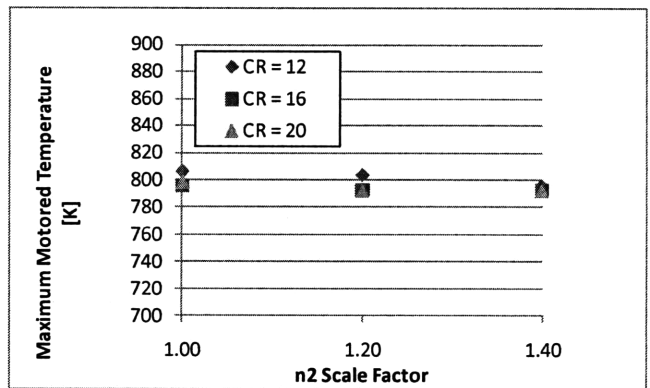


(b)

Figure 5-36 MPRR for n-heptane based fuel, impact of n_2 : (a) variable volume, uniform temperature distribution (b) variable volume, quadratic temperature distribution



(a)



(b)

Figure 5-37 Maximum motored temperature for n-heptane based fuel, impact of n_2 : (a) variable volume, uniform temperature distribution (b) variable volume, quadratic temperature distribution

5.7.5 Sensitivity to y_{NTC}

The parameter y_{NTC} represents the vertical length of the NTC region; see Figure 4-5 (e). The impact of changing y_{NTC} on the MPRR is given in Figure 5-38. With a uniform temperature, the rate of pressure rise increases slightly as the vertical length increases. This is due to the different path taken by the radicals after ignition, which alters the radical concentration at the point of maximum pressure rise. When a quadratic temperature distribution is introduced, the results do not follow a discernible trend. The location of ignition does not change (see Figure 5-39), but the rate of heat release of individual zones after ignition does change. Therefore, the interaction between the zones and the time delay

between ignition events would be altered. Since ignition is occurring in the NTC region, where zone combustion events do not occur in an ordered manner, it is not expected that any trend can be developed.

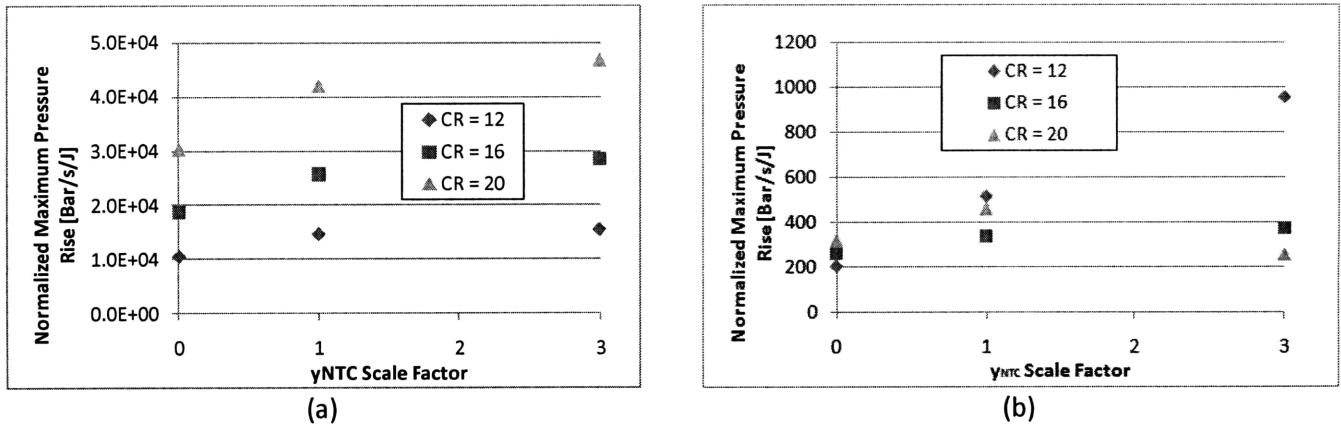


Figure 5-38 MPRR for n-heptane based fuel, impact of γ_{NTC} : (a) variable volume, uniform temperature distribution (b) variable volume, quadratic temperature distribution

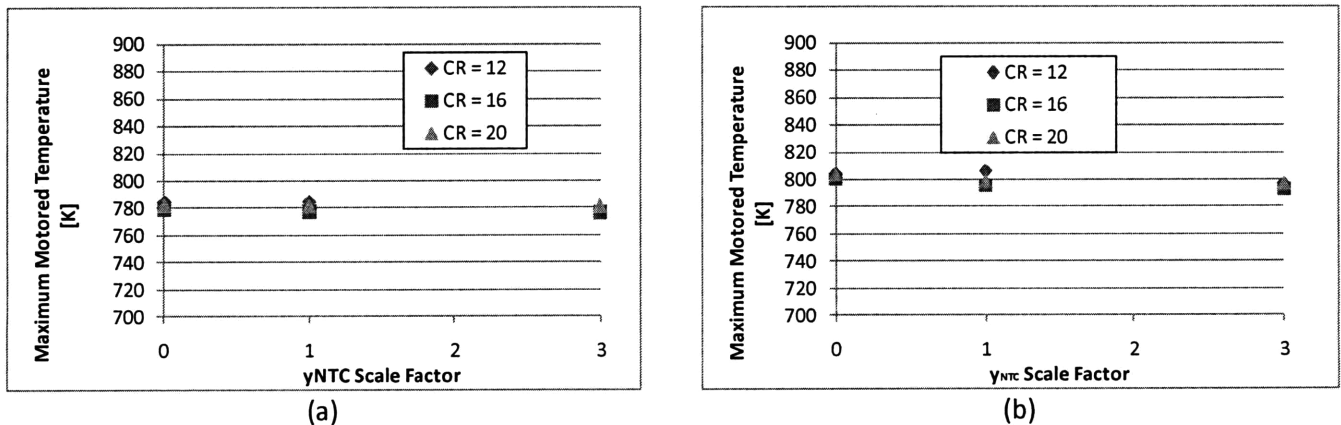


Figure 5-39 Maximum motored temperature for n-heptane based fuel, impact of γ_{NTC} : (a) variable volume, uniform temperature distribution (b) variable volume, quadratic temperature distribution

5.7.6 Sensitivity to Low Temperature Branching Global Parameter

The Shell Model parameter A_{f1} was used to change the low temperature branching agent formation rate; see Figure 4-6 (a). The dependence of the rate of pressure rise on A_{f1} is given in Figure 5-40. With regards to the uniform temperature distribution simulations, there is a sudden increase in the rate of pressure rise as A_{f1} decreases below a scale factor of 1. This occurs because the ignition point (obtained

from Figure 5-41) shifts from the NTC region to the high temperature region, which increases the radical concentration at the location of maximum pressure rise. Moving to the quadratic temperature distribution simulations, there is a peak around a scale factor of 1, which corresponds to ignition near the NTC region. Below this scale factor, ignition shifts to the low temperature region and above this scale factor ignition shifts to the high temperature region.

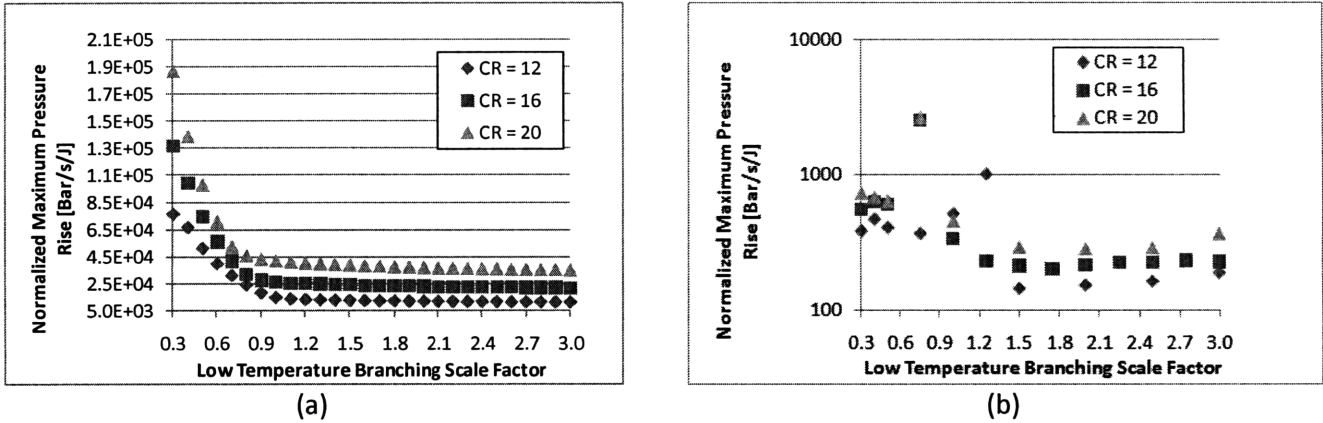


Figure 5-40 MPRR for n-heptane based fuel, impact of A_{f1} : (a) variable volume, uniform temperature distribution (b) variable volume, quadratic temperature distribution

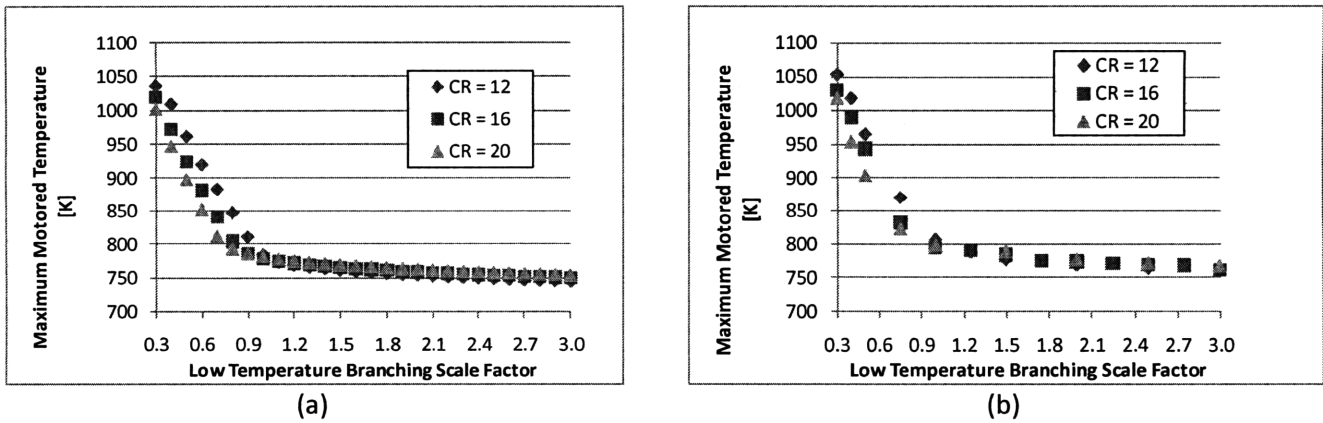


Figure 5-41 Maximum motored temperature for n-heptane based fuel, impact of A_{f1} : (a) variable volume, uniform temperature distribution (b) variable volume, quadratic temperature distribution

5.7.7 Sensitivity to High Temperature Branching Global Parameter

The Shell Model parameter A_{f2} was used to change the high temperature branching agent formation rate; see Figure 4-6 (b). The impact of changing A_{f2} on the MPRR is given in Figure 5-42. For the uniform

temperature simulations, the rate of pressure rise increases as A_{f2} increases, because A_{f2} governs the rate of heat release at the high temperatures. When a quadratic temperature distribution is added, there is a peak in the maximum pressure rise around a scale factor of 1. Once again, this corresponds to ignition in the NTC region, as shown in Figure 5-43.

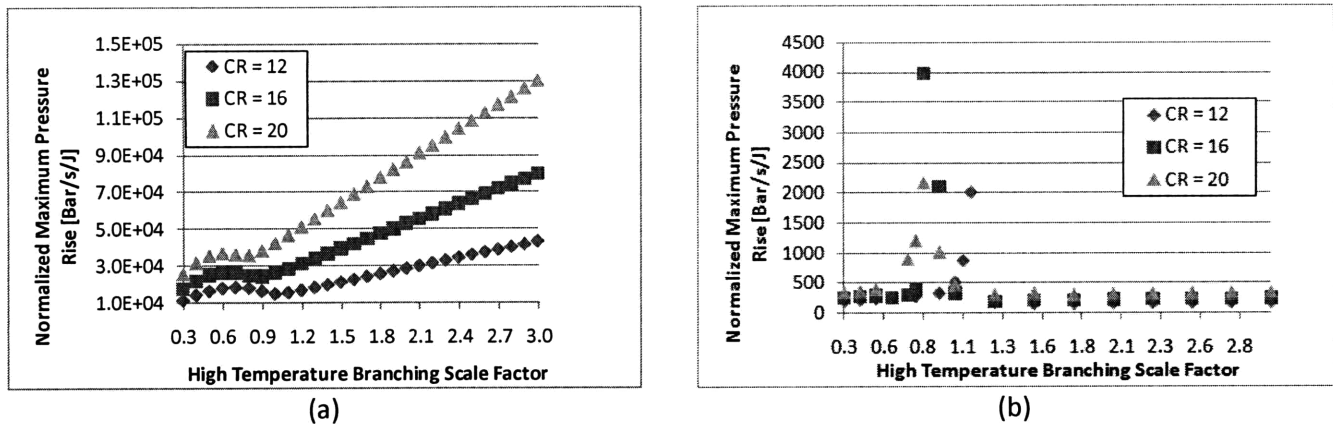


Figure 5-42 MPRR for n-heptane based fuel, impact of A_{f2} : (a) variable volume, uniform temperature distribution (b) variable volume, quadratic temperature distribution

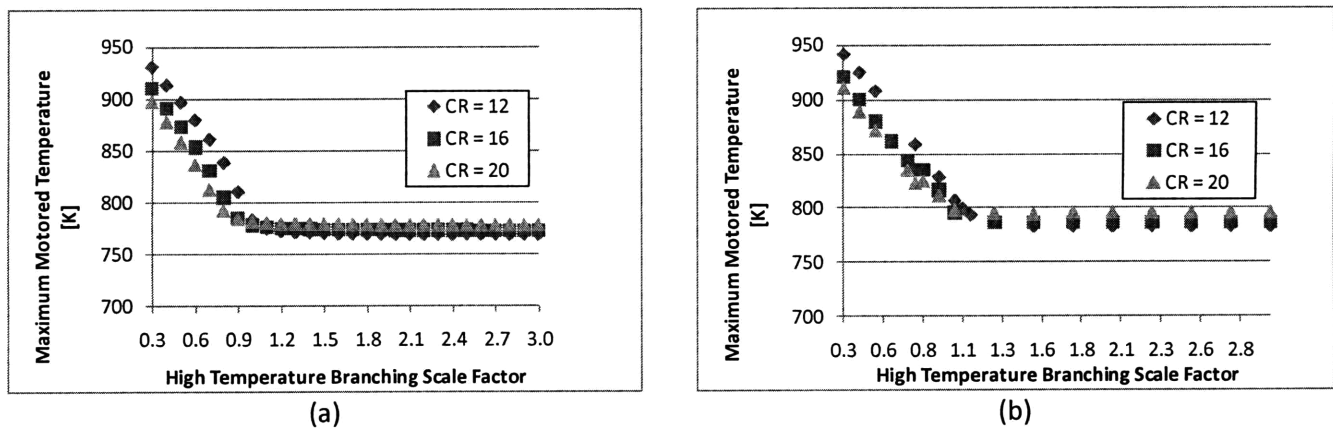


Figure 5-43 Maximum motored temperature for n-heptane based fuel, impact of A_{f2} : (a) variable volume, uniform temperature distribution (b) variable volume, quadratic temperature distribution

Chapter 6. Discussion and Summary

The objective of this report was to assess the impact of fuel on the rate of pressure rise in CAI engines by artificially changing the fuel ignition behavior. The fuel has a direct dependence through its combustion chemistry, particularly the kinetic parameters governing the high temperature heat release rate. The fuel also has an indirect dependence through its sensitivity on the operating conditions and charge stratification.

To study the impact of fuel on the rate of pressure rise, the fuel ignition delay curve was parameterized, and the impact of each parameter was studied. This was accomplished by manipulating the pseudo-kinetic parameters in the Shell Model, which is a well established model for predicting the ignition behavior for practical fuels. An optimization program was developed to translate a pre-defined ignition delay curve into parameter values for the fuel chemical model.

A summary of the dependence of the rate of pressure rise on the fuel parameters is given in Appendix F. It should be noted that the trends presented in Appendix F are only applicable for the range of the ignition delay parameter tested. Moving outside the tested range will likely introduce additional variations. This is not of concern, since the focus of this report is to understand the cause of the trends; not the actual trend. The main conclusions are presented in the following sections.

6.1 Minimizing MPRR in a Charge with a Uniform Temperature Distribution

- The kinetic rate parameters can have a large affect on the MPRR by increasing the rate of heat release at the temperature corresponding to the location of the MPRR. This effect would fall in the “combustion chemistry” column in Figure 1-4. For the simple reaction fuels, the rate of heat release can be easily correlated to the kinetic rate parameters and temperature. Therefore, the effect of changing the kinetic rate parameters can be easily determined.

- When ignition occurs in the high temperature region, it is beneficial to have a lower slope, n_2 , which would reduce the rate of heat release at the temperature corresponding to the MPRR
- When ignition occurs in the NTC region, the radical concentration later in the combustion process is reduced, which reduces the maximum rate of pressure rise.

6.2 Minimizing MPRR in a Charge with a Quadratic Temperature Distribution

- When a temperature distribution is present, the absolute slope of the ignition delay versus temperature curve is important. Unfortunately, the relationship between the absolute slope of the ignition delay curve and the rate of pressure rise is not straightforward. Having a larger slope can lead to a larger delay between zone combustion events, and consequently reduce the pressure rise rate. However, having a large slope can also increase the impact of the work interactions between the zones, which acts to increase the pressure rise rate.
- The impact of work interactions between the zones can be reduced by decreasing the heat release rate in each zone. This occurs because the zone combustion events become intertwined, so the work energy transfer has less impact on determining the time of ignition for subsequent zones.
- When comparing the slope of the ignition delay curves for different fuels, it is important to make the comparison at the temperature where the ignition occurs, which has been approximated by using the maximum motored temperature.
- When ignition occurs in the high temperature region, it is beneficial to have a lower slope n_2 . This reduces the negative impact of the zone work interactions.
- Combustion in the NTC region should be avoided. In all cases, the near zero ignition delay slope of the NTC region negates the benefits of having a temperature distribution.

References

1. Stanglmaier, R.H., Roberts, C.E., "Homogeneous Charge Compression Ignition (HCCI): Benefits, Compromises, and Future Engine Applications", SAE Paper 1999-01-3682, 1999.
2. Epping, K., Aceves, S., Bechtold, R., Dec, J., "The Potential of HCCI Combustion for High Efficiency and Low Emissions", SAE Paper 2002-01-1923, 2002.
3. Milovanovic, N., Chen, R., "A Review of Experimental and Simulation Studies on Controlled Auto-Ignition Combustion", SAE Paper 2001-01-1890, 2001.
4. Curran, H.J., Pitz, W.J., Westbrook, C.K., Callahan, C.V., Dryer, F.L., "Oxidation of Automotive Primary Reference Fuels at Elevated Pressures", Twenty-Seventh International Conference on Combustion, Boulder, CO, August 2-7, 1998.
5. Andrae, M.M., Cheng, W.K., Kenney, T., Yang, J., "On HCCI Engine Knock", SAE Paper 2007-01-1858, 2007.
6. Christensen, M., Johansson, B., Amneus, P., Mauss, F., "Supercharged Homogeneous Charge Compression Ignition", SAE Paper 980787, 1998.
7. Curran, H.J., Gaffuri, P., Pitz, W.J., Westbrook, C.K., "A Comprehensive Modeling Study of iso-Octane Oxidation", Combustion and Flame, 129:253-280, 2002.
8. Curran, H.J., Gaffuri, P., Pitz, W.J., Westbrook, C.K., "A Comprehensive Modeling Study of n-Heptane Oxidation", Combustion and Flame, 114:149-177, 1998.
9. Marinov, N.M., "A Detailed Chemical Kinetic Model for High Temperature Ethanol Oxidation", International Journal of Chemical Kinetics, 31:183-220, 1999.
10. Andrae, J.C.G., Bjornbom, P., Cracknell, R.F., Kalghatgi, G.T., "Autoignition of toluene reference fuels at high pressures modeled with detailed chemical kinetics", Combustion and Flame, 149:2-24, 2007.

11. Tanaka, S., Ayala, F., Keck, J., "A reduced chemical kinetic model for HCCI combustion of primary reference fuels in a rapid compression machine", *Combustion and Flame*, 133:467-481, 2003.
12. Griffiths, J.F., "Reduced Kinetic Models and their Application to Practical Combustion Systems", *Prog. Energy Combust. Sci.*, 21:25-107, 1995.
13. Halstead, M.P., Kirsch, L.J., Quinn, C.P., "The Autoignition of Hydrocarbon Fuels at High Temperatures and Pressures – Fitting of a Mathematical Model", *Combustion and Flame* 30:45-60, 1977.
14. Halstead, M.P., Kirsch, L.J., Prothero, A., Quinn, C.P., "A mathematical model for hydrocarbon autoignition at high pressures", *Proc. Roy. Soc.* A346:515-538, 1975.
15. Wang, Z., Shuai, S., Wang, J., Tian, G., An, X., "Modeling of HCCI Combustion: From OD to 3D", SAE Paper 2006-01-1364, 2006.
16. Wang, Z., Wang, J., Shuai, S., Zhang, F., "Numerical Simulation of HCCI Engine With Multi-Stage Gasoline Direct Injection Using 3D-CFD With Detailed Chemistry", SAE Paper 2004-01-0563, 2004.
17. Kong, S., Marriott, C.D., Reitz, R.D., Christensen, M., "Modeling and Experiments of HCCI Engine Combustion Using Detailed Chemical Kinetics with Multidimensional CFD", SAE Paper 2001-01-1026, 2001.
18. Li, G., Bo, T., Chen, C., Johns, R., "CFD Simulation of HCCI Combustion in a 2-Stroke DI Gasoline Engine", SAE Paper 2003-01-1855, 2003.
19. Aceves, S.M., Flowers, D.L., Westbrook, C.K., et. al., "A Multi-Zone Model for Prediction of HCCI Combustion and Emissions", SAE Paper 2000-01-0327, 2000.
20. Aceves, S.M., Martinez-Frias, J., Flowers, D.L., et. al., "A Decoupled Model of Detailed Fluid Mechanics Followed by Detailed Chemical Kinetics for Prediction of Iso-Octane HCCI Combustion", SAE Paper 2001-01-3612, 2001.

21. Easley, W.L., Agarwal, A., Lavoie, G.A., "Modeling of HCCI Combustion and Emissions Using Detailed Chemistry", SAE Paper 2001-01-1029, 2001.
22. Heywood, J.B., *Internal Combustion Engine Fundamentals*, McGraw-Hill, New York, 1988.

Appendix A

Shell Ignition Model:

The reaction mechanism for the modified Shell Model is given in Table A-1. Reaction number R9 was added to the mechanism published in [13] to produce the significant heat release due to CO oxidation.

Table A-1 Modified Shell Model

$RH + O_2 \xrightarrow{k_q} 2R$	Initiation	[R1]
$R \xrightarrow{k_p} R$	Propagation cycle	[R2]
$R \xrightarrow{f_1 k_p} R + B$	Propagation forming B	[R3]
$R + Q \xrightarrow{f_2 k_p} R + B$	Propagation forming B	[R4]
$R \xrightarrow{f_3 k_p} out$	Linear termination	[R5]
$R \xrightarrow{f_4 k_p} R + Q$	Propagation forming Q	[R6]
$2R \xrightarrow{k_t} out$	Quadratic termination	[R7]
$B \xrightarrow{k_B} 2R$	Degenerate branching	[R8]
$CO + R \xrightarrow{k_{CO}} CO_2 + R$	CO to CO ₂ conversion	[R9]

The reaction rate coefficients are given by the equations below. Note that there are 26 unknown parameters

$$k_q = A_q \exp\left(\frac{-E_q}{RT}\right) \quad [A.1]$$

$$k_{p1} = A_{p1} \exp\left(\frac{-E_{p1}}{RT}\right) \quad [A.2]$$

$$k_{p2} = A_{p2} \exp\left(\frac{-E_{p2}}{RT}\right) \quad [A.3]$$

$$k_{p3} = A_{p3} \exp\left(\frac{-E_{p3}}{RT}\right) \quad [A.4]$$

$$k_p = \frac{1}{\frac{1}{k_{p1}[O_2]} + \frac{1}{k_{p2}} + \frac{1}{k_{p3}[RH]}} \quad [A.5]$$

$$f_1 = A_{f1} \exp\left(\frac{-E_{f1}}{RT}\right) [O_2]^{x_1} [RH]^{y_1} \quad [A.6]$$

$$f_2 = A_{f2} \exp\left(\frac{-E_{f2}}{RT}\right) \quad [A.7]$$

$$f_3 = A_{f3} \exp\left(\frac{-E_{f3}}{RT}\right) [O_2]^{x_3} [RH]^{y_3} \quad [A.8]$$

$$f_4 = A_{f4} \exp\left(\frac{-E_{f4}}{RT}\right) [O_2]^{x_4} [RH]^{y_4} \quad [A.9]$$

$$k_t = A_t \exp\left(\frac{-E_t}{RT}\right) \quad [A.10]$$

$$k_B = A_B \exp\left(\frac{-E_B}{RT}\right) \quad [A.11]$$

$$k_{CO} = A_{CO} T^{n_{CO}} \exp\left(\frac{-E_{CO}}{RT}\right) \quad [A.12]$$

A_{CO} , n_{CO} , and E_{CO} in equation [A.12] were obtained from [22] and left constant.

Finally, the constant volume combustion equations are given by the equations below for a fuel with n carbon atoms and $2m$ hydrogen atoms.

$$\frac{d[R]}{dt} = 2k_q[RH][O_2] + 2k_B[B] - 2k_t - f_3 k_p[R] \quad [A.13]$$

$$\frac{d[B]}{dt} = f_1 k_p[R] + f_2 k_p[R][Q] - k_B[B] \quad [A.14]$$

$$\frac{d[Q]}{dt} = f_4 k_p[R] - f_2 k_p[R][Q] \quad [A.15]$$

$$\frac{d[RH]}{dt} = -\frac{1}{m} k_p[R] \quad [A.16]$$

$$\frac{d[O_2]}{dt} = -p k_p[R] - \frac{1}{2} k_{CO}[CO][R] \quad [A.17]$$

$$\frac{d[CO]}{dt} = \frac{n}{m} k_p[R] - k_{CO}[CO][R] \quad [A.18]$$

$$c_v \frac{dT}{dt} = \frac{1}{M} \{Q_1 k_p[R] + Q_2 k_{CO}[CO][R]\} \quad [A.19]$$

The oxygen consumption for each propagation cycle is given by p:

$$p = \frac{n + m}{2m} \quad [\text{A.20}]$$

Q_1 is the total exothermicity of a propagation cycle and Q_2 is the heat of reaction of CO to CO_2 conversion.

Appendix B

Equations Used to Determine Model Parameters:

Section 2.1.2 described the parameter optimization steps used to determine the parameters in the modified Shell Model. To accelerate the optimization process, a number of algebraic equations were used to help determine the required parameters. The equations were used in conjunction with the Steepest Descent Method to find the optimum parameters that would match the predefined ignition delay curve.

Before describing the algebraic equations that were developed, it is worth introducing a few new terms, following the terminology outlined in [14]. The branching factors are given by:

$$\phi = (2f_1 - f_3)k_p \quad [\text{B.1}]$$

$$\phi'' = (2f_1 + 2f_2Q - f_3)k_p \quad [\text{B.2}]$$

The branching factors can be used to gauge ignition delay times because it changes from positive to negative in the NTC region, and then back to positive during main ignition. The branching factor given in equation [B.1] assumes that the concentration of the intermediate species is zero, and can therefore be used in the low temperature region. Primary initiation generates radicals at a rate of:

$$v_q = 2k_q[O_2][RH] \quad [\text{B.3}]$$

The equilibrium radical concentration (found by setting the rate of change of R and B to zero) is given by:

$$\bar{R} = \frac{\phi'' + \sqrt{\phi''^2 + 8v_qk_t}}{4k_t} \quad [\text{B.4}]$$

Using the above definitions, the algebraic equations that were used to determine the appropriate model parameters can now be described. The first equation developed approximates the low temperature first stage ignition delay time by solving the following set of first order differential equations:

$$\frac{d[R]}{dt} = 2k_B[B] - 2k_t - f_3k_p[R] \quad [\text{B.5}]$$

$$\frac{d[B]}{dt} = f_1k_p[R] - k_B[B] \quad [\text{B.6}]$$

The first stage ignition delay time given by equation [B.7] is then assumed to be the time it takes for the radical concentration to reach its equilibrium value given by equation [B.4]. Note that at this stage, the intermediate species Q is set to zero.

$$\tau_1 = \frac{\log\left(\frac{\bar{R}}{c_1}\right)}{c_2} \quad [\text{B.7}]$$

$$c_1 = v_q \frac{c_3 + (4f_1k_p - f_3k_p + k_B)}{2c_3\phi} \quad [\text{B.8}]$$

$$c_2 = \frac{1}{2} [c_3 - f_3k_p - k_B] \quad [\text{B.9}]$$

$$c_3 = \sqrt{f_3^2k_p^2 - 2k_Bf_3k_p + 8k_Bf_1k_p + k_B^2} \quad [\text{B.10}]$$

The second equation developed (equation [B.11]) approximates the total ignition delay time in the high temperature region. The derivation follows the approach outlined in [14].

$$\tau_{TOTAL} = \frac{\phi^2}{4f_2f_4v_qk_p^2} \quad [\text{B.11}]$$

The third equation approximates the temperature at which the NTC region ends. This is derived by setting the branching factor in equation [B.1] to zero.

$$T_{NTC} = \frac{E_{f3} - E_{f1}}{R_u \log\left(\frac{Af_3}{2Af_1} [O_2]^{x_3-x_1} [RH]^{y_3-y_1}\right)} \quad [\text{B.12}]$$

Given a desired ignition delay curve, equations [B.7], [B.11], and [B.12] can then be used along with the Steepest Descent Method to determine appropriate model parameters. However, one issue that has been overlooked thus far is the shape of the heat release profile. To ensure that the model parameters give a first stage heat release profile that mimics real fuels, a shape factor was added to the

set of equations solved. Since the heat release rate is dictated by the radical concentration, the significance of the first stage ignition is given by the ratio of the local maximum and minimum radical concentrations:

$$\textit{Shape Factor} = \frac{R_{MAX}(T_{NTC-50})}{R_{MIN}(T_{NTC-50})} \quad [\text{B.13}]$$

Appendix C

Two-Stage Ignition Characteristics:

The analytical assessment presented in this report distinguishes fuels only with the shape of the ignition delay curve. The ignition delay curve is constructed by varying the initial temperature and molar concentrations in a constant volume batch reactor. Due to the significance of the ignition delay times in this report, it is worthwhile to mention how the first stage and total ignition delay times are defined.

Figure C-1 shows a temperature versus time plot for a sample constant volume batch reactor simulation (n-heptane, initial temperature of 800 K). The first stage and total ignition delay times are as indicated on the figure.

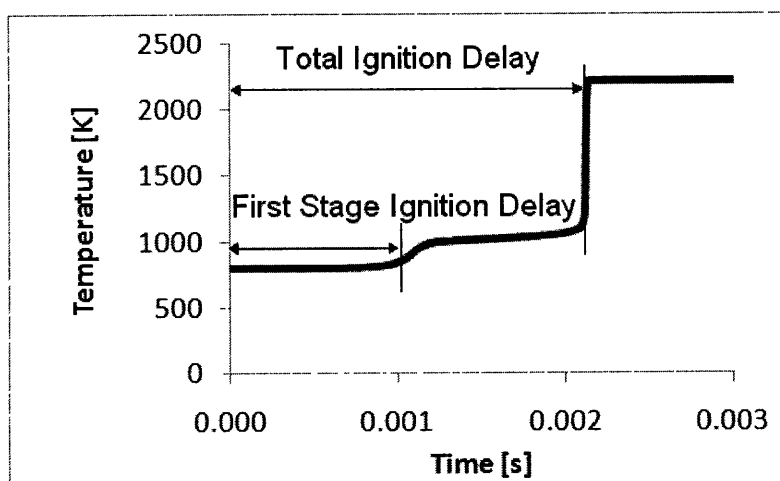


Figure C-1 Ignition characteristics

The first stage ignition delay time is defined as the time at which the branching agent concentration is maximized, as shown in Figure C-2. The total ignition delay time represents the time at which the rate of temperature rise is maximized.

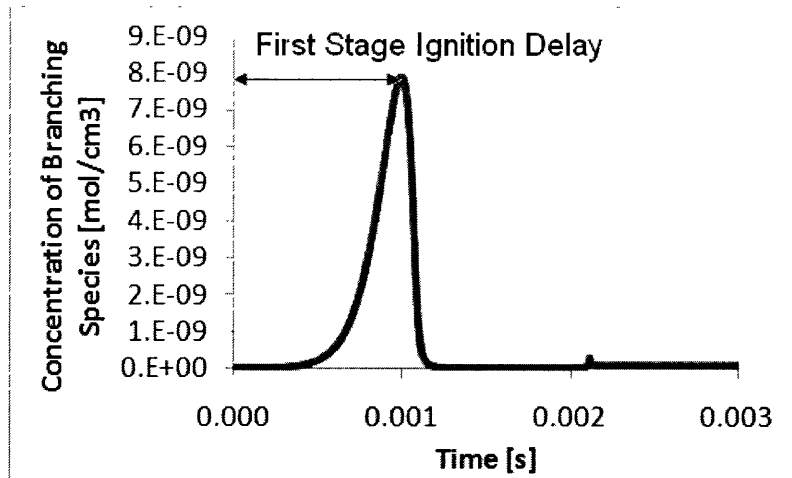


Figure C-2 First stage ignition delay time using branching agent concentration

Appendix D

Single-Zone and Multi-Zone Engine Model Equations:

To determine the MPRR with a uniform and non-uniform temperature distribution, each artificial fuel was inserted into a single zone and multi-zone engine simulation.

The single zone engine model is given below:

$$\frac{1}{V} \frac{dN_R}{dt} = 2k_q[RH][O_2] + 2k_B[B] - 2k_t - f_3k_p[R] \quad [D.1]$$

$$\frac{1}{V} \frac{dN_B}{dt} = f_1k_p[R] + f_2k_p[R][Q] - k_B[B] \quad [D.2]$$

$$\frac{1}{V} \frac{dN_Q}{dt} = f_4k_p[R] - f_2k_p[R][Q] \quad [D.3]$$

$$\frac{1}{V} \frac{dN_{RH}}{dt} = -\frac{1}{m}k_p[R] \quad [D.4]$$

$$\frac{1}{V} \frac{dN_{O_2}}{dt} = -pk_p[R] - \frac{1}{2}k_{CO}[CO][R] \quad [D.5]$$

$$\frac{1}{V} \frac{dN_{CO}}{dt} = \frac{n}{m}k_p[R] - k_{CO}[CO][R] \quad [D.6]$$

$$c_v \frac{dT}{dt} = \frac{RT}{V} \frac{dV}{dt} + \frac{1}{M} \{Q_1k_p[R] + Q_2k_{CO}[CO][R]\} \quad [D.7]$$

The cylinder volume, V , is calculated using engine kinematic equations presented in [22].

The multi-zone engine model uses the same equations as [D.1] to [D.6], except they are solved for each zone. Therefore, the volume, V , in the equations becomes the volume in each zone, V_i . Initially, the total volume is divided equally. However, to maintain a constant pressure, the zone volumes are calculated as:

$$V_i = \frac{N_i T_i}{\sum N_i T_i} V \quad [D.8]$$

An additional term representing the work transfer between the zones also needs to be added to the differential equation for temperature (equation [D.7]). The equivalent equation for the multi-zone model is:

$$c_P \frac{dT_i}{dt} = \frac{R_u T_i}{\sum N_j T_j} \sum N_j \frac{dT_j}{dt} + \frac{1}{M_i} \{Q_1 k_{P_i} [R]_i + Q_2 k_{CO_i} [CO]_i [R]_i\} \quad [D.9]$$

To simplify the equation, the change in the number of moles with time was neglected.

Appendix E

To ensure that the 50% heat release point occurs at top dead center, the initial charge temperature was modified for all of the engine simulations. This appendix will provide the initial temperatures used for all of the engine simulations. In the case of the simulations with a quadratic temperature distribution, the maximum temperature is plotted.

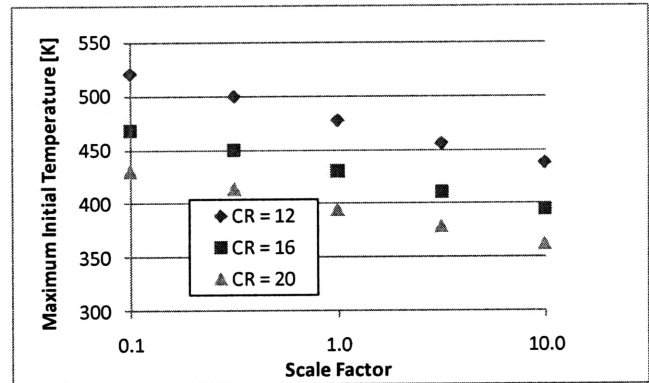
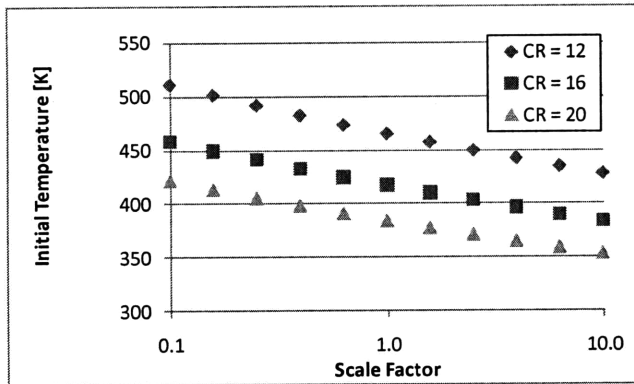


Figure E-1 Initial temperature for single reaction fuels, effect of position: (a) uniform temperature distribution (b) quadratic temperature distribution

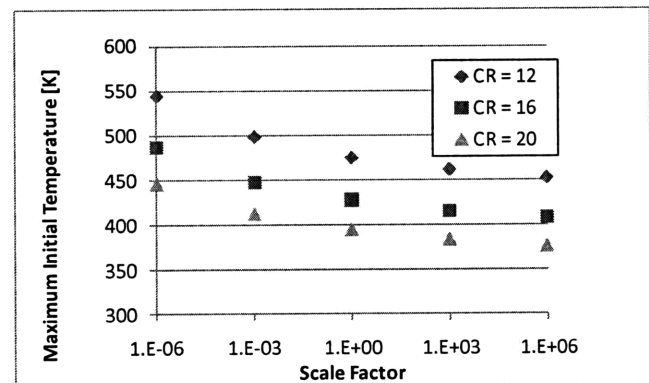
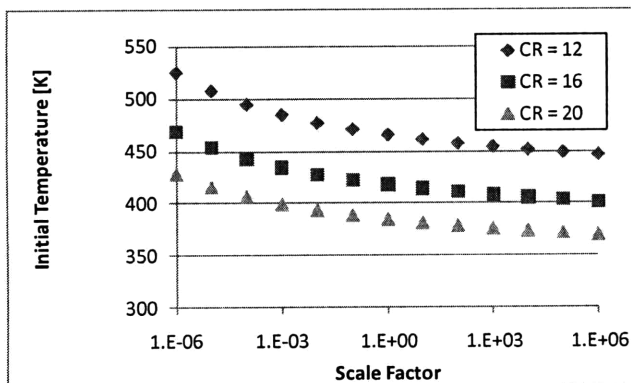


Figure E-2 Initial temperature for single reaction fuels, effect of slope with pivot at 900 K: (a) uniform temperature distribution (b) quadratic temperature distribution

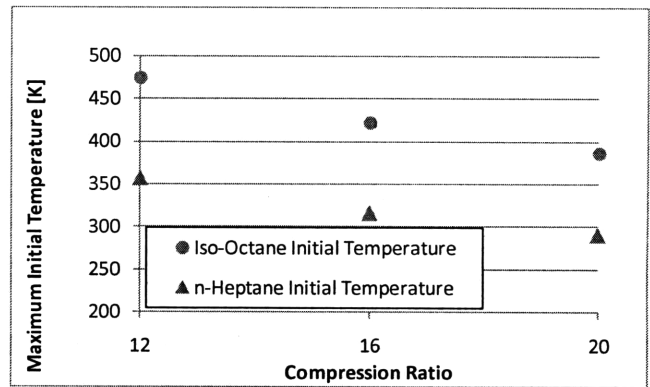
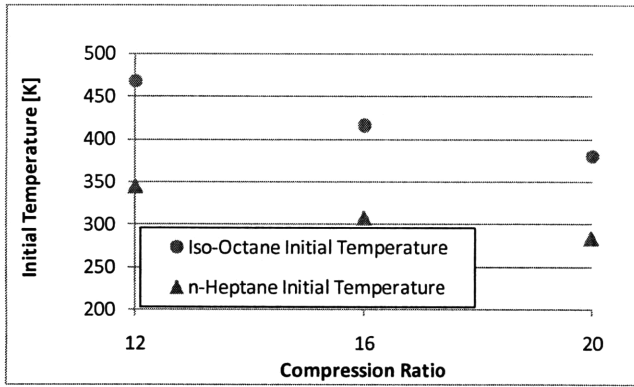


Figure E-3 Initial temperature for iso-octane and n-heptane simulations: (a) uniform temperature distribution (b) quadratic temperature distribution

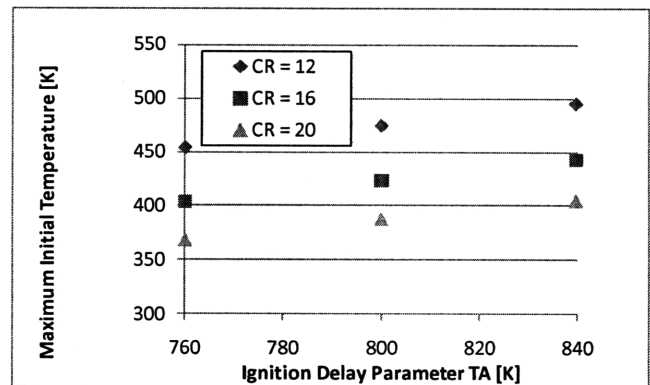
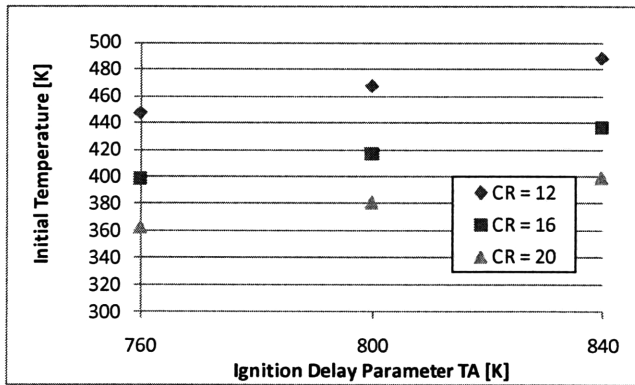


Figure E-4 Initial temperature for iso-octane based fuel, impact of T_A : (a) variable volume, uniform temperature distribution (b) variable volume, quadratic temperature distribution

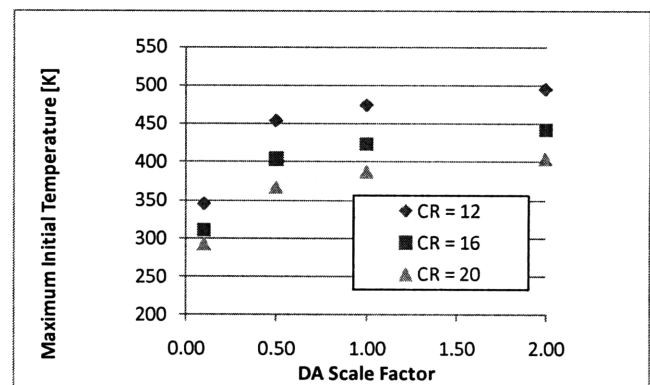
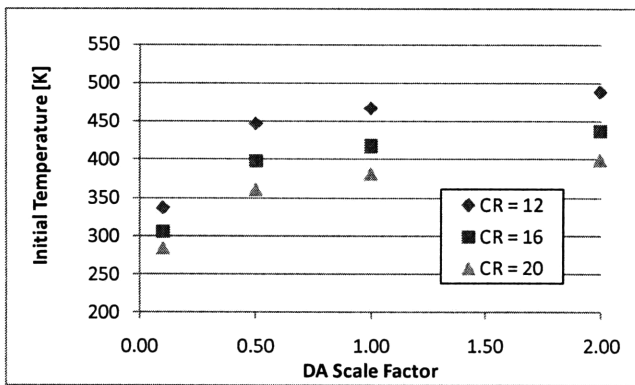


Figure E-5 Initial temperature for iso-octane based fuel, impact of D_A : (a) variable volume, uniform temperature distribution (b) variable volume, quadratic temperature distribution

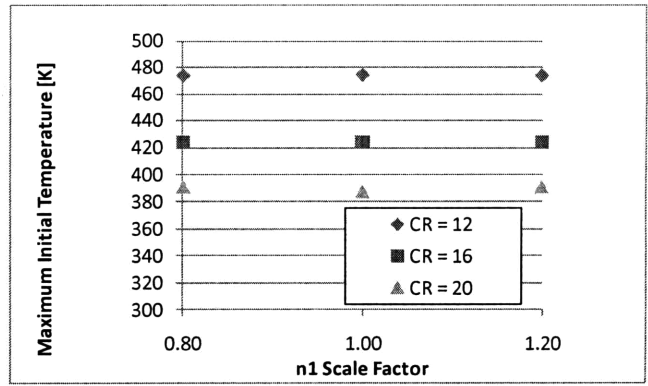
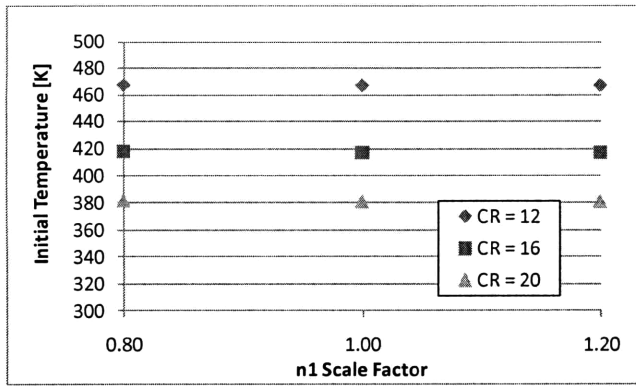


Figure E-6 Initial temperature for iso-octane based fuel, impact of n_1 : (a) variable volume, uniform temperature distribution (b) variable volume, quadratic temperature distribution

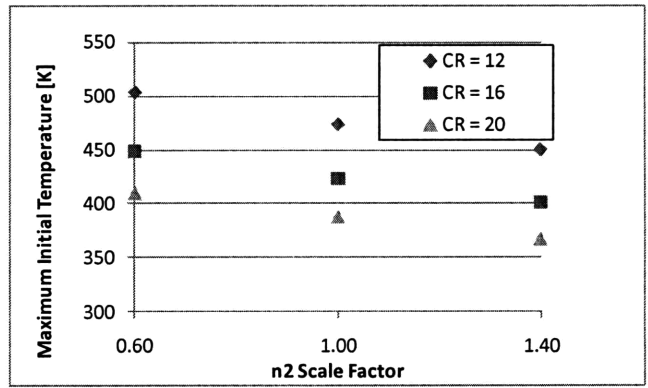
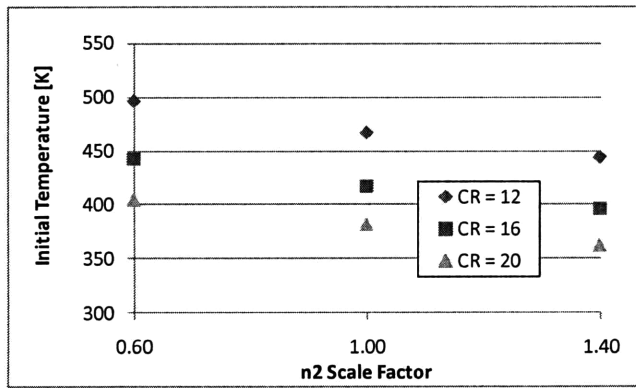


Figure E-7 Initial temperature for iso-octane based fuel, impact of n_2 : (a) variable volume, uniform temperature distribution (b) variable volume, quadratic temperature distribution

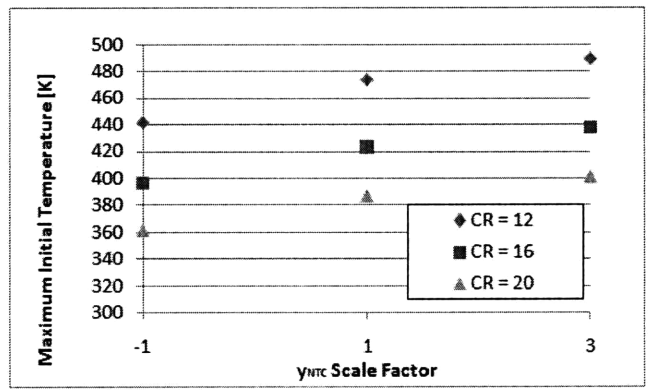
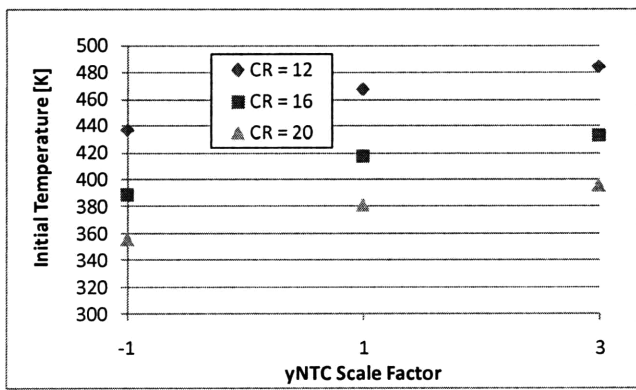


Figure E-8 Initial temperature for iso-octane based fuel, impact of γ_{NTIC} : (a) variable volume, uniform temperature distribution (b) variable volume, quadratic temperature distribution

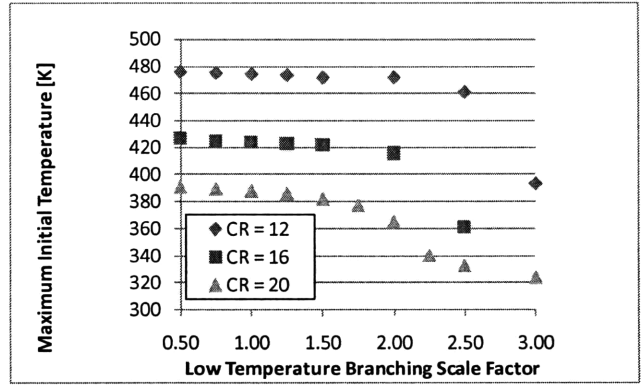
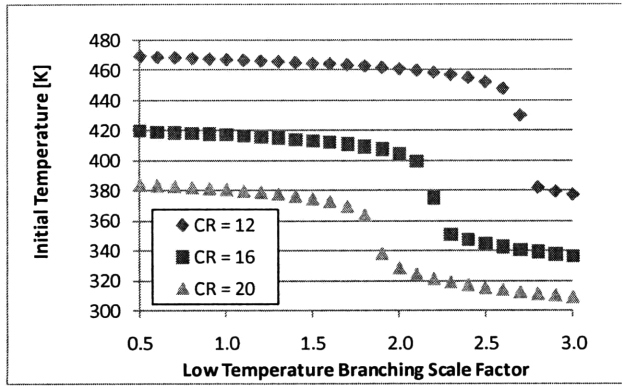


Figure E-9 Initial temperature for iso-octane based fuel, impact of A_{T1} : (a) variable volume, uniform temperature distribution (b) variable volume, quadratic temperature distribution

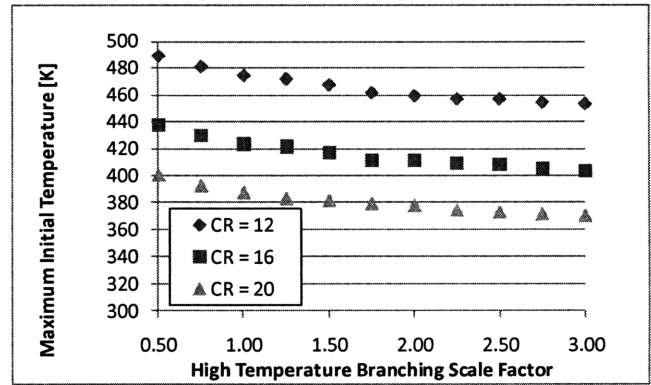
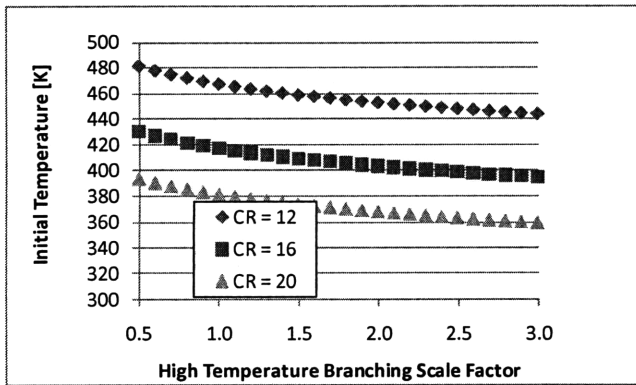


Figure E-10 Initial temperature for iso-octane based fuel, impact of A_{T2} : (a) variable volume, uniform temperature distribution (b) variable volume, quadratic temperature distribution

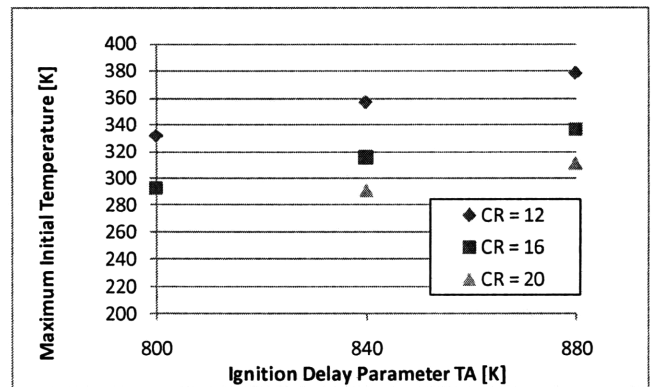
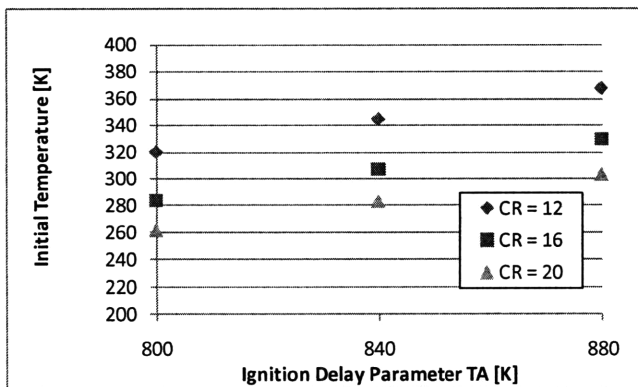


Figure E-11 Initial temperature for n-heptane based fuel, impact of T_A : (a) variable volume, uniform temperature distribution (b) variable volume, quadratic temperature distribution

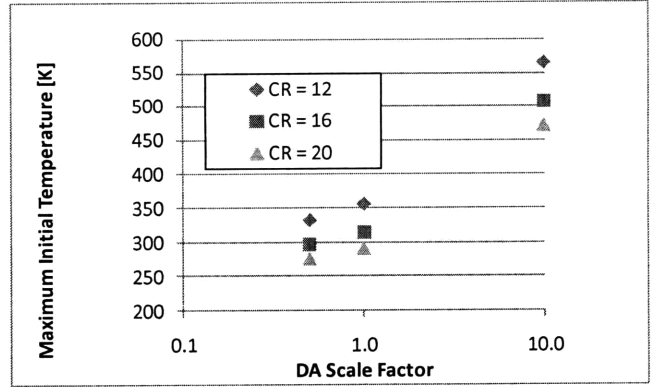
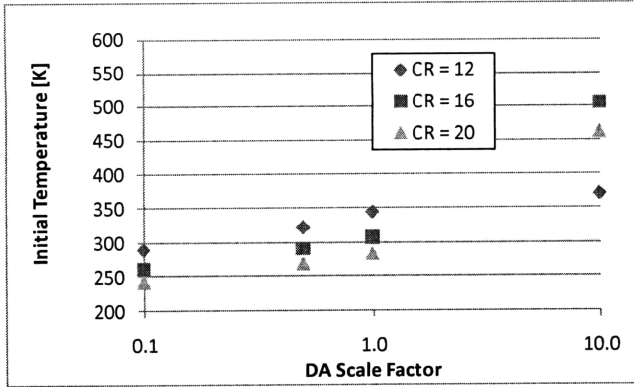


Figure E-12 Initial temperature for n-heptane based fuel, impact of D_A : (a) variable volume, uniform temperature distribution (b) variable volume, quadratic temperature distribution

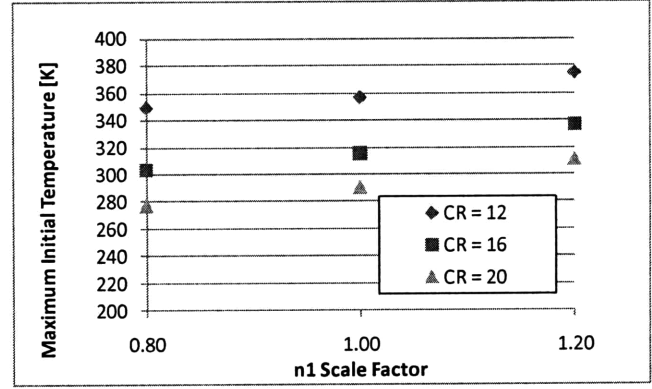
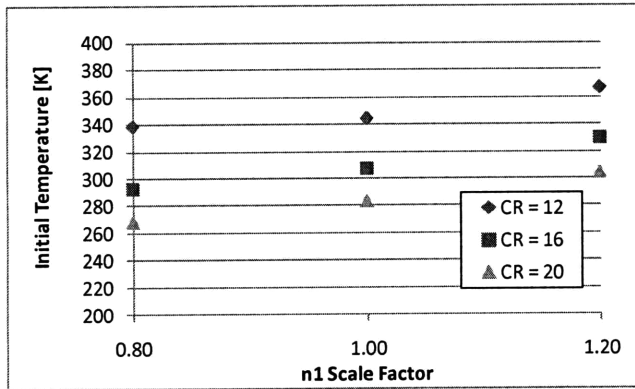


Figure E-13 Initial temperature for n-heptane based fuel, impact of n_1 : (a) variable volume, uniform temperature distribution (b) variable volume, quadratic temperature distribution

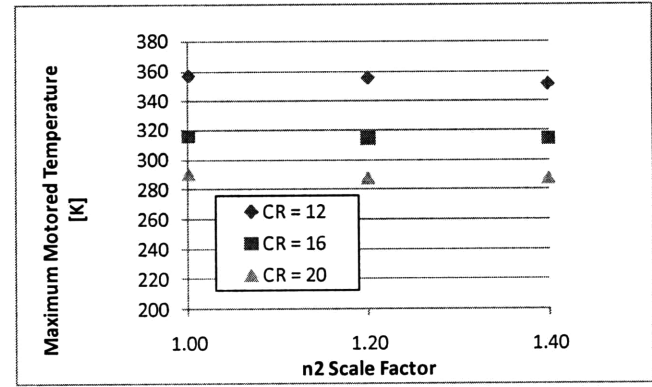
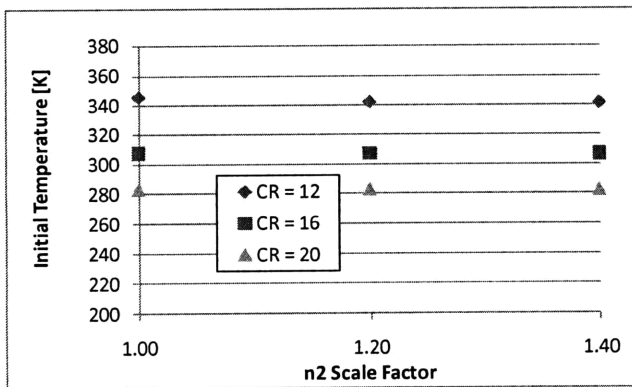


Figure E-14 Initial temperature for n-heptane based fuel, impact of n_2 : (a) variable volume, uniform temperature distribution (b) variable volume, quadratic temperature distribution

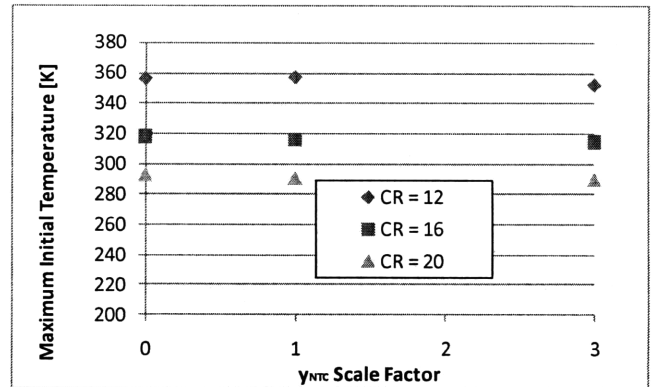
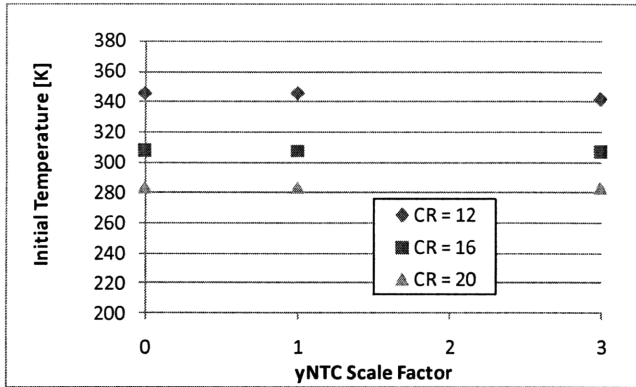


Figure E-15 Initial temperature for n-heptane based fuel, impact of γ_{NTC} : (a) variable volume, uniform temperature distribution (b) variable volume, quadratic temperature distribution

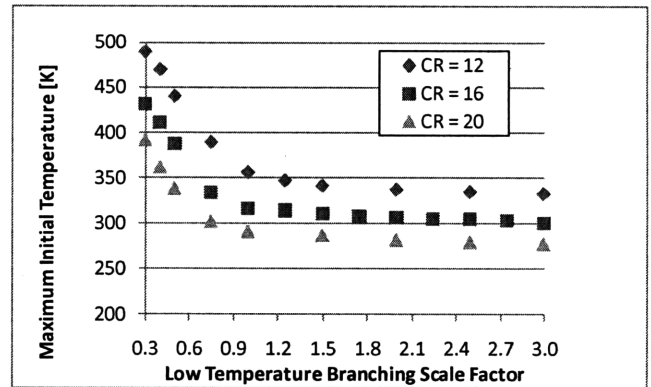
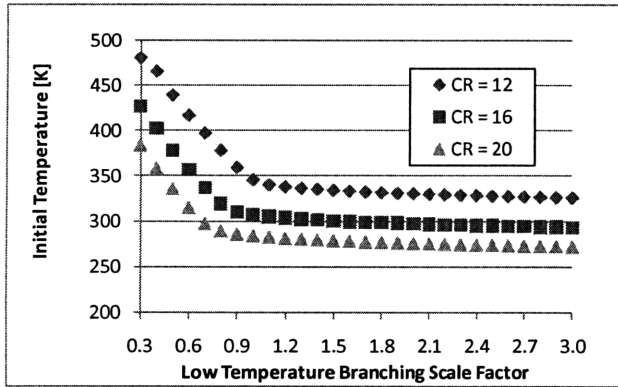


Figure E-16 Initial temperature for n-heptane based fuel, impact of A_{f1} : (a) variable volume, uniform temperature distribution (b) variable volume, quadratic temperature distribution

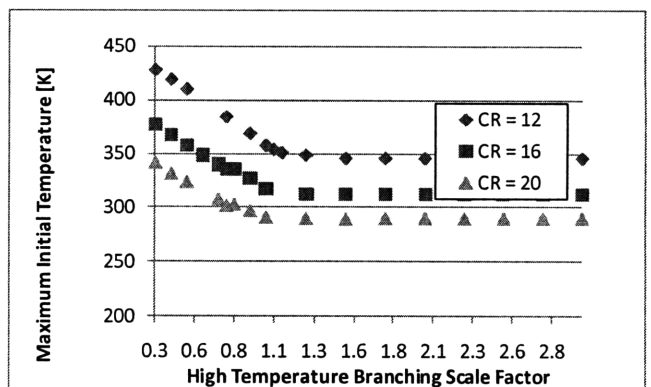
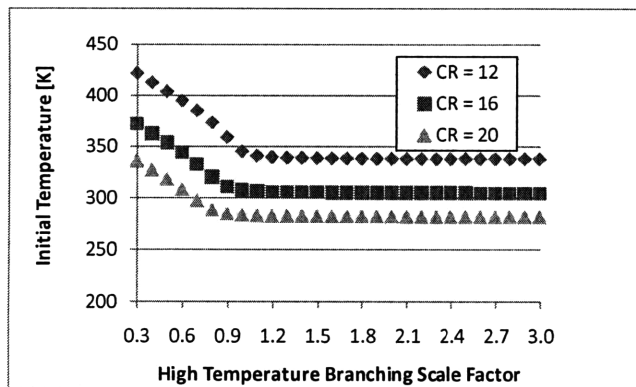







Figure E-17 Initial temperature for n-heptane based fuel, impact of A_{f2} : (a) variable volume, uniform temperature distribution (b) variable volume, quadratic temperature distribution

Appendix F

Summary of Impact of Ignition Delay Curve Features:

Figure F-1 provides a reference table on the impact of changing the ignition delay curve features on the MPRR. A detailed summary on the impact of each feature was given in Chapter 5.

No Change	Increase	Decrease	Local Max/Min	No Trend
				





























Fuel Parameter	Impact of increasing fuel parameter on Maximum Pressure Rise Rate			
	Uniform Temperature Distribution		Quadratic Temperature Distribution	
	Iso-Octane	n-Heptane	Iso-Octane	n-Heptane
T_A				
D_A				
n_1				
n_2				
Y_{NTC}				
A_{f1}				
A_{f2}				

Figure F-1 Summary of impact of ignition delay curve features on MPRR